The Effect of Water Partial Pressure on Low Temperature Iron Fischer-Tropsch Reaction Rate, Selectivity and Catalyst Structure

Thesis submitted for the Taught Masters in Catalysis degree in the Department of Chemical Engineering at the University of Cape Town

By

Herbert Benjamin Biel

B.Eng (Chemical), University of Stellenbosch

Promotor: Prof. Eric van Steen

Cape Town

2004

ACKNOWLEDGEMENTS

Technical and moral assistance was received from numerous sources during the course of this study. I hereby wish to extent my gratitude to the following:

- Professor Eric van Steen, my supervisor, for his support
- Dr. Alex Vogel and Philip Gibson for giving me the opportunity to undertake this project
- Cobus Malherbe for his assistance throughout the duration of the project
- Personnel of Sasol Technology R&D division who contributed to this work
- Sasol Technology R&D division for allowing me to undertake this project and their financial support
- My family for their love and support

SYNOPSIS

The Fischer-Tropsch synthesis catalysed by iron is a well-established process for the production of synthetic fuels, waxes and many other chemicals, yet there are many aspects that are still not totally understood. Controversy still exists as to what the active phase(s) is of the iron Fisher-Tropsch catalyst. A big drawback of the iron based Fischer-Tropsch synthesis is that one of its primary products, water, changes the structure and stability of the catalyst. Little is known about the effect that water partial pressure has on the phases present in the working catalyst.

During this study a generic iron Fischer-Tropsch catalyst was used in a bench scale reactor at 240°C and 20 bar to evaluate the effect of water partial pressure on the catalyst. The water partial pressure in the reactor was increased by co-feeding water to the reactor with an HPLC pump. The effect of water partial pressure on the activity and structure of the catalyst and the effect on the Fischer-Tropsch reaction rate, conversion and product distribution were evaluated.

The increase in the water partial pressure resulted in a change in the phases present in the catalyst. It was shown by both Mössbauer and XRD analyses that the spent base case catalyst (no water co-feeding) had Fe_2C present as the major phase. In addition, these analyses indicated that the spent catalyst that underwent 3 bar water addition contains magnetite as a major phase, which coincided with a drastic decrease in Fischer-Tropsch reaction rate and conversion. This strongly supports the theory which states that iron carbides are active for the Fischer-Tropsch synthesis and magnetite is inactive. The addition of 1 and 2 bar water to the feed did not lead to a drastic change in the catalyst structure, but did however show that the iron catalyst surface is very sensitive for small changes in water partial pressure. Hence, the addition of two bar water to the feed did cause a decrease in Fischer-Tropsch conversion and reaction rate,

but upon removal of water the catalytic activity was almost fully restored. Evidence of catalyst sintering at 3 bar water addition was obtained from XRD analyses.

The reaction rate data generated when the catalyst was exposed to a feed containing less than 2 bar water fitted various rate expressions well. The addition of 2 bar water to the feed and even more so, the addition of 3 bar water did however lead to deviations. Calculating the reaction rate of Fischer-Tropsch synthesis per gram of Fe_2C significantly reduced this deviation, which again suggests that the Fe_2C crystallites are the active sites for Fischer-Tropsch synthesis. Furthermore, when catalyst surface area loss is taken into account due to crystal growth the deviation even at 3 bar water addition is very little again showing evidence of catalyst sintering at high water partial pressures. The water-gas-shift reaction rate was not affected by any amount of water co-feeding.

The changes in the selectivity of the Fischer-Tropsch synthesis were mainly attributed to a reduction in the secondary reactions leading to a lower chain growth probability, decreased paraffin formation and decreased double bond isomerisation. Alcohol selectivity was however enhanced by the addition of water. The selectivity results obtained during this study support the following theories:

- Negligible olefin readsorption occurs at low carbon numbers
- Paraffins form both as primary and secondary products
- Internal olefins form mostly as secondary products
- Alcohol readsorption leads mainly to chain growth and paraffin formation

Evaluation of the chain growth probability and alcohol selectivity as a function of synthesis gas conversion revealed that the decrease in product readsorption is not only caused by a decrease in conversion after water addition, but also by a decrease in active iron carbide sites which are reoxidised to inactive magnetite.

TABLE OF CONTENTS

ACKNOWLEDGEMENTS	**I**
SYNOPSIS	**II**
TABLE OF CONTENTS	**IV**
NOMENCLATURE	**VIII**

CHAPTER 1

INTRODUCTION

1.1 THE FISCHER-TROPSCH PROCESS	**1**
1.1.1 Products of the Fischer-Tropsch Synthesis	**1**
1.1.2 Thermodynamic Aspects	**7**
1.1.3 Reactor and Process Development	**11**
1.2 MECHANISM OF THE FISCHER-TROPSCH REACTION	**17**
1.2.1 The 'Alkyl' (or Carbide) Mechanism	**17**
1.2.2 The "Enol" Mechanism	**19**
1.2.3 The 'CO-insertion' Theory	**21**
1.3 CATALYSTS FOR THE FISCHER-TROPSCH SYNTHESIS	**22**
1.3.1 The Active Phase in Iron-based Catalysts	**23**
1.4 THE EFFECT OF PROCESS PARAMETERS ON THE IRON CATALYSED FISCHER-TROPSCH SYNTHESIS	**27**
1.4.1 Activity Effects	**27**
1.4.2 Selectivity Effects	**30**
1.5 CONCLUSIONS	**31**

CHAPTER 2
EXPERIMENTAL

2.1 CATALYST PREPARATION	**32**
2.2 CATALYST CHARACTERISATION	**33**
2.2.1 Elemental Analysis	**33**
2.2.2 BET Surface Area and Pore Volume Determination	**33**
2.2.3 Mössbauer Analysis	**34**
2.2.4 X-Ray Diffraction Analysis (XRD)	**34**
2.3 EXPERIMENTAL SET-UP	**34**
2.3.1 Feed to the Reactor	**34**
2.3.2 The Reactor	**35**
2.3.3 Knock-out Pots	**38**
2.3.4 Gas Sample Points	**38**
2.4 PRODUCT ANALYSIS	**38**
2.4.1 Sampling Procedure	**38**
2.4.2 Analyses of Inorganic Gases and Methane	**39**
2.4.3 Analyses of Organic Product Compounds In Hot Tail Samples	**39**
2.4.4 Analyses of Oil Samples	**41**
2.5 DATA ANALYSIS	**42**
2.6 NORMAL REACTOR OPERATION	**45**
2.6.1 Reactor Start-up	**45**
2.6.2 Catalyst Reduction	**45**
2.6.3 Synthesis Conditions	**46**
2.6.4 Reactor Shut-down	**47**

CHAPTER 3
RESULTS

3.1 CHARACTERISATION OF CATALYST PRECURSOR 49

3.1.1 Elemental Analysis 49

3.1.2 BET Surface Area and Pore Volume Determination 50

3.2. SYNTHESIS RESULTS 50

3.2.1 Conditions in the Feed 50

3.2.2 Conditions in the Reactor 51

3.2.3 Effect of Water Partial Pressure on Conversion 54

3.2.4 Effect of Water Partial Pressure on Rate of Reaction 57

3.2.5 Effect of Water Partial Pressure on Selectivity 59

3.2.5.1 Chain Growth Probability 59

3.2.5.2 Secondary Hydrogenation 62

3.2.5.3 Double bond Isomerisation 65

3.2.5.4 Alcohol Selectivity 68

3.2.6 Reversibility of the Effects of Water Addition 71

3.3 CHARACTERISATION OF SPENT CATALYST 74

3.3.1 Mössbauer Analyses 74

3.3.2 XRD Analyses 78

CHAPTER 4
DISCUSSION

4.1 PHASES PRESENT IN THE IRON CATALYST 82

4.2 EFFECT OF WATER ON FISCHER-TROPSCH ACTIVITY 84

4.3 EFFECT OF WATER ON WATER GAS SHIFT ACTIVITY 91

4.4 SELECTIVITY OF THE FISCHER-TROPSCH SYNTHESIS 93

CHAPTER 5

CONCLUSIONS 97

REFERENCES 99

APPENDIX A

A1. Calculation of feed gas water partial pressure 111

A2. Calculation of reactor water partial pressure 114

APPENDIX B

Data gathered during experimental micro reactor runs 116

APPENDIX C

Results for calculations done from TCD analyses 122

APPENDIX D

Results for calculations done from the FID analyses 128

NOMENCLATURE

ABBREVIATIONS

AAS	Atomic Absorption Spectroscopy
AES	Atomic Emission Spectroscopy
ASF	Anderson-Schulz-Flory
CFB	Circulating Fluidised Bed
CSTR	Continuously Stirred Tank Reactor
FID	Flame Ionisation Detector
FT	Fischer-Tropsch
GC	Gas Chromatography
GTL	Gas To Liquids
HPLC	High Pressure Liquid Chromatography
ICP	Inductively Coupled Plasma
rpm	revolutions per minute
SAS	Sasol Advanced Synthol
TCD	Thermal Conductivity Detector
TPD	Temperature Programmed Desorption
TPR	Temperature Programmed Reduction
WGS	Water-Gas-Shift
XRD	X-Ray Diffraction

SYMBOLS

a	Kinetic parameter for FT reaction rate equation	[μmol/(g.s.bar$^{1.5}$)]
A_i	Peak area for component i in GC trace	[-]
b	Kinetic parameter for FT reaction rate equation	[bar^{-1}]
B_{hf}	Hyperfine magnetic field	[-]
f_i	Compound specific calibration factor	[-]

ΔG^R	Gibbs free energy for formation	[kJ/mol]
ΔH^R	Heat of reaction	[kJ/mol]
IS	Isometric Shift	[mm/s]
K_i	Equilibrium or adsorption constant	[-]
K_p	Equilibrium constant for WGS reaction	[-]
k_{WGS}	Reaction rate constant for WGS reaction	[mol/(gcat.s.bar)]
m_i	mass of component i	[g]
M_N	Molar content	[mol-%]
N	Number of carbon atoms	[-]
$\dot{n}_i$	Molar flow rate of component i	[mol/s]
P	Pressure	[bar]
$p_{d,N}$	Probability for desorption	[-]
$p_{g,N}$	Chain growth probability	[-]
pi	Partial pressure of component i	[bar]
$P_{r,N}$	Product with N carbon atoms	[-]
QS	Quadruple Splitting	[mm/s]
r	Rate of reaction	[mol/gcat/s]
$r_{d,N}$	Rate of desorption	[mol/gcat/s]
$r_{g,N}$	Rate of chain growth	[mol/gcat/s]
S_i	Selectivity of component i	[mol]
Sp_N	General surface species	[-]
T	Temperature	[°C]
X_i	Conversion of component i	[-]

GREEK LETTERS

α	Chain growth probability	[-]
τ	Residence time	[s]

1

INTRODUCTION

1.1 THE FISCHER-TROPSCH PROCESS

Almost a century ago the feasibility of producing liquid fuels from hydrogen and carbon monoxide with a group VIII metal catalyst was demonstrated in Germany (Dry, 1981). Fischer, Tropsch and Pichler were instrumental in the development of this polymerization process, which today is known as the Fischer-Tropsch Synthesis.

As early as 1902 it was observed that methane was formed from mixtures of hydrogen and carbon monoxide over nickel and cobalt catalysts. In 1923 Fischer and Tropsch (1926) reported their work using an alkalised iron catalyst at high pressures (10 to 15 MPa). At lower pressures hydrocarbons were produced, but it was found that the iron catalyst deactivated more rapidly. Development work on iron catalysts was continued in 1936 by Pichler who made the important discovery that when the pressure was increased from atmospheric to about 15 bar the life of the iron catalyst was markedly improved (Dry, 1981).

1.1.1 Products of the Fischer-Tropsch Synthesis

The Fischer-Tropsch Synthesis produces a complex product spectrum containing linear and branched hydrocarbons and oxygenated products. The selectivity of the process favours linear paraffins and linear α-olefins, but various amounts of alcohols, ketones, aldehydes and acids are also formed during synthesis (Gradassi, 1998; Dry, 1981). When operating at low temperatures (220 – 240°C)

the product selectivity is shifted towards high molecular weight products such as medium and hard waxes. When operating at high temperatures (320 – 340°C) the product selectivity is shifted towards lighter molecular weight products that are in the gasoline and diesel range (Dry, 1981).

The Fischer-Tropsch synthesis can be regarded as a surface polymerisation reaction, where the monomers for this polymerisation are produced in-situ from the reactants carbon monoxide and hydrogen (Schulz *et al.*, 1988). The polymerisation process seems to take place by the step-wise addition of C1-monomers (Herrington, 1946). Desorption of the growing chains on the catalyst surface leads to the actual product formation.

Schulz *et al.* (1988) developed a mathematical model to describe the product distribution using carbon number dependent reaction probabilities for chain growth and desorption, which are independent of the actual elemental reaction steps (see Figure 1.1). The model does not assume specific surface species, but defines a general surface species, Sp_N, which has N carbon atoms. In the simplest model developed by the authors, the surface species can grow or desorb as a product with N carbon atoms (Pr_N). The rate of chain growth is given by $r_{g,N}$ and the rate of desorption by $r_{d,N}$.

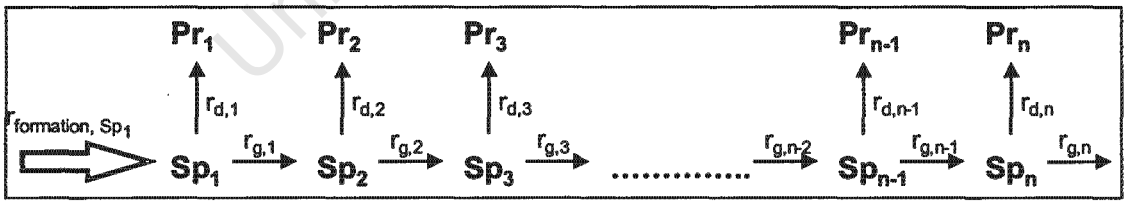

Figure 1.1: Model to describe the carbon number dependent chain growth model describing the Fischer-Tropsch synthesis (Schulz *et al.*, 1988)

A surface species has two possible reaction pathways: it can either grow or desorb. The probability with which chain growth takes place is defined as:

$$\alpha = p_{g,N} = \frac{r_{g,N}}{r_{g,N} + r_{d,N}} \tag{1.1}$$

(in literature the chain growth probability is often denoted as α). The probability for desorption of a growing chain is given by:

$$p_{d,N} = \frac{r_{d,N}}{r_{g,N} + r_{d,N}} \tag{1.2}$$

The rate of formation for a product with N carbon atoms is thus given by the rate of desorption of a surface species with N carbon atoms, Sp_N.

$$r_{Pr_N} = r_{d,N} \tag{1.3}$$

$$r_{Pr_N} = \frac{r_{d,N}}{r_{g,N} + r_{d,N}} \cdot \left(r_{g,N} + r_{d,N}\right) \tag{1.4}$$

$$r_{Pr_N} = p_{d,N} \cdot \left(r_{g,N} + r_{d,N}\right) \tag{1.5}$$

At steady-state the net rate of formation of a surface species with N carbon atoms equals zero. Thus, the rate of formation of the surface species with N carbon atoms through chain growth from a surface species with N-1 carbon atoms equals the rate of its consumption through chain growth and desorption.

$$r_{g,N-1} = r_{g,N} + r_{d,N} \tag{1.6}$$

The rate of formation of a product with N carbon atoms, Pr_N is thus given by:

$$r_{Pr_N} = p_{d,N} \cdot r_{g,N-1} = p_{d,N} \cdot \frac{r_{g,N-1}}{r_{g,N-1} + r_{d,N-1}} \cdot \left(r_{g,N-1} + r_{d,N-1}\right) \tag{1.7}$$

$$r_{Pr_N} = p_{d,N} \cdot p_{g,N-1} \cdot r_{g,N-2} \tag{1.8}$$

Continuing this substitution leads to:

$$r_{Pr_N} = p_{d,N} \cdot p_{g,N-1} \cdot \cdots\cdots \cdot p_{g,2} \cdot p_{g,1} \cdot r_{formation,Sp_1} \tag{1.9}$$

All product compounds contain one carbon atom originating from the initiating C_1-surface species. This means that at steady-state the sum of the molar rate of formation of all product compounds equals the rate of formation of the initiating C_1-species.

$$r_{formation,Sp_1} = \sum_{N=1}^{n=\infty} r_{Pr_N} \tag{1.10}$$

The molar content of a product compound with N carbon atoms, M_N, in the total number of moles of the product is thus given by

$$M_N = \frac{r_{Pr_N}}{\sum_{N=1}^{N=\infty} r_{Pr_N}} = p_{d,N} \cdot p_{g,N-1} \cdot \ldots\ldots \cdot p_{g,2} \cdot p_{g,1} \tag{1.11}$$

A special case can be derived, if the reaction probability for chain growth is independent of carbon number:

$$M_N = p_g^{N-1} \cdot p_d = p_g^{N-1} \cdot (1 - p_g) \tag{1.12}$$

The equation describing the product distribution in the Fischer-Tropsch process is thus identical to the equation describing the product distribution for homogeneous polymerisation (Schulz, 1935; Flory, 1936). A similar equation was also derived by Anderson *et al.* (1951).

According to equation 1.12, a semi-logarithmic plot of the molar content of the product distribution as a function of carbon number should yield a straight line with a slope equalling the logarithmic of the chain growth probability. These plots are in literature often denoted as the Anderson-Schulz-Flory (or ASF) distribution (see Figure 1.2).

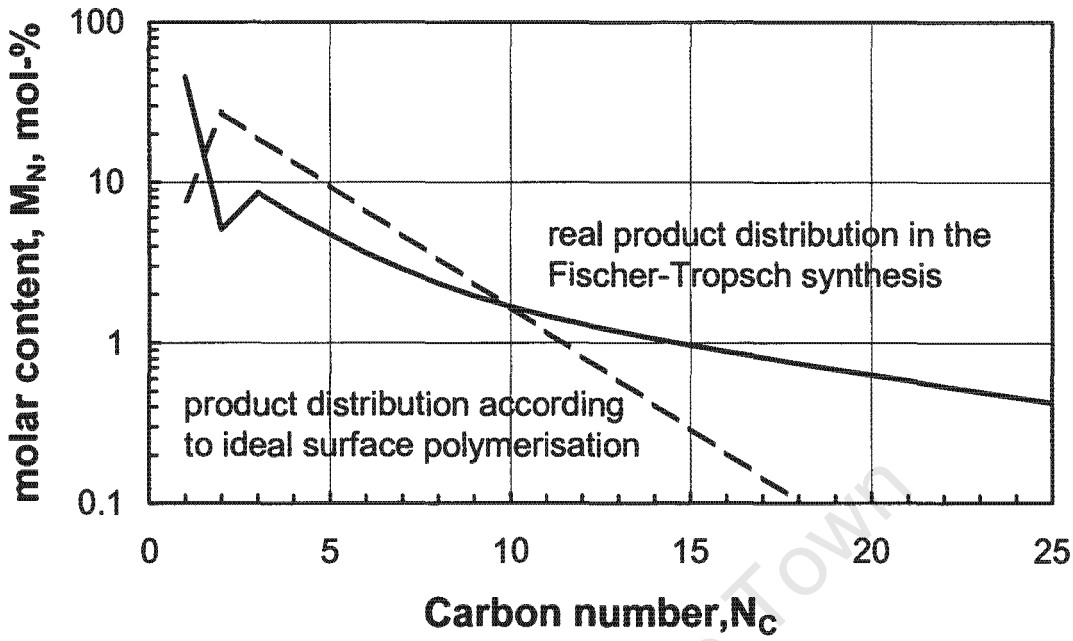

Figure 1.2: Comparison of the product distribution in the Fischer-Tropsch synthesis according to the ideal surface polymerisation with a carbon number independent rate of chain growth and rate of desorption and a realistic product distribution

Methane content in the ideal surface polymerisation with a carbon number independent rate of chain growth and rate of desorption should be lower than expected, since desorption of a C_1-surface species can only lead to the formation of a paraffin or an alcohol. Desorption of surface species with carbon number larger than one can lead to the formation of a paraffin, olefin, alcohol or aldehyde.

Real product distributions in the Fischer-Tropsch synthesis show three major differences to the ideal surface polymerisation with carbon number independent rate of chain growth and rate of desorption:

1. the formation of C_1-products (mainly methane) is higher than expected
2. the amount of C_2-products is lower than expected
3. the chain growth probability increases with increasing carbon number

The molar content of methane in the Fischer-Tropsch product is often much higher than expected. The reason for this phenomenon is presently unclear. Recently, it was proposed that methane is preferentially formed at sites with a high degree of coordination, whereas chain growth takes place preferentially at sites with a low coordination (Schulz *et al.*, 2002).

From an economic point of view, the carbon content of methane in the product is of greater relevance than the molar methane content. A high molar content of methane in the Fischer-Tropsch product does not necessarily mean a high carbon content of methane. The carbon or weight based content of methane in the total product depends highly on the chain growth probability (see Figure 1.3).

If the selectivity of any one carbon number species is altered, the selectivities of all the other species will also shift by a predictable amount (Dry, 1981). Based on the ideal surface polymerisation model (producing only paraffins), it is impossible to produce more than about 58 weight percent of C_2-C_4 hydrocarbons, about 45 percent of gasoline and about 30 percent of diesel. Dry (1981) reported typical ranges of α on ruthenium, cobalt and iron catalysts of 0.85-0.95, 0.7-0.8 and 0.5-0.7 respectively.

The assumption of a constant chain growth probability is however flawed. Some product compounds produced in the Fischer-Tropsch synthesis can undergo secondary reactions. The low molar content of C_2-compounds is often ascribed to the high reactivity of these compounds for secondary reactions (Schulz and Claeys, 1999a). Re-adsorption of reactive product compounds can lead to enhanced chain growth probability at high carbon numbers (Schulz and Claeys, 1999b; Iglesia *et al.*, 1991).

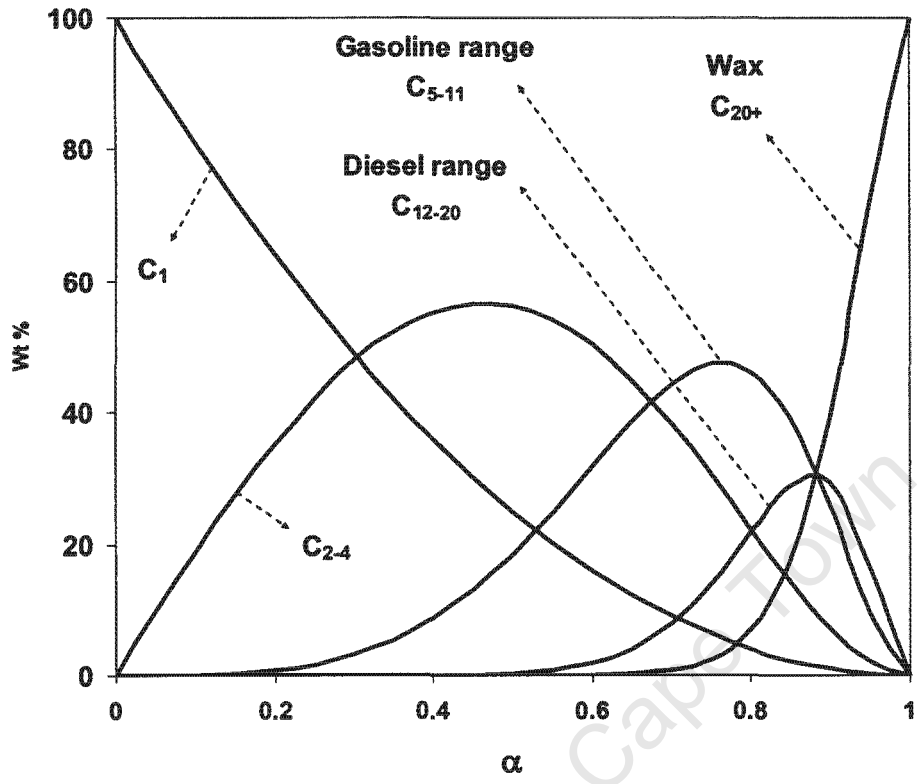

Figure 1.3: Hydrocarbon selectivity (wt.-%) as a function of chain growth probability *α*.

1.1.2 Thermodynamic Aspects

The Fischer-Tropsch process is mainly kinetically controlled, hence the product distribution is mainly a function of catalyst properties and operating conditions rather than being controlled by thermodynamic constraints. However, valuable information on the attainable equilibrium yields and the influence of temperature and pressure on the equilibrium composition can be obtained from thermodynamic analysis. The thermodynamics discussed in this section are mainly from the extensive work done by Anderson (Storch *et al.*, 1951) and Dry (1981).

The reaction stoichiometry of the Fischer-Tropsch synthesis can be represented as:

$$CO + \left(2 + \frac{1}{n}\right)H_2 \rightarrow \frac{1}{n}C_nH_{2n+2} + H_2O \quad (1.13)$$

$$CO + 2H_2 \rightarrow \frac{1}{n}C_nH_{2n} + H_2O \quad (1.14)$$

$$CO + 2H_2 \rightarrow \frac{1}{n}C_nH_{2n+1}OH + (1 - \frac{1}{n})H_2O \quad (1.15)$$

in which equations 1.13 1.14 and 1.15 represent the reactions producing paraffins, olefins and alcohols respectively. The water-gas-shift reaction can also take place under Fischer-Tropsch conditions

$$CO + H_2O \Leftrightarrow CO_2 + H_2 \quad (1.16)$$

The formation of carbon during the Fischer-Tropsch reaction takes place via the Boudouard reaction.

$$2CO \rightarrow CO_2 + C \quad (1.17)$$

Figure 1.4 shows the Gibbs free energy of reaction for the formation of the various product compounds. The formation of all these product compounds is thermodynamically feasible (i.e. the Gibbs free energy for the formation of all products is less than 0), with the exception for the formation of methanol ($\Delta G^R(250°C)$= 26.8 kJ/mol) and formaldehyde ($\Delta G^R(250°C)$= 60.7 kJ/mol).The formation of methane is thermodynamically highly favoured ($\Delta G^R(250°C)$ = -90.7kJ/mol CO converted) over long chain hydrocarbons (e.g. for n-decane $\Delta G^R(250°C)$ = -34.7 kJ/mol CO converted). Therefore, the suppression of undesirable methane formation is a definite problem in the Fischer-Tropsch process.

The Gibbs free energy of reaction for the formation of n-paraffins is the lowest showing that these are the most stable product compounds in a given carbon number fraction. Olefins are at these conditions less stable than paraffins, and they can thus be converted in secondary reactions to the corresponding paraffin. Alcohols and aldehydes are the least stable products formed in the Fischer-Tropsch synthesis and these product compounds may undergo secondary reactions yielding olefins and paraffins.

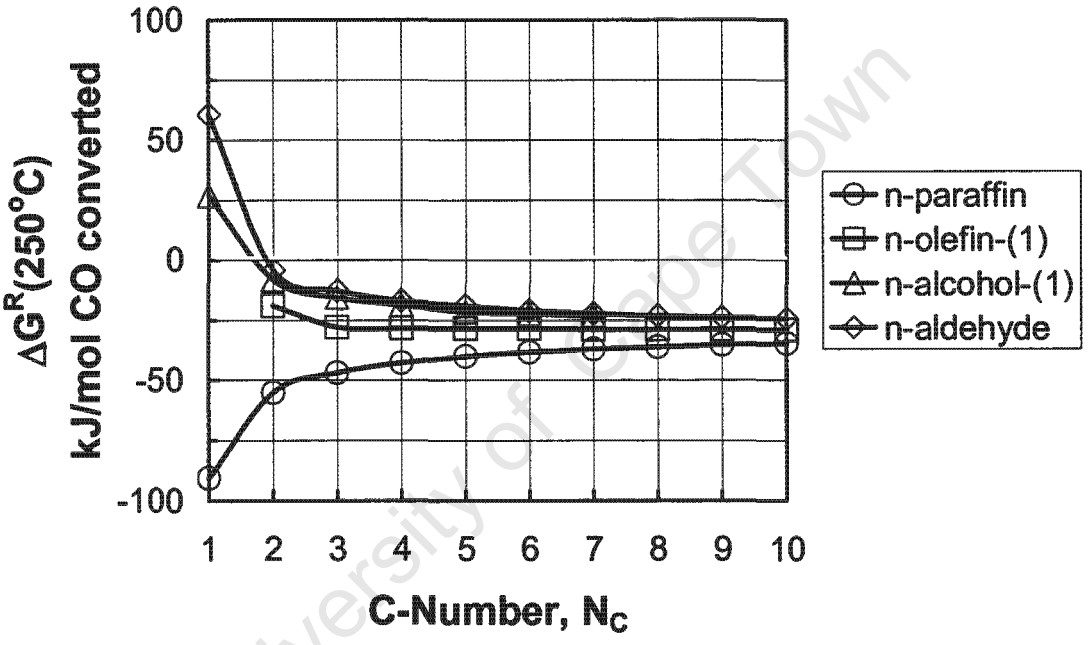

Figure 1.4: Gibbs free energy of reaction at 250°C per mol of carbon monoxide converted for the formation of

Paraffins: $CO + (2+1/n)\ H_2 \rightarrow 1/n\ C_nH_{2n+2} + H_2O$

Olefins: $CO + 2H_2 \rightarrow 1/n\ C_nH_{2n} + H_2O$

Alcohols: $CO + (2+1/n)\ H_2 \rightarrow 1/n\ C_nH_{2n+1}OH + (1-1/n)\ H_2O$

Aldehydes: $CO + (2-1/n)\ H_2 \rightarrow 1/n\ C_{n-1}H_{2n-1}CHO + (1-1/n)\ H_2O$

(Gibbs free energy calculated using data from Daubert *et al.*, 1993)

The heats of reaction are important because this energy must be removed from the reactor, which is a difficult engineering problem for the Fischer-Tropsch

process. The heats of reaction vary only slightly with temperature. Figure 1.5 shows the heat of reaction for the formation of various product compounds per mole of carbon monoxide converted as a function of carbon number. The formation of methane has the highest heat of reaction at 250°C (-215 kJ/mol), which is similar to the one reported by Storch *et al.* (1951; -211kJ/mol at 190°C). The heat of reaction for the formation of paraffins decreases with increasing carbon number and is approximately –161 kJ/mol of carbon monoxide converted for the formation of n-decane. Due to the exothermic nature of the reactions lower temperatures favour the formation of longer chain hydrocarbons.

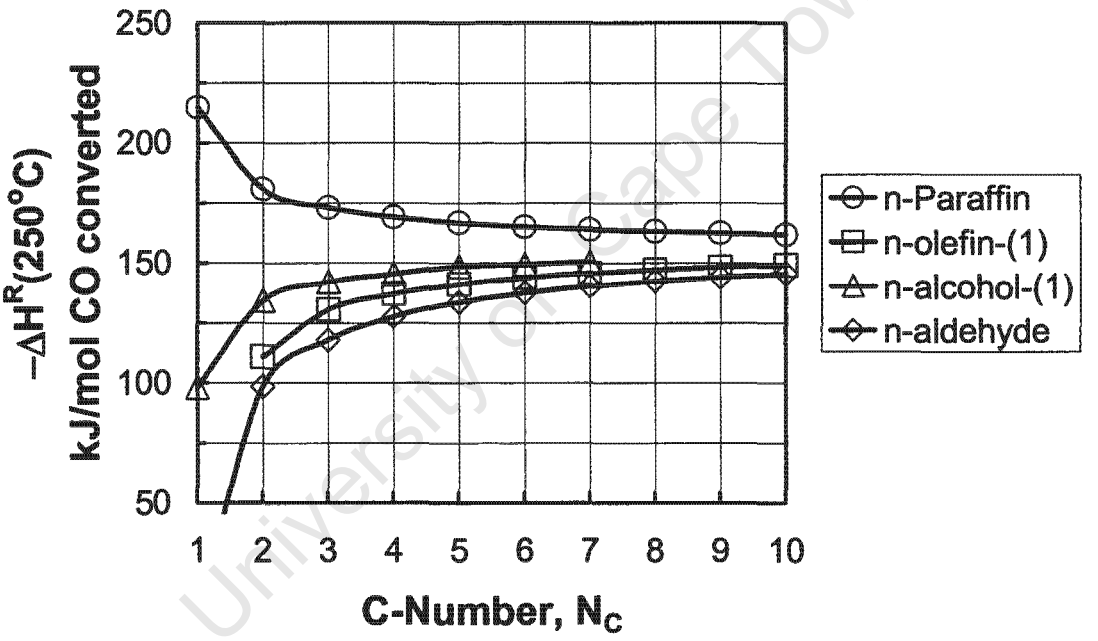

Figure 1.5: Heat of reaction at 250°C per mol of carbon monoxide converted for the formation of

Paraffins: $CO + (2+1/n)\ H_2 \rightarrow 1/n\ C_nH_{2n+2} + H_2O$

Olefins: $CO + 2H_2 \rightarrow 1/n\ C_nH_{2n} + H_2O$

Alcohols: $CO + (2+1/n)\ H_2 \rightarrow 1/n\ C_nH_{2n+1}OH + (1-1/n)\ H_2O$

Aldehydes: $CO + (2-1/n)\ H_2 \rightarrow 1/n\ C_{n-1}H_{2n-1}CHO + (1-1/n)\ H_2O$

(Heat of reaction calculated using data from Daubert *et al.*, 1993)

The water-gas shift and Boudouart reactions are both exothermic reactions. At 250°C the heat of reaction for the water-gas shift reaction is about -39kJ/mol while it's about -125kJ/mol for the Boudouart reaction. The selectivity towards carbon dioxide and free carbon would be expected to increase with temperature, since the heats of these reactions are smaller than for hydrocarbon synthesis,

1.1.3 Reactor and Process Development

Up to and during the Second World War several production plants were operated in Germany. After the discovery of large crude oil deposits in the Middle East in the 1950's interest in Fischer-Tropsch Synthesis was mostly lost. During this period the only development was the construction of the Sasol 1 plant which came on line in 1955 and has been in operation to this day. Several books and articles (Storch *et al.*, 1951; Anderson, 1956) have been written which cover the above time period. Presently, the following Fischer-Tropsch plants are commercially operating:

1. Sasol 1 is situated in Sasolburg (South Africa). Synthesis gas is produced from coal in Lurgi gasifiers. This is followed by Fischer-Tropsch synthesis at lower temperatures in both fixed bed and slurry reactors over a precipitated iron catalyst to produce high quality waxes and a variety of chemicals (Dry, 1982; Jager *et al.*, 1995). The coal gasifiers will be replaced by natural gas reformers in the course of 2004.
2. Sasol 2 & 3 are situated in Secunda (South Africa). Synthesis gas is produced from coal in Lurgi gasifiers. This is followed by Fischer-Tropsch synthesis at higher temperatures in fluidised bed reactors over a fused iron catalyst to produce sulphur free gasoline and diesel, solvents and α-olefins from coal (Jager *et al.*, 1990; Jager *et al.*, 1991).
3. PetroSA (formally known as Mossgas) operates in Mosselbay (South Africa) and utilises steam reforming of natural gas followed by Fischer-Tropsch synthesis at higher temperatures in circulating fluidised bed reactors over a fused iron catalyst to produce environmentally friendly liquid fuels and a variety of chemicals (Knottenbelt, 2002).

4. The Shell Middle Distillate Synthesis Process, operated in Bintulu (Malaysia), uses steam reforming of natural gas followed by Fischer-Tropsch synthesis over a cobalt catalyst to produce automotive fuels, speciality chemicals and high quality waxes. (Eilers *et al.*, 1990; Sie *et al.*, 1991; Senden, 1995)

The low cost of natural gas in the Middle East (Qatar and Iran) together with strict regulations against flaring natural gas in Nigeria has sparked interest in the utilisation of gas-to-liquid technology in these areas (Brown *et al.*, 2002). Both Sasol and Shell are developing GTL plants to be commissioned in these areas in the near future.

Taking the basic Fischer-Tropsch reaction as:

$$CO + 2H_2 \rightarrow (CH_2) + H_2O$$

with the CH_2 units subsequently forming a range of olefins, the heat released per reacted carbon atom averages at about 150 kJ (Anderson, 1956; Dry, 1996). Rapid removal of this heat is a major consideration in the design of suitable reactors. The objective is to minimise the temperature rise within the catalyst bed and to achieve this requires rapid heat removal in the direction perpendicular to the flow of the reactants.

One approach is to pack the catalyst particles into narrow tubes (see Figure 1.6), which are surrounded on the outside by water. A high flow of synthesis gas is passed through the tubes. This type of reactor is known as a Tubular Fixed Bed Reactor. The use of the narrow tubes ensures that the distance between the hot catalyst particles and the heat exchanger surface is short and also that the ratio of the heat exchanger surface area to the catalyst mass is high. This type of reactor was first introduced in Germany in 1936. Thereafter Ruhrchemie and Lurgi jointly developed the ARGE reactors. The first commercial ARGE reactors were commissioned at Sasol One site in 1955 and are still in operation (Dry, 1996).

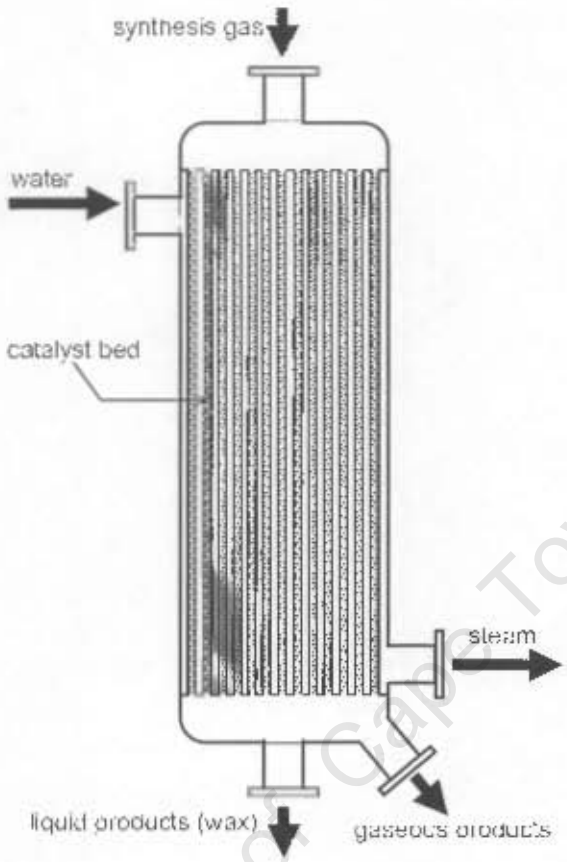

Figure 1.6: Schematic drawing of the ARGE multi tubular fixed bed reactor for the Fischer-Tropsch synthesis

The multi tubular fixed bed reactors are simple to operate (Dry, 1996). Furthermore, they can be used over wide temperature ranges irrespective of whether the FT products are gaseous or liquids, or both, under reaction conditions. There is also no problem separating liquid products from the catalyst. There are however many economic disadvantages in using multi-tubular reactors, since they are expensive to construct. Furthermore, the high gas flow rate through the packed bed results in a high differential pressure over the reactor leading to high compressor costs. To minimise pressure drop larger catalyst particle sizes are implemented at the cost of increased mass transfer

limitations. The catalyst, which looses its activity with time on line, has to be replaced periodically.

The slurry phase reactor (see Figure 1.7) was developed by Sasol. It is much simpler than the tubular fixed bed reactor and 40% less expensive to fabricate (Espinoza *et al.*, 1999). It consists of a shell fitted with cooling coils in which steam is generated. Synthesis gas is distributed at the bottom and it rises through the slurry. The slurry consists of liquid reaction products, predominantly wax, with catalyst particles suspended in it.

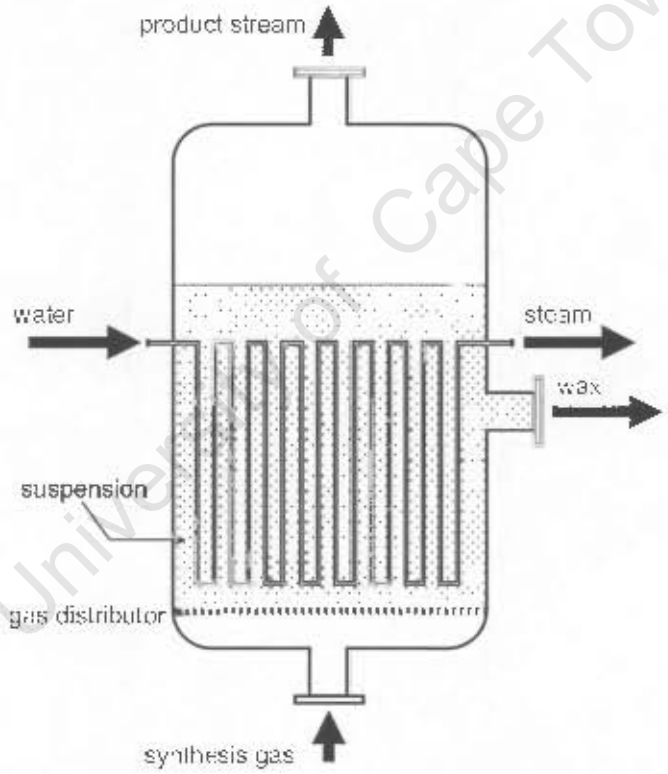

Figure 1.7: Schematic drawing of the slurry bed reactor for the Fischer-Tropsch synthesis

Kölbel and co-workers did a considerable amount of work on the concept of slurry bed reactors in the 1950's to the late 1970's (Kölbel and Ralek, 1980).

Isothermal conditions are maintained much better in the slurry bed than in a multi tubular fixed bed reactor. The pressure drop over the slurry bed is significantly lower, which translates to lower compression costs. The reactor can stay on-line for longer times than the tubular fixed bed reactors and the catalyst can be replaced on-line.

The Synthol or Circulating Fluidised Bed reactors (see Figure 1.8) are used commercially in South Africa and have a long history of continuous development and improvement. With this set-up the catalyst powder flows down a standpipe as a dense phase aerated powder. Pressure builds up on going down the standpipe to give the highest pressure in the system at the bottom. The catalyst flows through a slide valve and is picked up by the high velocity synthesis gas stream and is carried into the vertical reactor section. The heat of reaction is removed from the reactor section by cooing coils. On leaving the reactor section,

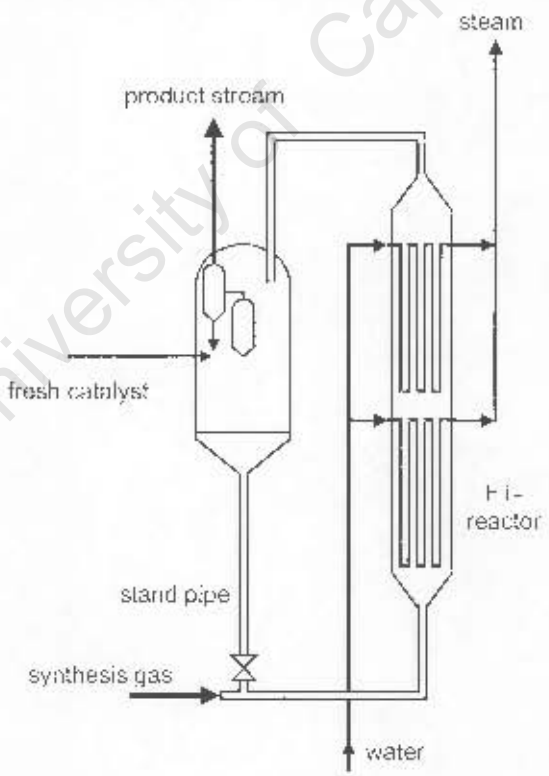

Figure 1.8: Schematic drawing of the circulating fluidised bed reactor for the Fischer-Tropsch synthesis

the catalyst passes through the upper transfer bend into a hopper and flows down the standpipe.

Hydrocarbon Research Inc. and Standard Oil Co in the USA first developed fluidised bed reactors for FT synthesis. During 1947-1951 the Kellogg Company in the USA developed a circulating fluidised bed reactor, which was scaled up by Sasol during the commissioning of the Sasol I plant in 1955. Although the CFB reactors have performed successfully they are complex to operate (Steynberg *et al.*, 1999; Dry, 1996).

The Sasol Advanced Synthol (SAS) reactor (see Figure 1.9) is a conventional fluidised bed that may be designed to operate at pressures ranging from 20 to 40

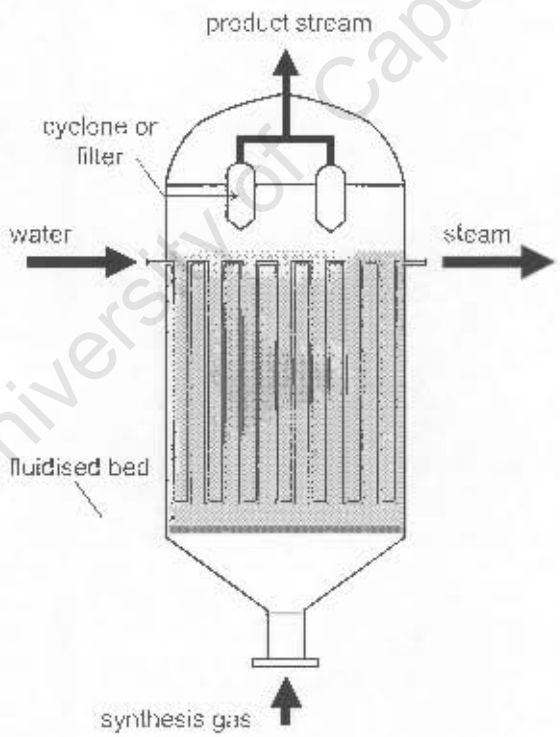

Figure 1.9: Schematic drawing of the fluidised bed reactor for the Fischer-Tropsch synthesis

bar and temperatures of around 340°C using an iron catalyst similar to that used in the CFB reactors.

The fluidised bed reactor consists of a vessel with a gas distributor, a fluidised bed containing the catalyst, cooling coils in the bed and cyclones to separate entrained catalyst from the gaseous product stream. Sasol has replaced the 16 Synthol reactors at Secunda with eight SAS reactors. The advantages of the fluidised bed reactor compared to the Synthol circulating fluidised bed reactor are numerous. The fluidised bed reactor is much cheaper to construct. Erosion problems are eliminated and therefore the need for regular inspection/ maintenance. The total amount of catalyst is in the reaction zone; therefore higher conversions are achieved (Steynberg *et al.*, 1999; Dry, 1996).

1.2 MECHANISM OF THE FISCHER-TROPSCH REACTION

Various mechanisms have been postulated for the chain growth reactions of Fischer-Tropsch synthesis. Most of the proposed mechanisms can account for the product spectrums, but the evidence used is usually indirect and can be interpreted incorrectly. According to the surface entities formed, a variety of mechanisms have been postulated. The three main categories which can be distinguished for the mechanism of the Fischer-Tropsch reactions are the so-called 'alkyl' (carbide), 'enolic' and the 'CO insertion' mechanisms.

1.2.1 The 'Alkyl' (or Carbide) Mechanism

The alkyl mechanism is currently the most widely accepted mechanism for chain growth in the FT synthesis. Fischer and Tropsch (1926) first suggested the carbide theory, which was later elaborated by Craxford (1939).

According to this mechanism, the first step in the process is the dissociation of carbon monoxide on the catalyst surface. This was confirmed by Araki *et al.* (1976) and Sachtler *et al.* (1979). Araki *et al.* (1976) observed that with reaction

mixture of ^{12}CO-H_2 in contact with a nickel surface pre-covered by $^{13}C_s$ yielded mainly $^{13}CH_4$. Sachtler *et al.* (1979) obtained similar results with cobalt, ruthenium and rhodium catalysts. According to these findings it is generally accepted tha: CO adsorbs chemically onto an active site, dissociates and is subsequently hydrogenated. Blyholder (1964) postulated that CO is bonded to the metal surface in a carbon-down position with its molecular axis perpendicular to the surface. Surfaces, which facilitate electron donation into the $2\pi^*$ antibonding orbital of the CO molecule, will exhibit a higher probability of the C-O bond cleavage.

Surface carbon is then thought to undergo subsequent hydrogenation. This results in the formation of CH_x species 1, 2 and 3.

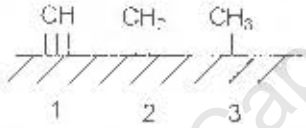

During the hydrogenation of carbon monoxide over a nickel catalyst the existence of species 1, 2 and 3 were proven by employing mass spectroscopy (Kaminsky *et al.*, 1986).

Chain growth can take place by the combination of a surface alkyl group with a reactive surface carbon, CH-species or CH_2-species, which results in the formation of the following species:

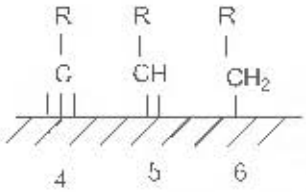

Brady and Petitt (1980, 1981) showed the involvement of surface CH_2-species in the chain growth process. They converted diazomethane in the presence and absence of hydrogen over transition metal catalysts. Ethene was the only product formed in the absence of hydrogen implying a CH_2-coupling and subsequent desorption. In the presence of hydrogen a product spectrum similar to that of the

Fischer-Tropsch synthesis was obtained. This shows that CH_2 surface species can act as the monomer or are involved in the formation of monomer species for the formation of long chain hydrocarbons.

The formation of branched compounds may occur if species 5 combines with an adsorbed methyl species, which will result in the formation of species 7.

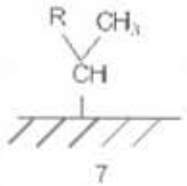

7

In the termination steps adsorbed alkyl species can either desorb as olefins by H elimination or it can be hydrogenated yielding a paraffin as illustrated below:

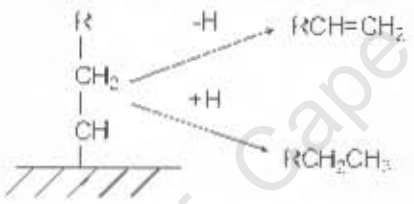

1.2.2 The "Enol" Mechanism

Storch *et al.* (1951) gave a detailed description of the enolic theory, which can account for the formation of oxygenates, olefins and paraffins. In this mechanism an associatively adsorbed linear CO molecule is partly hydrogenated according to reaction 1.18:

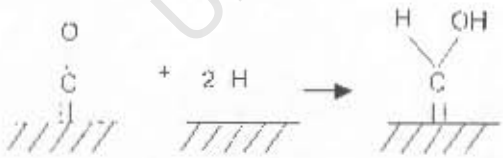

(1.18)

Chain growth can occur through condensation of two adjacent enolic species, followed by hydrogenation. (Equations 1.19 and 1.20):

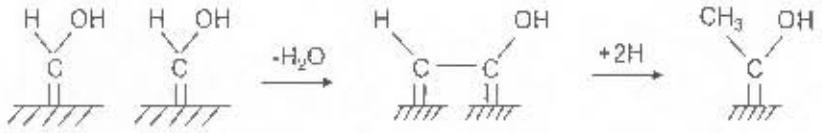

(1.19)

General case:

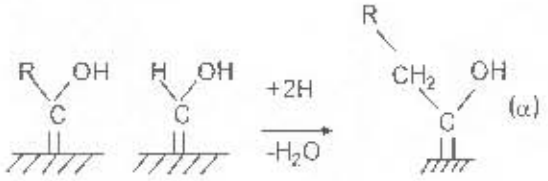

(1.20)

Alternatively, chain growth takes place by combination of adjacent-to-end carbons as in equations 1.21 and 1.22:

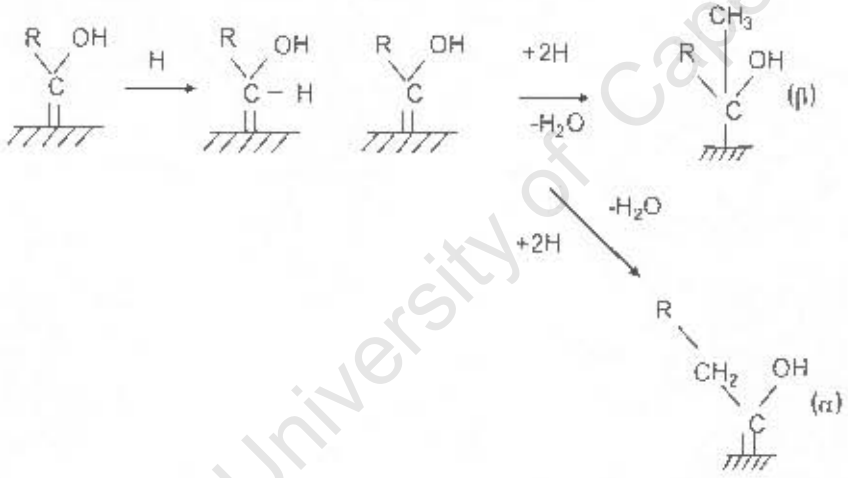

(1.21)

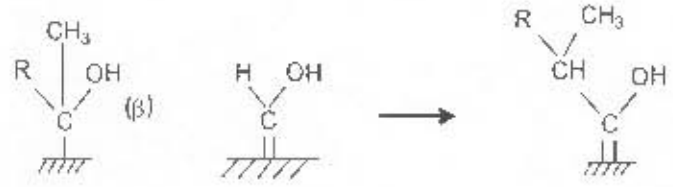

(1.22)

It is postulated that the double bonds between carbon and metal atoms are more resistant to hydrogenation if the carbon atom is also attached to a hydroxyl group. In the adjacent-to-end growth process hydrogenation of the carbon-to-

metal bond occurs and proceeds according to reactions 1.21 and 1.22. The intermediate 3 may grow by reaction 1.21 to form a group with a methyl side chain. The termination of growth is illustrated by reaction 1.23 and 1.24:

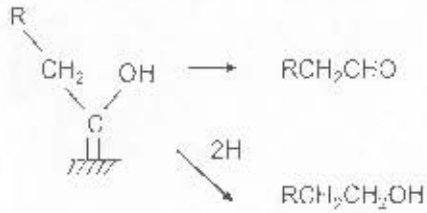

(1.23)

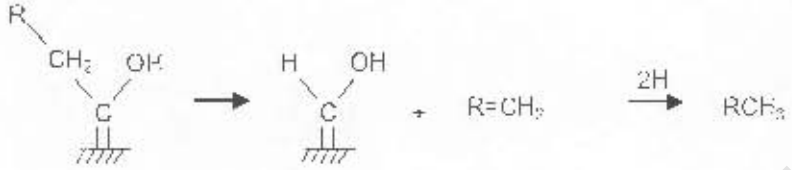

(1.24)

Aldehydes and alcohols may result from desorption and dehydrogenation of the alcohol like groups at the surface (equation 1.23). Acids may result from Cannizzaro type of reactions of the primarily formed aldehydes or by reactions of carbon monoxide with water or alcohols. Esters can be produced by subsequent reactions. The decomposition of the alcohol-like intermediates results in the formation of olefins and paraffins (equation 1.24).

1.2.3 The 'CO-insertion' Theory

The 'CO-insertion' mechanism was originally proposed by Sternberg and Wender (1959) and Roginski (1965) and fully developed by Pichler and Schulz (1970). In this mechanism carbon monoxide is chemisorbed onto the metal surface without dissociation. It inserts into either an H-M or C-M bond where M represents the catalyst surface site (Sternberg and Wender, 1985; Pichler and Schulz, 1970). The 'CO-insertion' mechanism is viewed by many researchers as the main reaction pathway leading to the formation of oxygenates (Anderson *et al.*, 1985; Dry, 1990). A generalisation of the CO insertion method is given below.

Chain initiation:

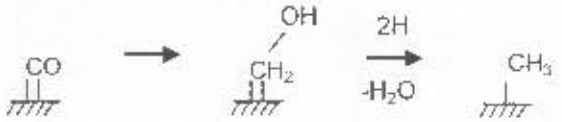

(1.25)

Propagation:

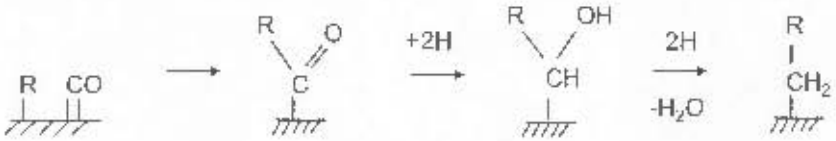

(1.26)

Termination/Desorption:

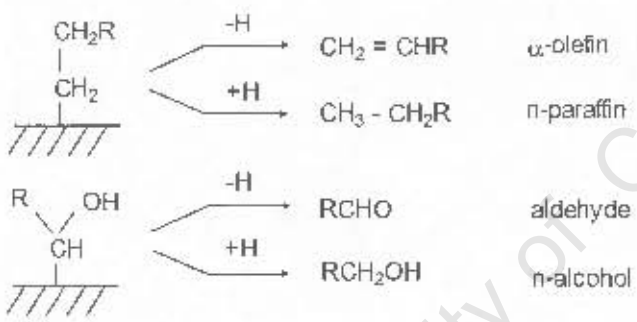

1.3 CATALYSTS FOR THE FISCHER-TROPSCH SYNTHESIS

The group VIII metals are known to catalyse the formation of hydrocarbons from hydrogen and carbon monoxide. The activities and selectivities of these metals, with the exception of Os, were investigated by Vannice (1975) at low CO-conversions. The reactor unit was operated at a pressure of 100 kPa and 240-280°C. High space velocities of 2500-10000hr^{-1} were typically used to keep the CO conversion around 5% or less. Ordering the metals according to their specific activities yields the following sequence:

Ru > Fe > Ni > Co > Rh > Pd > Pt > Ir

Ordering the metals according to the average molecular weight of their hydrocarbon products gave the following results:

Ru > Fe > Co > Rh > Ni > Ir > Pt > Pd

The low activities of Rh, Pd, Pt an Ir combined with the fact that they are rare and expensive make them not suitable for commercial use. The methane selectivity with nickel is very high. It is therefore commonly used as a methanation catalyst. Ruthenium is a very active and versatile catalyst, in that at higher temperatures it is an excellent methanation catalyst while at low temperatures and high pressures it produces large amounts of very high molecular mass waxes. Ruthenium has a high potential as a catalyst for converting synthesis gas into a variety of hydrocarbons, but is a very rare and costly metal (Dry, 1981).

Despite the high initial cost, cobalt can be considered as a Fischer-Tropsch catalyst for the production of middle distillates. At high enough reactor pressures, wax selectivities of higher than 50% can be obtained. The cobalt based Fischer-Tropsch kinetics are not inhibited by reaction water and high per pass syngas conversions can be achieved (van Berge and Everson, 1997).

To date Sasol has commercially only used iron-based catalysts in both high and low temperature Fischer-Tropsch applications. Not only is iron much cheaper than the alternative metals, but it also produces more olefins (Dry, 1988). Iron catalysts also catalyses the water-gas shift reaction, which permits the use of synthesis gas with a low H_2/CO ratio, e.g. synthesis gas obtained by the gasification of coal (Xu *et al.*, 1998).

1.3.1 The Active Phase in Iron-based Catalysts

Dry (1981) found that even if the catalyst loaded to a Fischer-Tropsch reactor is 100 percent metallic iron, the metal is very rapidly converted into a mixture of magnetite and iron carbides. Figure 1.6 illustrates the changes that occur in an iron catalyst in the case of a fluidized bed reactor operating at about 327°C. The units are undefined as the figure is only intended to illustrate the trends.

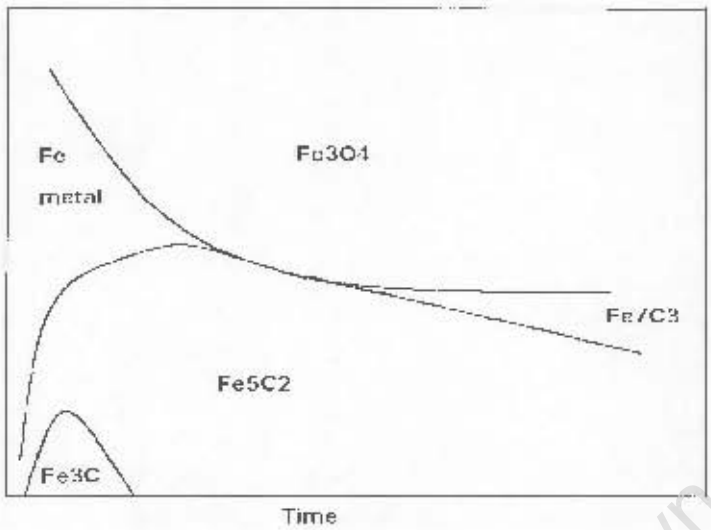

Figure 1.10: The change in composition of an iron catalyst during the FT reaction (Dry, 1981).

Dry (1981) reported that initially an unstable carbide phase, pseudo cementite (Fe_3C) is formed. This phase disappears after a few hours and Hägg carbide (Fe_5C_2) is then the only carbide present. After several days another carbide phase called Eckstrom-Adcock (Fe_7C_3) carbide appears and its concentration slowly increases with time.

More recently Senzi *et al.* (2001) did an in situ X-ray absorption spectroscopy study on iron oxide precursors and found that the presence of synthesis gas leads to structural and chemical changes in the precursors and to the formation of active sites required for the Fischer-Tropsch synthesis. They also found that the activation of these precursors occur via reduction of Fe_2O_3 followed by carburisation to form FeC_x. Figure 1.11 shows an example of a potassium promoted iron oxide precursor's change after exposure to synthesis gas with time on line.

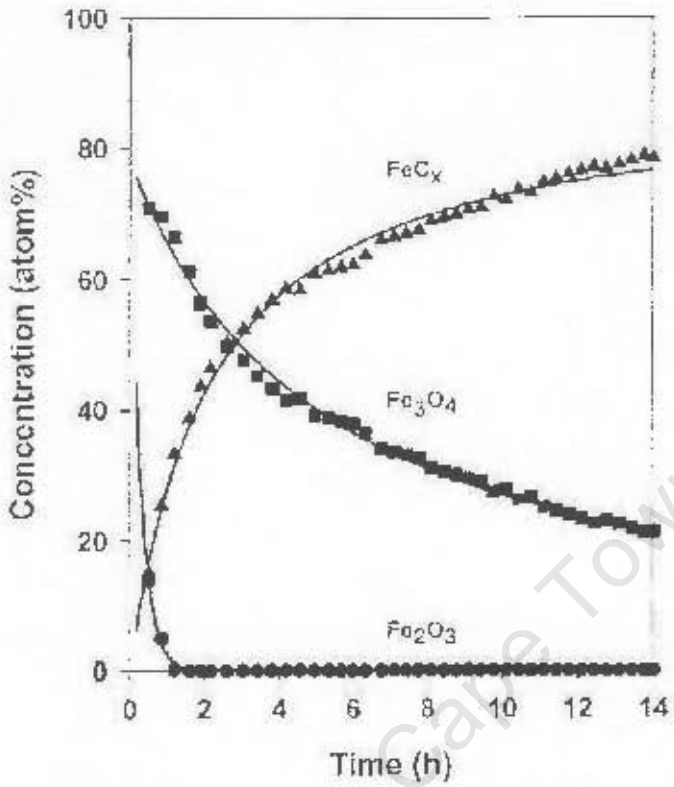

Figure 1.11: The phase change of a potassium promoted iron oxide precursor with time on line after exposure to synthesis gas at 250°C (Senzi *et al.*, 2001).

Analyses of the different size fractions of the catalyst of a fluidized bed reactor indicate that as the particle size decreases, the carbide/oxide ratio increases, with the very fine particles containing no oxides at all (Dry, 1981). Re-oxidation of iron within the core of the catalyst particles was postulated. As the synthesis gas diffuses into the porous catalyst particles the H_2 and CO are consumed in the FT reaction and H_2O and CO_2 is produced. Therefore the gas becomes progressively less reducing as it penetrates into the particles and beyond a certain depth it must become oxidising. For large catalyst particles the fraction of the catalyst, which is exposed to an oxidising atmosphere, will be larger. This will result in more oxide being present in large catalyst particles. Iron carbides are much more resistant to oxidation than metallic iron (Dry, 1981).

Although iron based catalysts for Fischer-Tropsch synthesis have been known for a long time, a controversy still exists regarding the composition of the catalytically active phase of the iron. The difficulty arises from the fact that under reaction conditions, iron exists as magnetite, α-iron and several iron carbides. The distribution of these phases is a sensitive function of reaction conditions and time on line (Dictor and Bell, 1985).

Some researchers have linked the formation of magnetite to catalyst deactivation. However, Huang *et al.* (1993) reported that according to their XRD patterns Fe_3O_4 is the only crystalline phase present in the catalyst, when it shows its highest activity. Based on this observation they imply that either Fe_3O_4 is the active phase or that the active phase cannot be detected by XRD.

Dwyer and co-workers and Bonzel and co-workers have shown that while α-iron is quite active for Fischer-Tropsch synthesis, it rapidly deactivates due to formation of a graphitic over layer (Dwyer and Somorjai, 1978; Krebs and Bonzel, 1979; Bonzel and Krebs, 1980, 1982; Dwyer and Hardenbergh, 1984).

Many workers believe iron carbides to be the active phase (Datye *et al.*, 2000). Amelse *et al.* (1978) observed using Mössbauer spectroscopy that the iron catalyst they tested carburised within 90 minutes of Fischer-Tropsch synthesis to the extent that no metallic iron could be detected in the Mössbauer spectra. As the catalyst carburised the methane formation rates increased and the product selectivity shifted towards higher hydrocarbon content.

Raupp and Delgass (1979) concluded from in situ Mössbauer investigations on a supported iron catalyst that the FT reaction rate follows the extent of bulk carbide formation. Dictor and Bell (1985) concluded from their work using X-ray diffraction analyses the active phase of iron-based Fischer-Tropsch catalysts is a mixture of carbides and a small amount of α-iron.

Mansker *et al.* (1999) concluded from X-ray diffraction analyses on a slurry phase iron catalysts that in its most active form the iron catalyst contains the Fe_7C_3 carbide with small amounts of α-iron while the Fe_5C_2 carbide also present in differing amounts during each run, appeared to be less active.

1.4 THE EFFECT OF PROCESS PARAMETERS ON THE IRON CATALYSED FISCHER-TROPSCH SYNTHESIS

1.4.1 Activity Effects

The effect of the reaction parameters on the activity of the Fischer-Tropsch synthesis has been investigated extensively (see e.g. Frohning *et al.*, 1977). It has been generally observed that the rate of reaction is increased with increasing hydrogen partial pressure and decreased with increasing carbon monoxide partial pressure.

Huff and Satterfield (1984) derived a rate expression for the rate of synthesis gas conversion based on a mechanistic model, which fitted the data well for a fused iron catalyst:

$$-r_{H_2+CO} = \frac{a \cdot p_{CO} \cdot p_{H_2}^2}{p_{H_2O} + b \cdot p_{CO} \cdot p_{H_2}} \qquad 1.27$$

Recently, van Steen and Schulz (1999) developed an alternative model, which fitted the data obtained on a precipitated iron catalyst:

$$-r_{H_2+CO} = \frac{a \cdot \dfrac{p_{CO} \cdot p_{H_2}^{1.5}}{p_{H_2O}}}{\left(1 + b \cdot \dfrac{p_{CO} \cdot p_{H_2}}{p_{H_2O}}\right)^2} \qquad 1.28$$

The rate expression proposed by Huff and Satterfield predicts a decrease in the activity with increasing water partial pressure, whereas the rate expression

proposed by van Steen and Schulz predicts the rate of reaction to pass through a maximum with increasing water partial pressure.

Karn *et al.* (1960) added up to 30 mol % of water in the synthesis gas feed when investigating the effect of water on an iron Fischer-Tropsch catalyst. The results of the water co-feeding experiments were compared to other runs where inert gases were added to the feed, and it was concluded that water caused a decrease in the FT reaction rate over and above that which is observed due to the dilution of the synthesis gas. It was however reported that the rate of the water-gas-shift reaction was up to four times higher than that of the FT reaction rate during some of the experiments where water was added to the feed.

Reymond *et al.* (1980) investigated the effect of water addition on the conversion of synthesis gas to hydrocarbons over a fused iron catalyst at atmospheric pressure. Since methane was the main product of the reaction, its production rate was taken as a measure of the FT reaction rate. According to the graphical representation of the results, water addition decreased the methane production rate by about 70 %. The decrease in activity might also have been caused by the dilution in these experiments.

Satterfield *et al.* (1986a, 1986b) performed various studies on co-feeding water to the Fischer-Tropsch synthesis to investigate its effect on iron Fischer Tropsch catalysts. They found that an increase in water vapour in the feed (27 mol %) caused a decrease in the Fischer-Tropsch reaction rate, but that the effect was completely reversible upon removal of the water vapour. However, in these experiments the total reactor pressure was kept constant, and thus the decrease in activity might have been caused by the decrease in the hydrogen and carbon monoxide partial pressure. They also found that when the added water was increased to 42 mol-% of the feed, the loss of catalytic activity seemed to be permanent due to irreversible catalyst re-oxidation.

Schulz *et al.* (1997) studied the effect of water on a cobalt catalyst in a stirred reactor by increasing the water partial pressure with a temperature-controlled saturator. They found that the CO conversion is not influenced significantly upon water addition. Hilmen *et al.* (1999) found that a cobalt catalyst deactivates when water is added during Fischer-Tropsch synthesis, which was attributed to the oxidation of the catalyst as shown using TPR, TPD and surface area analyses. Claeys and van Steen (2002) investigated the effect of water on a ruthenium catalyst and found a significant increase in product formation rates.

Water seems to affect the rate of the Fischer-Tropsch synthesis and with iron-based catalyst a decrease in activity seems to be most commonly observed (although the decrease in activity in a number of studies might also have been caused by dilution of the synthesis gas). The decline in activity can be predicted by the proposed rate expressions by Huff and Satterfield (1984) and by van Steen and Schulz (1999). However, these proposed rate expressions do not take phase changes within the catalyst into account. It was however proposed by Dry (1981) that water might cause the formation of magnetite in the catalyst at the expense of iron carbide. The addition of large quantities of water has been shown to oxidise an iron catalyst (Satterfield *et al.*, 1986b). The phase change may cause a change in the activity, if the different phases possess a different intrinsic activity.

Furthermore, water may enhance catalyst sintering, which may also attribute to an observed loss in activity. It has been shown that the catalyst near the exit of a fixed bed reactor (where the water partial pressure is at its highest) is more deactivated than catalyst higher up in the reactor. These observations fit the commonly observed fact that water vapour enhances the rate of sintering of high surface area catalysts (Dry, 1981). Crystallites located next to each other can consume water, combine to form one bigger crystallite and simultaneously release water. Thus, an investigation in the effect of water on the Fischer-Tropsch synthesis must take the possibility of sintering into account.

1.4.2 Selectivity Effects

Table 1.1 summarises the effect of process parameters on several aspects of general Fischer–Tropsch synthesis (iron, cobalt and ruthenium catalysts) (Claeys, 1997).

Table 1.1. The effect of process parameters on the selectivity of general Fischer-Tropsch synthesis (Claeys, 1998).

	Parameter					
	T	P_T	τ	K (Iron only)	P_{H2}	P_{CO}
Methane Selectivity	+	-	+	-	+	-
Chain Length	-	+	~	+	-	+
Branching	+	-	~	-	~	~
Olefins Selectivity	~	~	-	+	-	+
Oxygenates Selectivity	-	+	-	+		
Deposition of Carbon	+	~	~	+		+

Temperature and pressure have a substantial effect on Fischer-Tropsch synthesis. An increase in pressure forces the adsorbed molecules onto the catalyst surface and therefore increases the chain growth probability. This leads to the formation of longer chain hydrocarbons. An increase in temperature makes larger molecules thermodynamically less stable and leads to a decrease in chain growth probability and increase in methane selectivity.

Promoting an iron catalyst with potassium reduces methane selectivity and therefore increases chain growth probability. Hydrogen is a molecule that can terminate chain growth of an adsorbed molecule and therefore, if its partial pressure is increased, chain growth probability is decreased. An increase in carbon monoxide however, increases chain growth probability as more carbon molecules are provided for the chain growth reaction.

Schulz *et al.* (1997) studied the effect of water on a cobalt catalyst in a stirred reactor by increasing the water partial pressure with a temperature-controlled

saturator. They found that the selectivity is positively affected since methane formation is suppressed and chain growth enhanced. All effects were completely reversible upon removal of water vapour. Claeys and van Steen (2002) reported similar findings for the effect of water on the performance in the Fischer-Tropsch synthesis over a supported ruthenium catalyst. They found a significant increase in product formation rates and significant changes in product selectivity. They observed that the addition of water leads to a lower methane selectivity and improved chain growth.

1.5. CONCLUSIONS

The Fischer-Tropsch synthesis catalysed by iron is a well-established process for the production of synthetic fuels, waxes and many other chemicals, yet there are many aspects that are still not totally understood. Controversy still exists as to what the active phase(s) is of the iron Fisher-Tropsch catalyst. A big drawback of the iron based Fischer-Tropsch synthesis is that one of its primary products, water, changes the structure and stability of the catalyst. Little is known about the effect that water partial pressure has on the phases present in the working catalyst.

This study will concentrate on the effect of water partial pressure on the following aspects of the iron catalysed Fischer-Tropsch synthesis:

- The effect of water partial pressure on the activity of the catalyst.
- The effect of water partial pressure on the catalyst structure/phases.
- The influence that water partial pressure has on the FT product distribution.
- Establish whether the effects of an increase in water partial pressure are reversible upon removal of water.

2

EXPERIMENTAL

2.1 CATALYST PREPARATION

A generic iron Fischer-Tropsch catalyst was used in this study. The catalyst was prepared by the precipitation of a water soluble iron salt (such as $Fe(NO_3)_3$), with or without promoters (such as KNO_3 and $Cu(NO_3)_2$) and binders such as silica (Mansker *et al.*, 1999). A carbonate was used as the precipitation agent. The use of carbonates of potassium, sodium and ammonia as precipitating agent results in better catalysts than when hydroxides are used (Dry, 1981). The use of metal sulphates and chlorides generally results in catalysts with low activity (Dry, 1981; Espinoza *et al.*, 1999). The addition of copper to the catalyst was found to enhance the rate of reduction and enables reduction to be carried out at lower temperatures (Dry, 1981). The addition of potassium enhances the activity of the catalyst and shifts its product selectivity to longer chain hydrocarbons (Dry, 1981).

The precipitated iron hydroxide (FeOOH) was subsequently washed and re-slurried to add promoters. The catalyst precursor was subsequently calcined at temperatures above 200°C to form hematite (Fe_2O_3) and spray-dried. It was found that spray drying the catalyst results in more rounded catalyst particles and it therefore is less susceptible to attrition in the turbulent environment of the slurry phase reactor (Dry, 1981).

The spray-dried hematite is then activated by pre-treatment with H_2, CO, or synthesis gas. Activation alters the catalyst composition to what is thought to be a mixture of iron oxides (Fe_2O_3, Fe_3O_4), various carbides (Fe_3C, Fe_5C_2, Fe_7C_3) and iron metal (α-Fe) (Mansker *et al.*, 1999).

2.2 CATALYST CHARACTERISATION

The iron-based Fischer Tropsch catalyst used in this study was characterised in detail to obtain the properties needed to do a comprehensive analysis of the effect of water partial pressure on the catalyst.

In order to characterise the working catalyst, it is necessary to prevent changes in the catalyst upon transfer of the catalyst and during the characterisation measurement. Hence, the catalyst was transferred in wax and characterisation measurements were done with the catalyst loaded in wax to prevent oxidation.

2.2.1 Elemental Analysis

The iron content in the catalyst was determined by method of titration. The sample is dissolved in hydrochloric acid. Stannous chloride is added to a suitable volume to reduce ferric to ferrous iron. The ferrous iron is titrated with a 0.05M $K_2Cr_2O_7$ solution with sodium di-phenyl amine sulphonate as indicator.

The other elements present in the catalyst were analysed using Inductively Coupled Plasma Atomic Adsorption Spectroscopy (ICP-AAS). The sample is dissolved under reflux in a known quantity of hydrochloric acid and diluted to a specific volume. After digestion the sample is analysed on the Vista AZ CCD simultaneous ICP-AES.

2.2.2 BET Surface Area and Pore Volume Determination

The BET surface area of the catalyst was determined using a Micrometrics Gemini. The sample is degassed under a nitrogen blanket for one hour and ten

minutes at 90°C. The oven temperature is then increased to 250°C for another 4 hours to clean up the catalyst surface. The saturation pressure is set to at least 600 mm Hg and the measurement is done at 77K.

2.2.3 Mössbauer Analysis

The Mössbauer experiments were performed with a 50 mCi (initial activity) Co-57 source in a Rhodium matrix. The analyses were performed at ca. 25°C with the catalysts still in the wax medium to prevent re-oxidation. The data was analyzed using a least-square fitting routine that models the spectra as a combination of quadruple doublets and sextuplets based on a Lorentzian line-shape profile. The spectral components were identified based on their isomeric shift (IS), quadruple splitting (QS) and hyperfine magnetic field (B_{hf}). The isomeric shift values were reported relative to metallic iron (α-Fe) and the iron content of each phase was determined from their relative peak areas.

2.2.4 X-Ray Diffraction Analysis (XRD)

The samples were analysed with the Philips XRD-2 System with the catalyst still in the wax medium to prevent re-oxidation. The conditions at which the diffractometer was set for the qualitative identification of the phases are given in Table 2.1. The radiation source used was an X-ray tube, Cobalt target, wavelength (λ) Co K α= 1.7889 Angstrom, ceramic, Long Fine Focus (LFF-type).

2.3 EXPERIMENTAL SET-UP

A bench scale stirred tank micro reactor was used to investigate the effect of water on the performance of an iron-based Fischer-Tropsch catalyst. The experimental set-up is schematically shown in Figure 2.1.

2.3.1 Feed to the Reactor

The experimental set-up has three feed lines, for feeding synthesis gas, argon and water to the reactor. Argon is used as an internal standard during the experiments. All gas flows (synthesis gas or argon) are controlled using Brooks

Table 2.1: Experimental Conditions for XRD Analyses

Voltage	40 kV
Current	40 mA
Divergence slit	0.5°
Anti-scatter slit	1°
Range (2θ)	5°-105°

mass flow controller. The feed line for synthesis gas can also be used for feeding pure hydrogen to the reactor.

Distilled water is fed using an HPLC-pump (Rheos 4000). Argon is bubbled continuously through the water container to remove dissolved oxygen. The total amount of water fed is monitored using a scale.

The water and gas streams flow through and are mixed in a heated and insulated gas bomb filled with glass beads. The temperature of the gas bomb is controlled at 200°C to ensure that all the water is in the vapour phase before entering the reactor. The gas bomb also ensures sufficient mixing of the feed gasses and acts as a buffer to any pulses in the water feed that might damage the catalyst.

2.3.2 The Reactor

A stirred reactor was used in this study, which acts as a steady-state operating CSTR for the reactants and the light product compounds (see Figure 2.2). The reactor volume is 650 ml and the wall thickness is 35mm. The reactor has a double-blade stirrer to ensure good mixing of both phases under reaction conditions. The top stirrer is slightly smaller in diameter to leave sufficient space

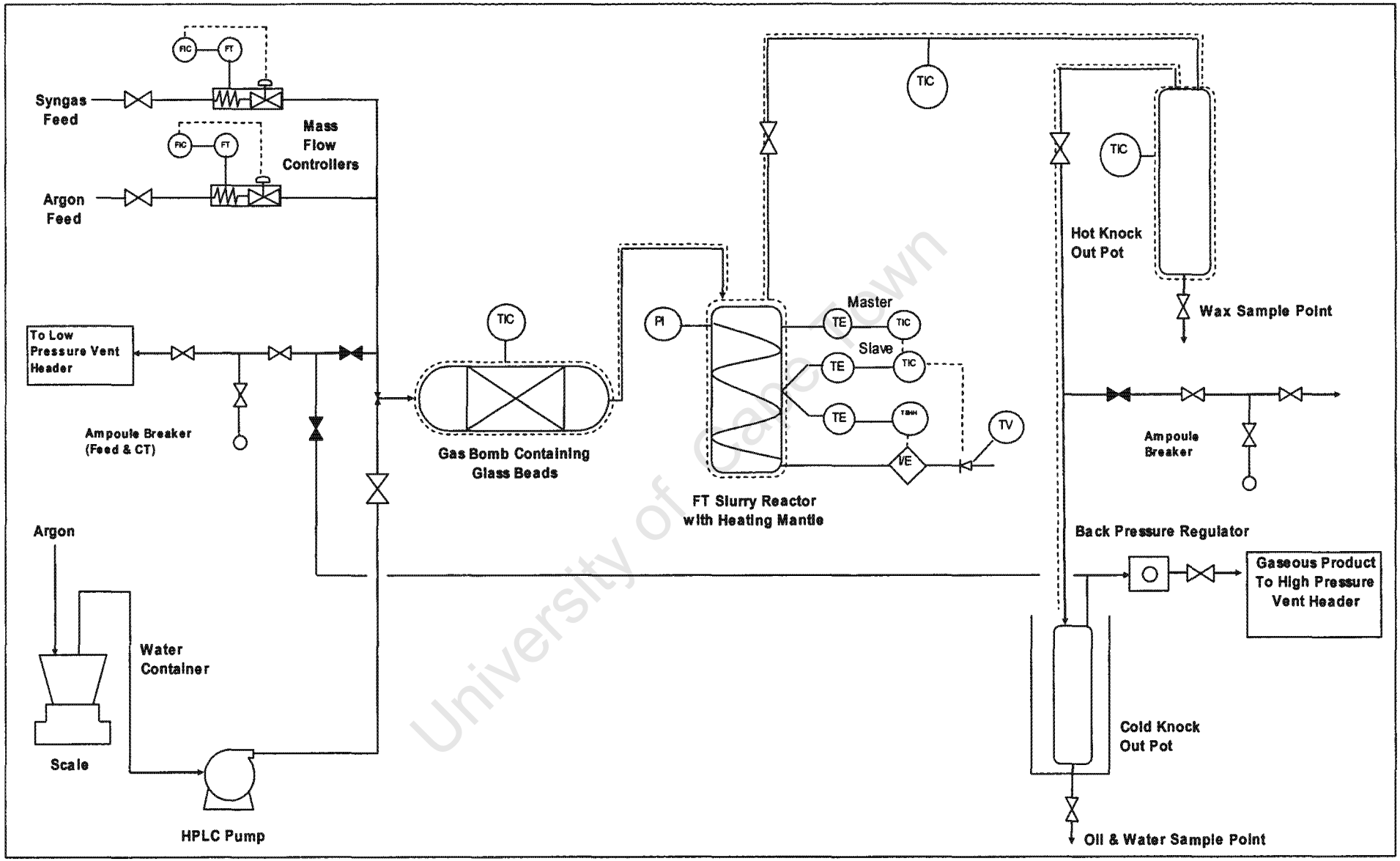

Figure 2.1: Schematic representation of the experimental set-up for the Fischer-Tropsch synthesis

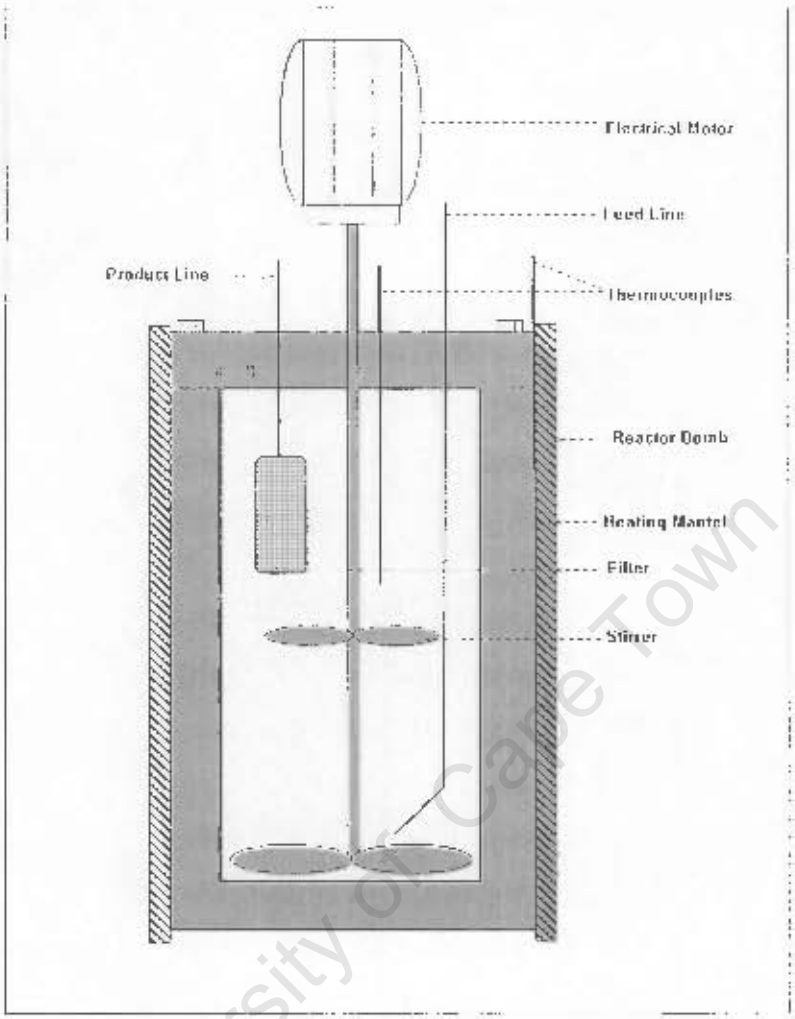

Figure 2.2: Stirred tank micro reactor used for the Fischer-Tropsch Synthesis

for the feed line. The feed line enters the reactor at the top and reaches all the way down to 5mm above the bottom stirrer. It is also slightly bent inwards resulting in the opening being 5mm from the centre of the reactor. Both the gaseous and liquid products leave the reactor through a filter to ensure that the catalyst remains in the reactor.

The reactor is heated by a heating mantle. The temperature in the reactor is measured by two thermocouples, one of which measures the temperature in the reaction medium and the other one is inserted between the heating mantle and the reactor wall. The thermocouple inside the reactor is used by the master

temperature controller, and the thermocouple between the reactor wall and the heating mantle is used by the slave temperature controller.

2.3.3 Knock-out Pots

The product stream flows to a hot pot where the wax is knocked out. The heated, hot knock-out pot was kept at 200°C. The volume of this vessel is 500ml and it has a valve at the bottom for draining wax.

The product stream flows then to a cold pot where an oil fraction and reaction water is knocked out. The cold knock-out pot, which is situated in a water bath to keep it at room temperature, has also a volume of 500ml and has a valve at the bottom for draining reaction water and oil. The line between the hot and cold knock-out pots is insulated and controlled at 200°C. The "hot tail" gas sample is taken from it.

2.3.4 Gas Sample Points

Two gas sample points are available on the set-up, one hot tail gas sample point (fed by the stream leaving the hot knock-out trap) and one cold tail sample point (feeding from after the cold knock-out trap), which is also used to sample the feed gas. The hot tail gas sample point is controlled at 200°C., whereas the cold tail sample point was kept at room temperature. Ampoule samples (Schulz *et al.*, 1984a) can be taken from these streams for later analysis using gas chromatography.

2.4 PRODUCT ANALYSIS

2.4.1 Sampling Procedure

Two gas sample points were available on the set-up. The hot tail gas sample point temperature was controlled at 200°C. The two tail gas samples were always completed before the knockout traps were drained, as the gas samples

would otherwise not be representative. The samples of the two tail gas sample points were always drawn before the feed gas sample point was bubbled.

The protruding ampoules were heated with a portable butane burner for 10 seconds. This is necessary for especially the hot tail gas sample point, to prevent possible selective condensation of the sample gas. Condensation could result in the sample not being representative. Care was taken when heating and sealing off the ampoules, as excessive heating could induce thermal cracking.

The reactor knockout traps were drained every +/-24 hours to retrieve samples and prevent possible carry-over of products. The hot trap was drained before the cold knockout trap, to prevent any possible carryover of wax. The traps were drained into a beaker, by opening the sample point needle valves. The reaction water and oil sample from the cold knockout trap was left for 10 minutes to allow sufficient separation and then separated in a funnel.

2.4.2 Analyses of Inorganic Gases and Methane

The gaseous feed and cold tail samples were analysed on the Gomac CD 600 gas chromatograph equipped with a Thermal Conductivity Detector (TCD). The gaschromatographic separation was performed using a molecular sieve capillary column and a Porapak-Q packed column. The analysis conditions are given in Table 2.2. A typical TCD trace can be seen in Figure 2.3.

2.4.3 Analyses of Organic Product Compounds in Hot Tail Samples

The hot tail samples were analysed on a GC (Agilent 6890) equipped with a Flame Ionisation Detector. The separation was achieved using a PETROCOL DH 150 capillary column utilising a temperature programme. The analysis conditions are given in Table 2.3.

Table 2.2: Conditions for analyses of inorganic feed and product compounds

Injector	Splitless
Injector Temp	100°C
Head Pressure	20 psi
Carrier Gas	H2 - 20 ml/min
Column Type & Dimensions	Molecular sieve Capillary column and Porapack-Q packed column
Temperature	70°C
Detector	TCD
Detector Temperature	100°C

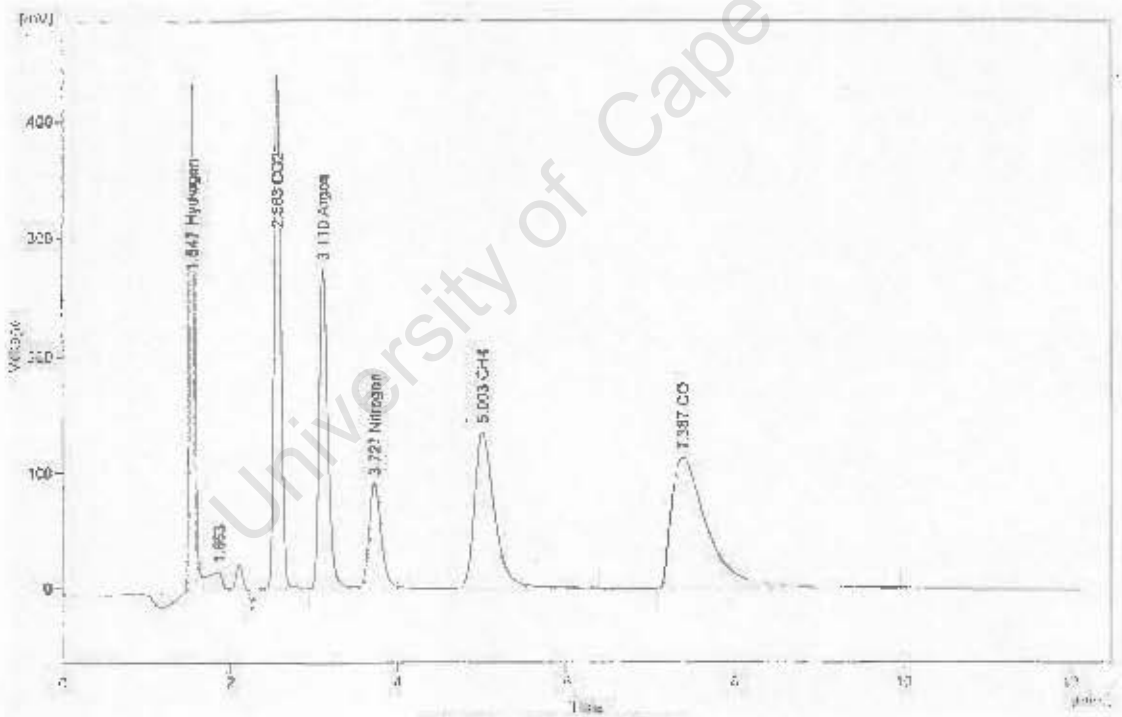

Figure 2.3: Typical GC trace for the analyses of inorganic gases and methane

Table 2.3 Conditions for analyses of organic product compounds in the hot tail samples

Injector	Split-injector
Injector Temp	250 °C
Head Pressure	175 kPa(g)
Split Ratio	1 to 100
Carrier Gas	H_2 - 27 cm/sec (2.4 ml/min)
Column Type & Dimentions	PETROCOL DH 150 Capillary Column 150m x 0.25mm x 1.0µm film thickness
Temperature program	Initial: -60 °C Hold: 10 min Heating rate: 20 °C/min Temp: -20°C Hold: 0 min Heating rate: 2 °C/min Final: 220 °C Hold: 48 min
Detector	FID
Detector Temperature	300 °C
Fuel gas	Hydrogen: 40 ml/min
Air	450 ml/min
Make-up	Nitrogen: 25 ml/min

2.4.4 Analyses of Oil Samples

The oil samples were analysed using the Agilent 6890 gas chromatograph equipped with a Flame Ionisation Detector. The analysis conditions are given in Table 2.4.

Table 2.4: Conditions for GC-analyses of the oil samples

Injector Type	Split/Splitless
Injector Temp	250 oC
Head Pressure	122 kPa(g)
Split Ratio	1 to 200
Carrier Gas	Hydrogen
Column Type & Dimensions	HP-PONA 50m x 0.2mm x 0.5µm
Temperature program	Initial: 50 oC Hold: 1 min Oven rate: 4 oC/min Final Temp: 290°C Hold: 29 min
Detector	FID
Detector Temperature	300 °C
Fuel gas	Hydrogen: 30 ml/min
Air	450 ml/min
Make-up	Nitrogen: 30 ml/min

2.5 DATA ANALYSIS

The addition of an internal standard, Ar, at an exactly determined flow rate allows the calculation of the flow rates of the inorganic compounds and methane using the peak areas obtained in the gaschromatographic analysis with a TCD.

$$\dot{n}_i = f_i \cdot \frac{A_i}{A_{Ar}} \cdot \dot{n}_{Ar,feed} \qquad (2.1)$$

with $\dot{n}_i$: the molar flow rate of compound i

f_i: compound specific calibration factor

A_i: peak area for compound i in GC trace

The molar flow rate of water can be calculated using the oxygen balance knowing the molar flow rates of CO and CO_2 in the feed and at the outlet of the reactor and the inlet molar flow rate of water, which is determined gravimetrically. In the calculation the molar flow rate of water the oxygen content in the organic products is neglected. This constitutes only a small error in the total molar flow rate of water.

$$\dot{n}_{H_2O,outlet} = \dot{n}_{H_2O,feed} + \dot{n}_{CO,feed} + 2 \cdot \dot{n}_{CO_2,feed} - \dot{n}_{CO,outlet} - 2 \cdot \dot{n}_{CO_2,outlet} \quad (2.2)$$

The molar flow rates of the organic product compounds can be obtained having determined the molar flow rate of methane in the product stream and the product composition using in the hot tail samples:

$$\dot{n}_i = f_i \cdot \frac{A_i}{A_{CH_4}} \cdot \dot{n}_{CH_4,outlet} \quad (2.3)$$

(the factor f_i corresponds to the reciprocal value of the carbon number of the compound for paraffins and olefins; for oxygenates the lower sensitivity of the detector for these compounds were taken into account according to Claeys (1997)).

the partial pressure of each component can be calculated knowing the total molar composition of the gaseous phase within the reactor and assuming the reactor to be well-mixed.

$$p_i = \frac{\dot{n}_i}{\sum_i \dot{n}_i} \quad (2.4)$$

Carbon monoxide in the iron-catalysed Fischer-Tropsch synthesis is used for the formation of organic product compounds (r_{FT}) and for the formation of CO_2 (r_{WGS}). The rate of formation of organic product compounds can be calculated from the amount of carbon monoxide being consumed and the amount of carbon dioxide

being formed. The rate of the water-gas shift reaction can be determined from the amount of carbon dioxide being formed.

$$r_{FT} = \frac{\dot{n}_{CO,feed} - \dot{n}_{CO,outlet} - (\dot{n}_{CO_2,feed} - \dot{n}_{CO_2,outlet})}{m_{unreduced\ catalyst}} \quad (2.5)$$

$$r_{WGS} = \frac{(\dot{n}_{CO_2,feed} - \dot{n}_{CO_2,outlet})}{m_{unreduced\ catalyst}} \quad (2.6)$$

Catalytic results are often evaluated in terms of conversion and selectivity. The conversion of the individual compounds, H_2 and CO, can be defined as:

$$X_i = \frac{(\dot{n}_{i,feed} - \dot{n}_{i,feed})}{\dot{n}_{i,feed}} \quad (2.7)$$

The synthesis gas conversion is defined as the amount of CO plus H_2 being converted:

$$X_{synthesis\ gas} = \frac{(\dot{n}_{CO,feed} + \dot{n}_{H_2,feed} - \dot{n}_{CO,outlet} - \dot{n}_{H_2,outlet})}{\dot{n}_{CO,feed} + \dot{n}_{H_2,feed}} \quad (2.8)$$

The usage ratio of hydrogen to carbon monoxide is defined as the amount of hydrogen being consumed relative to the amount of carbon monoxide being consumed:

$$usage\ ratio = \frac{(\dot{n}_{H_2,feed} - \dot{n}_{H_2,outlet})}{\dot{n}_{CO,feed} - \dot{n}_{CO,outlet}} \quad (2.9)$$

The selectivity for a compound can principally be defined as the amount of that compound formed relative to the amount of carbon monoxide being converted. It is often more useful to define the selectivity for a certain product as the amount of this product formed relative to the amount of carbon monoxide consumed for the formation of organic product compounds.

$$S_i = \frac{\dot{n}_i}{\dot{n}_{CO,feed} - \dot{n}_{CO,outlet} + \dot{n}_{CO_2,feed} - \dot{n}_{CO_2,outlet}} \quad (2.10)$$

In the Fischer-Tropsch synthesis, methane selectivity is often recorded as a measure for chain growth and economic viability. The methane selectivity in this study cannot be determined accurately, since the feed contains a large amount of methane (see Chapter 2.6). The accurate rate of formation of methane, which requires the subtraction of the molar feed rate of methane from the molar flow rate of methane leaving the reactor, is therefore not possible.

As selectivity characteristics ratios of molar flow rates were used (see Chapter 3).

2.6 NORMAL REACTOR OPERATION

2.6.1 Reactor Start-up

The catalyst was dried in an oven at 120 °C for 2 hours, prior to weighing and loading. This prevents inaccuracy in catalyst mass loaded due to the moisture content. The start-up slurry medium used was 350g of Sasol H2 wax flakes. After loading the wax to the reactor, the reactor temperature was raised to 150°C to melt the wax. 20 g of the dried catalyst was then slowly added to the wax. The reactor was sealed, heated to 240°C and pressurised to 20 bar using argon.

2.6.2 Catalyst Reduction

The catalyst was reduced in a hydrogen atmosphere. The reduction conditions are given in Table 2.5. Hydrogen was fed over the feed line for synthesis gas. After adjusting the hydrogen and argon flow, the stirrer speed was adjusted to 450 rpm. The reduction was carried out at 240°C and 20 bar for 16 hours. When the reduction was completed, the hydrogen flow was stopped and the stirrer speed was adjusted to 200 rpm.

Table 2.5: Reduction conditions of the iron-based Fischer-Tropsch catalyst in this study

Catalyst mass, g	20
Reduction unit	CSTR
Reduction temperature, °C	240
Reduction pressure, bar	20
H_2-flow rate (ml (NTP)/(g min)	100
Ar-flow rate (ml (NTP)/(g min)	10
Stirrer speed, rpm	450

2.6.3 Synthesis Conditions

The standard synthesis conditions for the Fischer-Tropsch synthesis are given in Table 2.6. The synthesis gas feed line was opened and the flow rate adjusted to the desired value. Subsequently, the stirrer speed was slowly increased to 450 rpm. Small corrections to the system pressure were necessary as synthesis flow rates varied from the initial start-up flow rates.

Table 2.6: Standard conditions for the Fischer-Tropsch synthesis

Reactor	CSTR
H_2/CO	1.85
Flow rate synthesis gas (ml(NTP)/(g min)	930
Ar flow rate (ml(NTP)/(g min)	93
Reaction pressure, bar	20
Reaction temperature, °C	240

The feed fluctuates slightly with time, since the feed is taken from the industrial unit. The composition of the feed was checked regularly. The typical molar composition of the feed to the reactor is given in Table 2.7.

Table 2.7: Typical molar feed composition during the standard Fischer-Tropsch synthesis

H_2	CO	CH_4	N_2	CO_2	Ar[1]
0.51	0.28	0.12	0.01	0.01	0.08

[1] internal standard

Water was only added after the catalyst had been exposed to the standard conditions for ca. 100 hrs on-line. Before co-feeding started the water line was detached from the set-up and totally filled with water (by starting the pump) to ensure that air bubbles trapped in the line were removed. The line was then reattached to the set-up and the pump primed to 18 bar. The pressure was kept lower than the reactor pressure to ensure that no excess water was pumped into the reactor when the valve was opened. The water co-feeding valve was then opened slowly until the pump was under the reactor's pressure. The valve was then opened fully and the pump flow rate set to the desired value.

It was decided to keep the reactor pressure constant throughout the entire duration of a run. As a result of this the partial pressures of hydrogen and carbon monoxide in the feed decreased after water addition. The amount of water added to the reactor and the resulting inlet partial pressures are given in Table 2.8.

2.6.4 Reactor Shut-down

All the gas flows to the system except argon was terminated by closing all valves. The reactor temperature was lowered to 130°C and the pressure lowered to atmospheric. When the reactor temperature reached 130°C the stirrer was switched off. The reactor was opened while it was still hot to prevent the wax from solidifying on the internals.

The reactor bomb containing the wax and catalyst was left to cool down under argon. When the wax was totally solidified it was tipped out of the reactor bomb and the bottom part containing the catalyst was cut off and sent for analyses.

Table 2.8: Amount of liquid water fed to the reactor and the resulting inlet partial pressures to the reactor

Amount of liquid water added ml/min	$p_{H2,inlet}$ atm	$p_{CO,inlet}$ atm	$p_{CO2,inlet}$ atm	$p_{H2O,inlet}$ atm	$p_{inerts,inlet}$[1] atm	$p_{Ar,inlet}$[2] atm
0	10.2	5.6	0.2	**0.0**	2.4	1.6
0.05	9.7	5.3	0.2	**1.0**	2.3	1.5
0.10	9.3	5.1	0.1	**1.9**	2.2	1.4
0.175	8.6	4.8	0.1	**3.1**	2.0	1.3

[1]inerts in synthesis gas from plant (CH_4 and N_2);

[2]added as internal standard to the feed

3

RESULTS

3.1 CHARACTERISATION OF CATALYST PRECURSOR

3.1.1 Elemental Analysis

Elemental analyses were done on the catalyst precursor before and after calcination. Two samples were taken from each batch and they were analysed once (see Table 3.1). The potassium and sodium content of the catalyst precursor was re-calculated as K_2O and Na_2O and the silicon content as SiO_2.

Table 3.1: Elemental analysis of the catalyst precursor

Element	Units	Uncalcined			Calcined		
		1	2	Average	1	2	Average
Fe	wt.- %	52.6	53.1	52.9	57.4	58.1	57.8
Cu	g/100g Fe	4.8	5.4	5.1	4.8	5.1	4.9
K_2O	g/100g Fe	4.1	4.1	4.1	4.2	4.2	4.2
Na_2O	g/100g Fe	0.1	0.1	0.1	0.1	0.1	0.1
SiO_2	g/100g Fe	23.9	23.2	23.6	23.2	24.1	23.7

The difference in the mass of the metal and metal oxide and the total mass of the catalyst precursor must be ascribed to the elements, which were not analysed, i.e. oxygen, hydrogen (and possibly carbon). The difference is higher for the uncalcined catalyst precursor (0.30 gram per gram of uncalcined catalyst precursor) than for the calcined catalyst precursor (0.23 gram per gram of

calcined catalyst precursor). This indicates some removal of water and/or carbon dioxide during the calcination process at temperatures higher than 200°C.

The difference in catalyst precursor mass upon calcination might be ascribed solely to the presence of oxygen. It can be assumed that 1 mole of oxygen is associated with 1 mole of copper. The molar ratio of iron to oxygen can then be estimated to be equal to 1:1.3-1.4, which corresponds roughly to the presence of Fe_2O_3.

3.1.2 BET Surface Area and Pore Volume Determination

The catalyst was analysed for BET surface area and total pore volume before and after calcination (see Table 3.2). The catalyst precursor has a reasonably high surface area of 193 m^2/g, which was maintained during calcination at temperatures higher than 200°C. Similarly, the pore volume is maintained upon calcination. The obtained surface area and pore volume means that the average pore diameter in the catalyst precursor is ca. 13.6nm.

Table 3.2: BET surface area and total pore volume analysis of the catalyst precursor

Element	Units	Uncalcined	Calcined
BET Surface Area	m^2/g	192	193
Total Pore Volume	cm^3/g	0.61	0.66

3.2 SYNTHESIS RESULTS

3.2.1 Conditions in the Feed

The commercial Lurgi coal gasifiers supplied the synthesis gas, which was used as feed to the Fischer-Tropsch reactor. A molar ratio of H_2 to CO of 1.85 was targeted, but changes in conditions in the upstream plant had a slight effect on this ratio. Figure 3.1 illustrates the fluctuation in H_2/CO ratio during the runs.

When the results of the experiments are interpreted, this change in H_2/CO ratio must be considered.

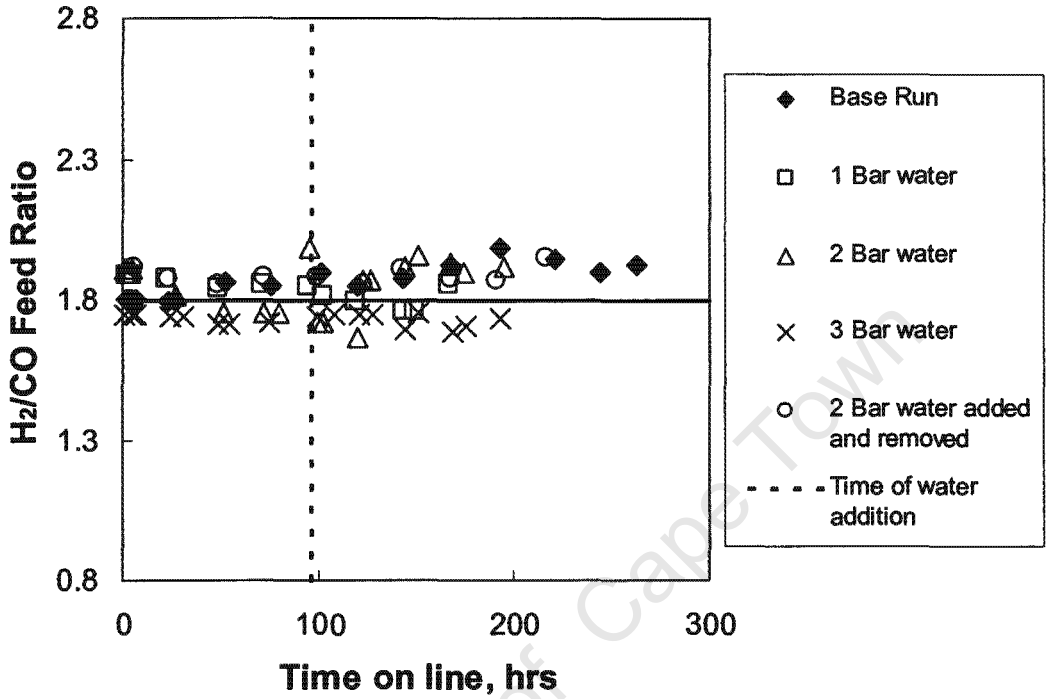

Figure 3.1: Molar H_2 to CO ratio in the feed gas as a function of time on-line for the different experiments performed (dotted line indicates the time at which co-feeding of water was started)

3.2.2 Conditions in the Reactor

The Fischer-Tropsch synthesis is at constant space velocity only affected by the partial pressures within the reactor. In this study the partial pressure of water in the feed was increased keeping the total pressure in the reactor constant. This means that the partial pressure of the components carbon monoxide and hydrogen in the feed decreased upon the addition of water to the feed (see Table 2.8).

Figure 3.2 shows the partial pressure of water in the reactor as a function of time-on-line. The initial increase in the water partial pressure over the first 48 hrs,

which could be reasonably reproduced in the various runs, is most likely caused by the change in the catalytic activity of the iron catalyst with time (a residence time effect can be excluded on the basis of the flow rate through the reactor (ca. 1020 ml(NTP)/min) and the gas volume in the reactor (ca. 350 ml) and the volume of the hot knock-out pot (500 ml)). The change in catalytic activity with time-on-line is well documented for iron-based catalysts (see e.g. Schulz *et al.*, 1990).

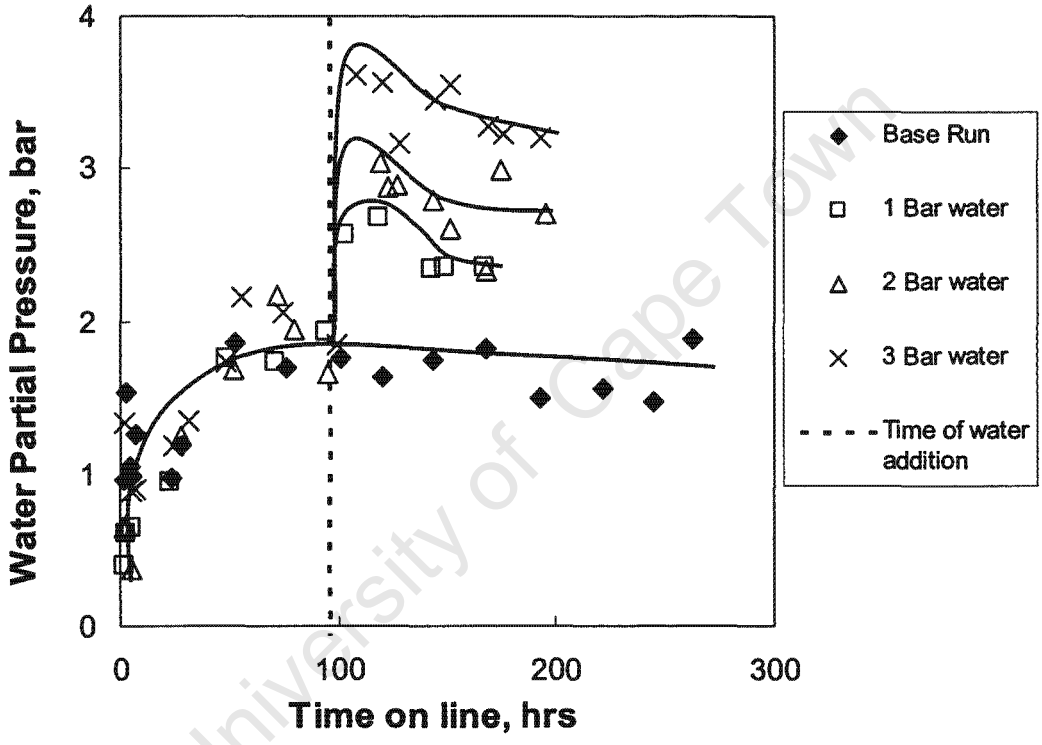

Figure 3.2: Partial pressure of water in the reactor as a function of time-on-line (dotted line: starting time of co-feeding water)

Upon the introduction of water, the water partial pressure in the reactor rises rapidly and declines with time-online, before approaching a constant value.

Although the partial pressures of hydrogen and carbon monoxide were decreased in the feed as a result of water addition, their partial pressures in the reactor were not significantly affected (see Figure 3.3 and 3.4). This might be attributed to a decrease in conversion that occurs after water addition. A

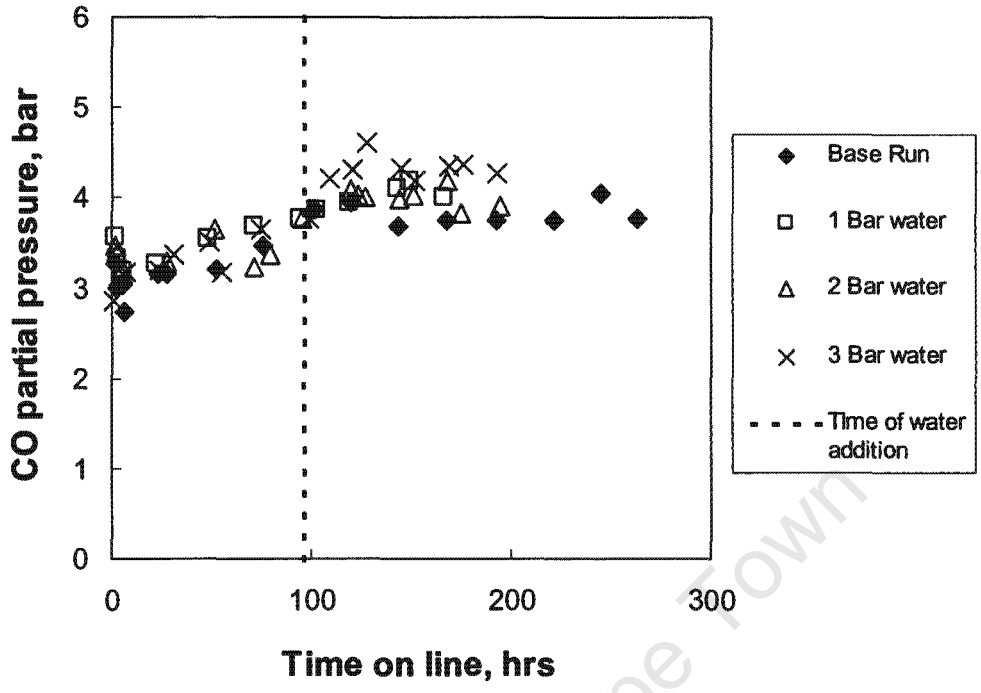

Figure 3.3: Partial pressure of carbon monoxide in the reactor as a function of time-on-line (dotted line: starting time of co-feeding water)

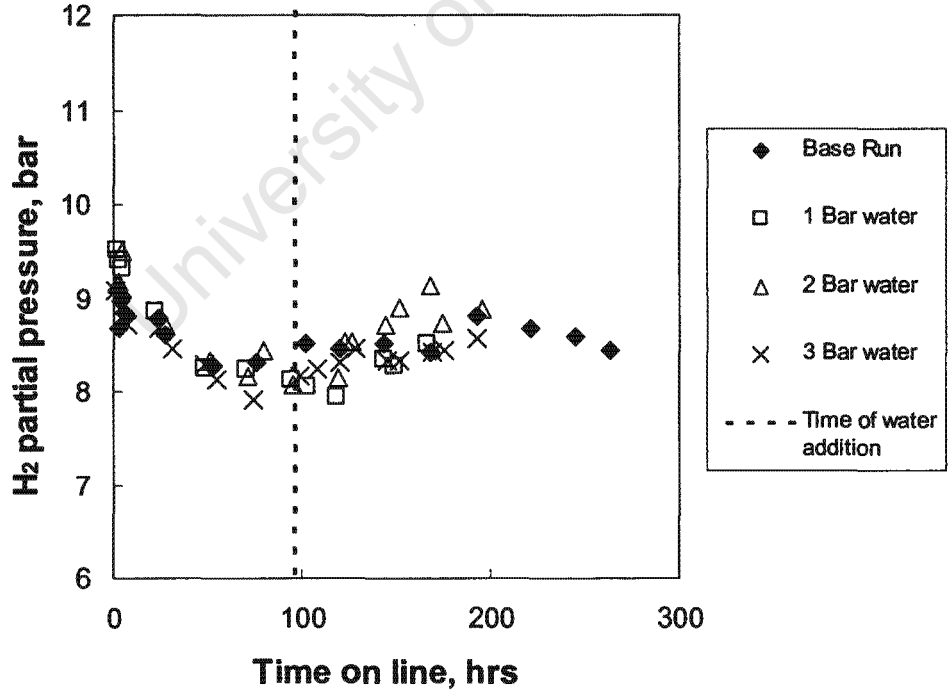

Figure 3.4: Partial pressure of hydrogen in the reactor as a function of time-on-line (dotted line: starting time of co-feeding water)

decrease in the conversion of hydrogen and carbon monoxide will lead to an increase in their partial pressures in the reactor.

3.2.3 Effect of Water Partial Pressure on Conversion

The conversion of synthesis gas, CO plus H_2, decreases upon the introduction of water into the feed (see Figure 3.5). This must be attributed to the change in the partial pressure of water in the reactor, since the partial pressure of hydrogen and carbon monoxide remain unchanged compared to the run, in which no water was added to the reactor. The decrease in the synthesis gas conversion could have been expected based on the rate expression proposed by Huff and Satterfield (1984). This rate expression predicts that the rate of hydrogen plus carbon monoxide consumption decreases upon increasing the water partial pressure.

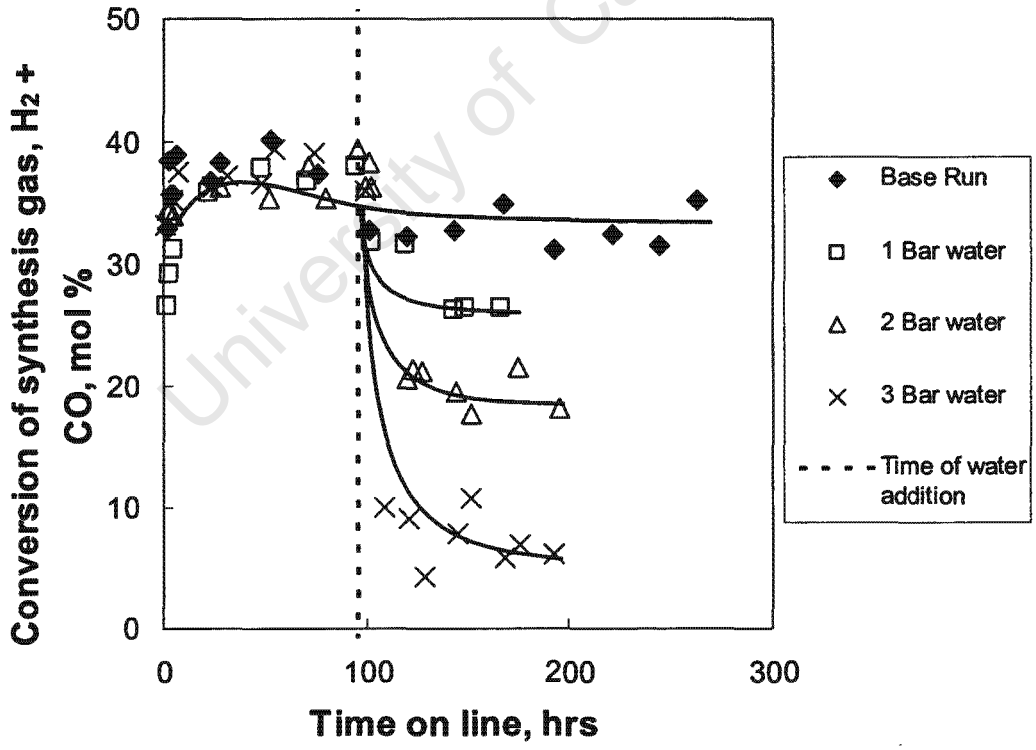

Figure 3.5: Conversion of synthesis gas as a function of time-on-line (dotted line: starting time of co-feeding water)

The usage ratio is defined as the amount of hydrogen consumed relative to the amount of carbon monoxide consumed during synthesis. The usage ratio in the Fischer-Tropsch synthesis should be between 0.67 and 2 for a feed containing no water. With time-on-line the usage ratio increases for the base run, in which no water was added (see Figure 3.6). Upon the addition of water the usage ratio decreases, which might indicate that the amount of hydrogen produced through the water gas shift reaction relative to the amount of hydrogen consumed for the formation of organic product compounds increases. The usage ratio is more severely affected by the addition of 3 bar of water to the feed than by the addition of 1 and 2 bar of water.

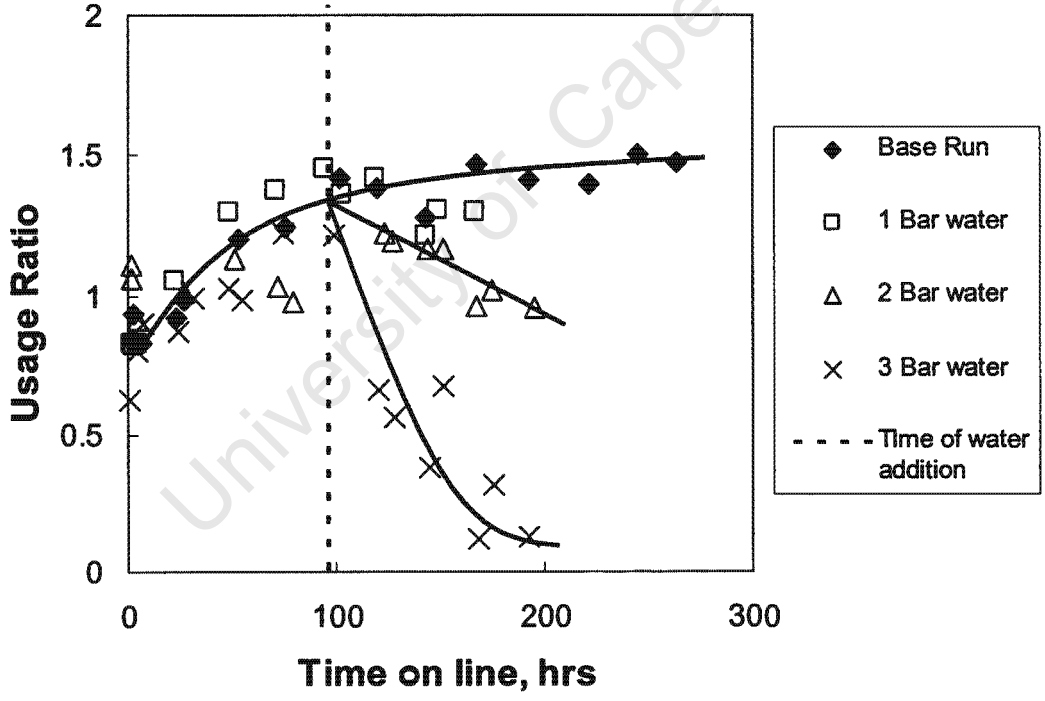

Figure 3.6: Usage ratio (amount of hydrogen consumed relative to the amount of carbon monoxide consumed) as a function of time-on-line (dotted line: starting time of co-feeding water)

Figure 3.7 shows the amount of carbon monoxide, which is consumed for the formation of carbon dioxide in relation to the amount of consumed carbon monoxide as a function of time-on-line. The fraction of carbon monoxide, which is consumed to form carbon dioxide, passes initially a maximum. This might be attributed to the change in the catalyst structure (Schulz *et al.*, 1990). Upon the introduction of water in the feed, the fraction of carbon monoxide, which is converted to carbon dioxide, increases rapidly. This indicates that the rate of the water-gas shift reaction relative to the rate of formation of organic product compounds increases.

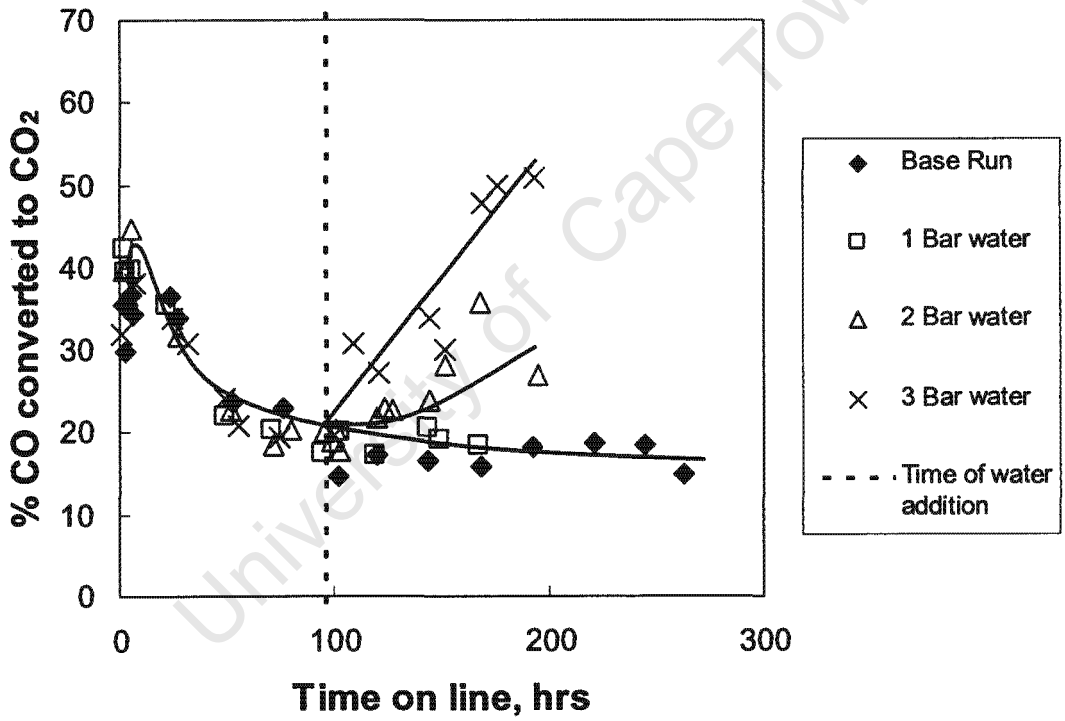

Figure 3.7: Relative amount of carbon monoxide, which is consumed for the formation of carbon dioxide in relation to the amount of consumed carbon monoxide as a function of time-on-line (dotted line: starting time of co-feeding water)

3.2.4 Effect of Water Partial Pressure on Rate of Reaction

The rate of the Fischer-Tropsch synthesis equals the rate of formation of organic product compounds on carbon basis. Initially the rate of the Fischer-Tropsch synthesis seems to pass a maximum (see Figure 3.8). Upon the introduction of water in the feed, which led to an increase in the partial pressure of water in the reactor, the rate of the Fischer-Tropsch synthesis drops rapidly. This might have been expected based on the rate expression proposed by van Steen and Schulz (1999), who predict that the rate of reaction passes a maximum with increasing partial pressure of water.

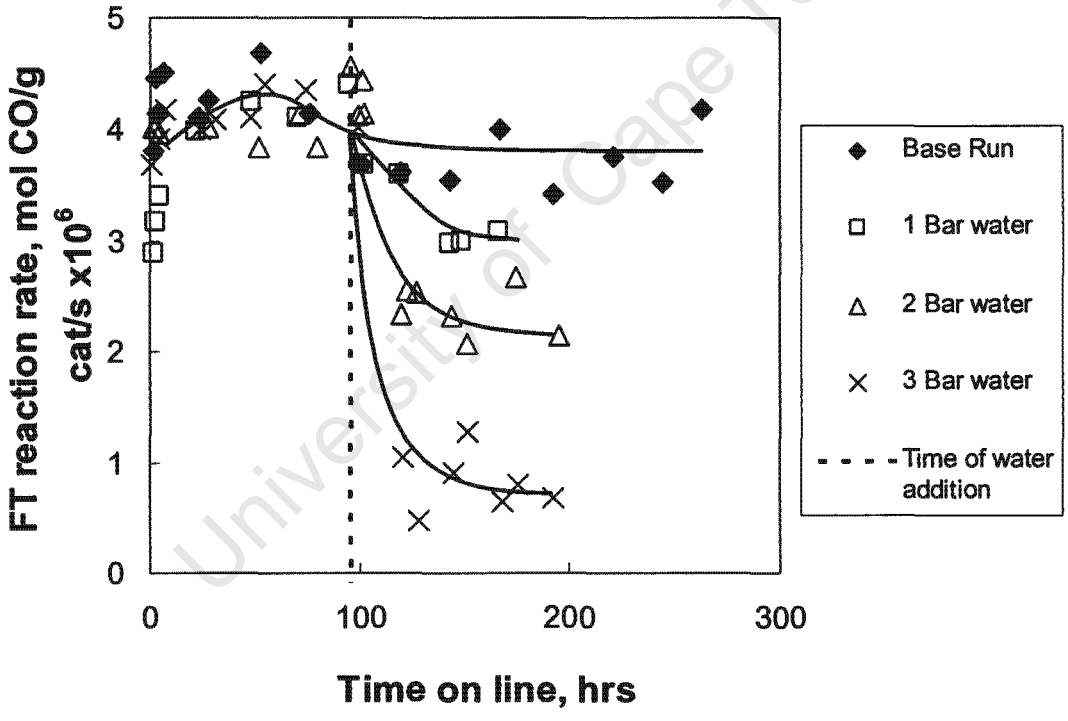

Figure 3.8: Rate of the Fischer-Tropsch synthesis (in moles of CO converted for the formation of organic product compounds /gram of unreduced catalyst/second x 10^6) as a function of time-on-line (dotted line: starting time of co-feeding water)

Only a few rate expressions have been proposed to describe the rate of CO_2-formation (rate of water-gas shift reaction) under Fischer-Tropsch conditions over a precipitated iron catalyst (see e.g. van der Laan and Beenackers, 2000).

$$r_{WGS} = \frac{k_{WGS} \cdot \left(p_{CO} \cdot p_{H_2O} - \frac{p_{CO_2} 2 \cdot p_{H_2}}{K_p} \right)}{\left(1 + K_1 \cdot p_{CO} + K_2 \cdot p_{H_2O}\right)^2} \qquad (3.1)$$

According to the rate expression for the water-gas shift reaction during the Fischer-Tropsch synthesis proposed by van der Laan and Beenackers (2000) water should inhibit the rate of the water-gas shift reaction, but this is not observed (see Figure 3.9).

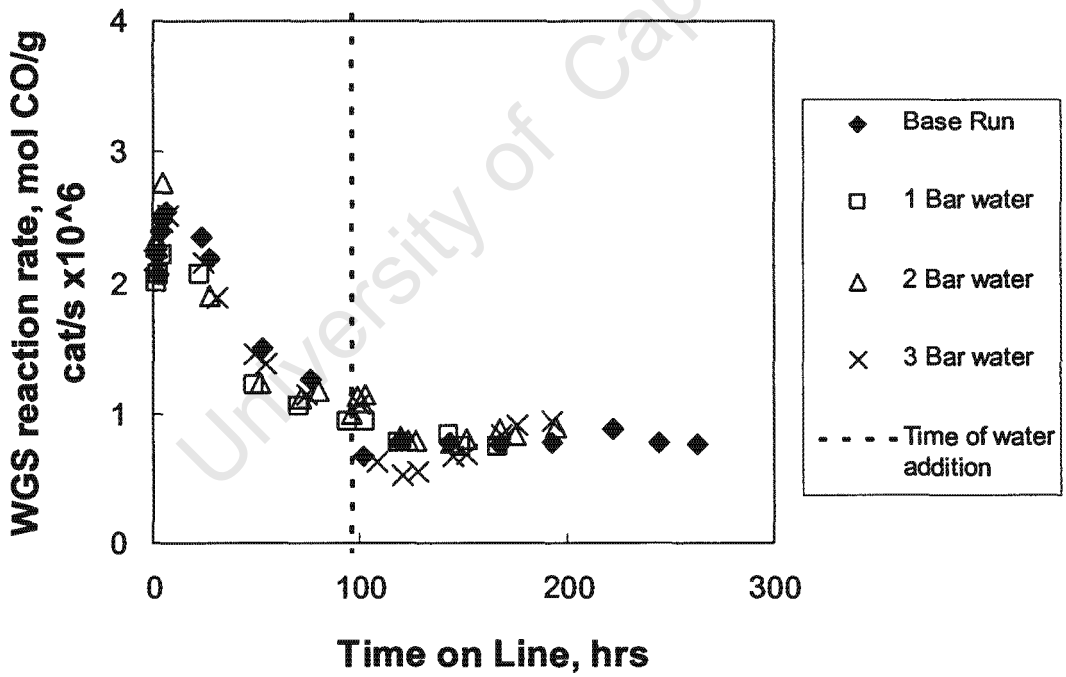

Figure 3.9: Rate of water-gas-shift reaction (moles of CO converted for the formation of carbon dioxide/gram of unreduced catalyst/second x 10^6) as a function of time-on-line (dotted line: starting time of co-feeding water)

3.2.5 Effect of Water Partial Pressure on Selectivity

3.2.5.1 Chain Growth Probability

As an initial indication of the chain growth probability, the ratio of the amount of wax collected relative to the amount of oil collected over a constant time period was evaluated. A high production of the amount of wax collected relative to the amount of oil collected indicates a high chain growth probability. Figure 3.10 shows the ratio of the production rate of wax relative to the production rate of oil as a function of time-on-line for the various runs. Water affects the wax production relative to the oil production negatively. Thus, the chain growth probability is expected to decrease as well upon introduction of water in the feed.

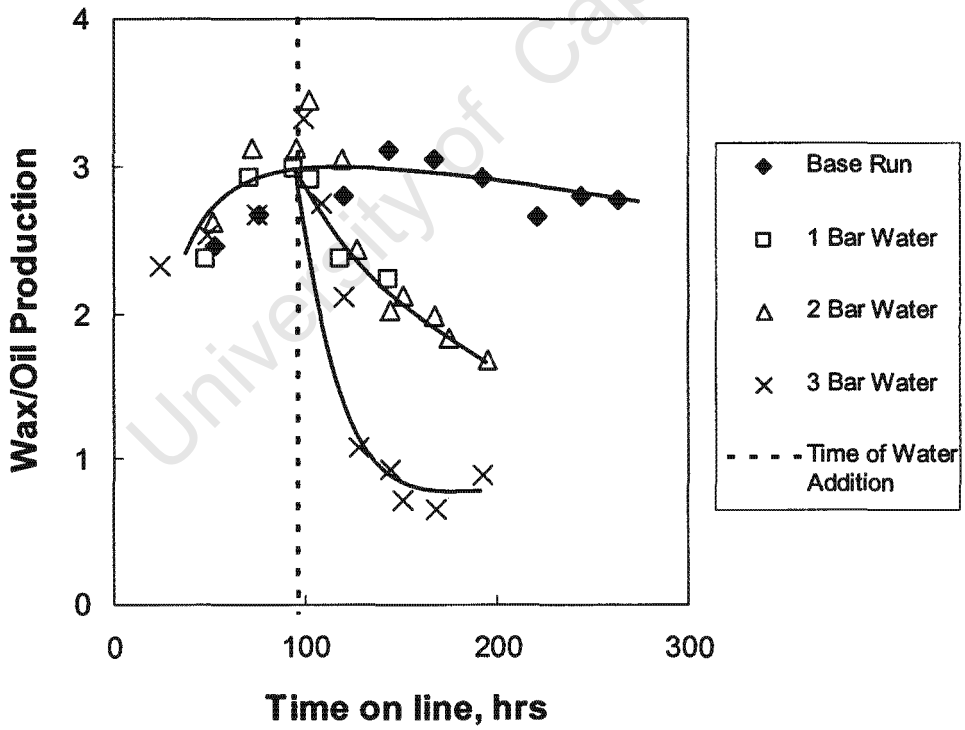

Figure 3.10: Rate of wax production relative to the rate of oil production as a function of time-on-line (dotted line: starting time of co-feeding water)

The decrease in the rate of wax production relative to the rate oil production is also not sudden, but rather a gradual decrease over a 100 hour period. With the addition of 3 bar water to the feed the decrease in production rate of wax relative to the production rate of oil was more severe than with 1 and 2 bar water addition. The organic product compounds follow the Anderson-Schulz-Flory distribution. A typical distribution of the hydrocarbon products in the hot tail gas stream between C_4 and C_{10} is shown in Figure 3.11. It can be seen that the hydrocarbon distribution in this range can be reasonably well described with a single chain growth probability.

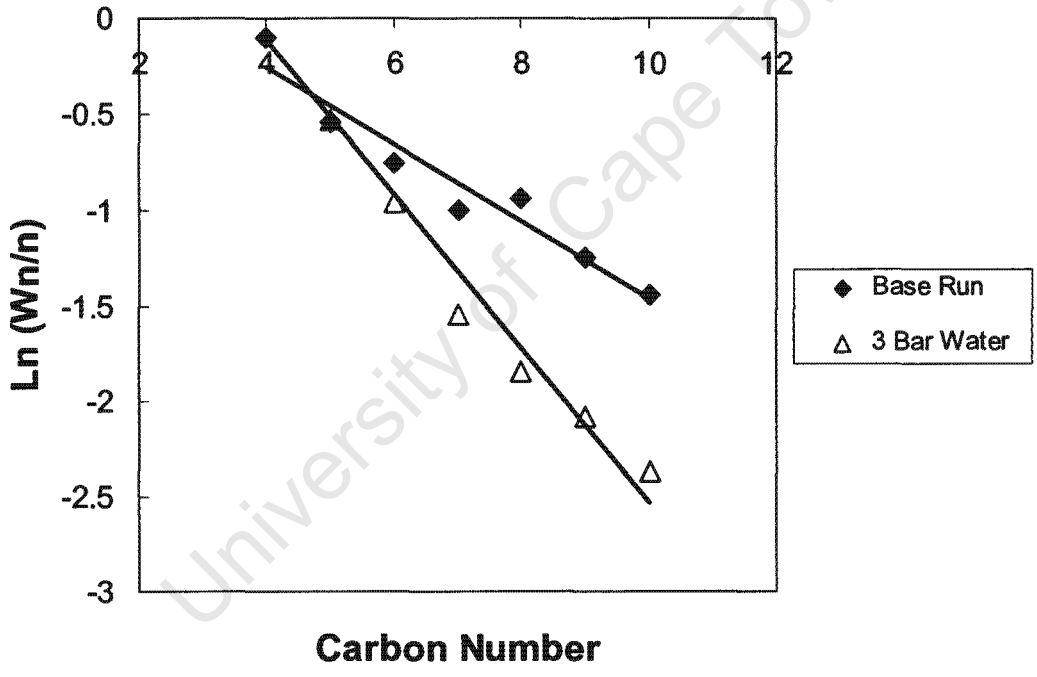

Figure 3.11: Anderson-Schulz-Flory plot for the products between C_4 and C_{10} in the hot tail gas for the base case and 3 bar water addition after 170 hrs on-line

Figure 3.12 shows the chain growth probability (α) as determined from the Anderson-Schulz-Flory plot for the products between C_4 and C_{10} in the hot tail gas as a function of time-on-line. The observed chain growth probability

increases with increasing time-on-line (a similar increase was observed for the rate of wax production relative to the rate of oil production). This might be caused by the slow saturation of the wax with olefins, which can be re-incorporated leading to higher, observed chain growth probabilities (Schulz and Claeys, 1999a).

The addition of 1 bar water to the feed did not have a significant effect on the chain growth probability. This is seemingly in contradiction to the observed decrease in the rate of wax production relative to the rate of oil production upon the addition of 1 bar of water. It must, however, be kept in mind that the chain growth probability is typically not a constant, but increases with increasing carbon number (typically beyond the carbon numbers from which in this study the chain growth probability was determined). Although the chain growth probability in the range C_4-C_{10} seems hardly affected, the chain growth probability at higher carbon numbers might still be affected.

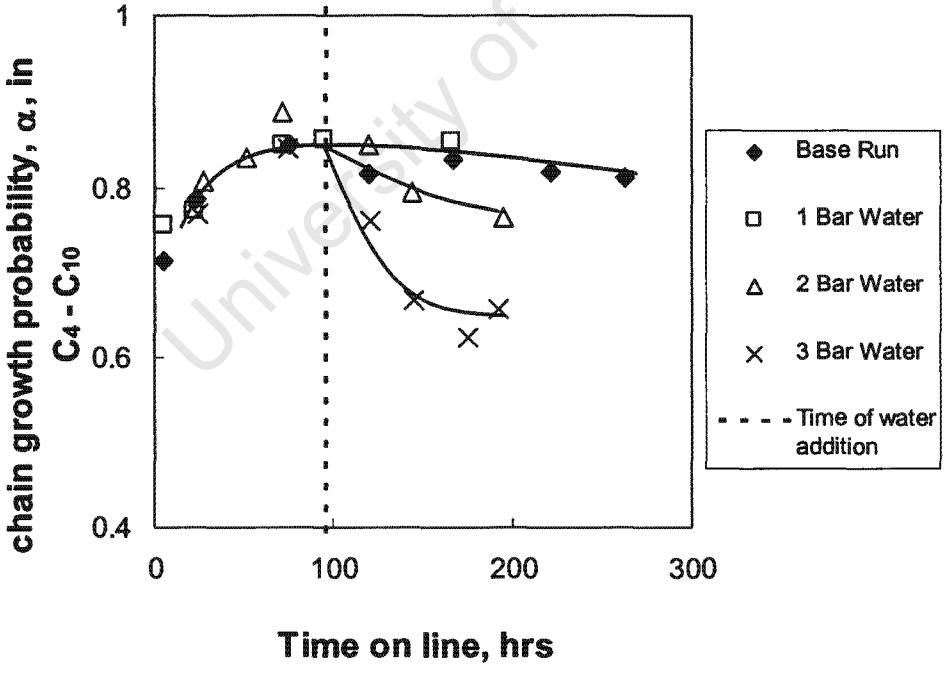

Figure 3.12: Chain growth probability in the range C_4-C_{10} determined from the product analysis of the hot tail gas as a function of time-on-line (dotted line: starting time of co-feeding water)

The addition of 2 bar and 3 bar of water did yield a significant decrease in the chain growth probability in the range of C_4-C_{10} as was already indicated by the decline in the ratio of the wax production rate relative to the oil production rate. The decrease in the chain growth probability was gradual over 100 hours as opposed to a step change immediately after water addition. The findings from the hot tail gas analysis thus correspond to the results from the wax/oil production.

3.2.5.2 Secondary Hydrogenation

Both olefins and paraffins are thought to be primary products of the Fischer-Tropsch synthesis (Schulz and Gökcebay, 1984b). However, olefinic product compounds can undergo secondary hydrogenation yielding n-paraffins. The mol fraction of the n-paraffin in the fraction of linear hydrocarbons is therefore an indication of the extent of secondary hydrogenation taking place in the reaction system. It has been assumed that the primary Fischer-Tropsch product contains ca 20% n-paraffins in the fraction of linear hydrocarbons (Schulz and Gökcebay, 1984b).

The effect of water partial pressure on the molar fraction of the n-paraffin in the fraction of linear hydrocarbons in a carbon number fraction was examined for C_3, C_{10} and C_{14}. The paraffin fraction in C_3 and n-C_{10} was obtained from FID analyses on the hot tail gas, whereas the paraffin fraction in n-C_{14} was obtained from a GC analysis on the oil fraction. n-C_{14} was chosen because it is the highest in the oil fraction for which the GC analyses still accurately detects both the linear olefins and paraffins.

Figure 3.13 shows the paraffin content in the C_3-fraction as a function of time-on-line. Propene is rather much less reactive than ethene under typical Fischer-Tropsch conditions (Schulz and Claeys, 1999b). The propane content in the fraction of C_3-hydrocarbons is typically a good indicator for the effect on primary olefin selectivity in the Fischer-Tropsch synthesis. With increasing time-on-line

the paraffin content in the fraction of C_3-hydrocarbons decreases slightly. After ca. 100 hrs on-line a paraffin content of ca. 20% is obtained indicating primary selectivity (Schulz and Gökcebay, 1984b).

Increasing the water partial pressure in the feed (and thus in the reactor) does not seem to affect the paraffin content in the fraction of C_3-hydrocarbons indicating that water does not affect primary olefin selectivity in the Fischer-Tropsch synthesis.

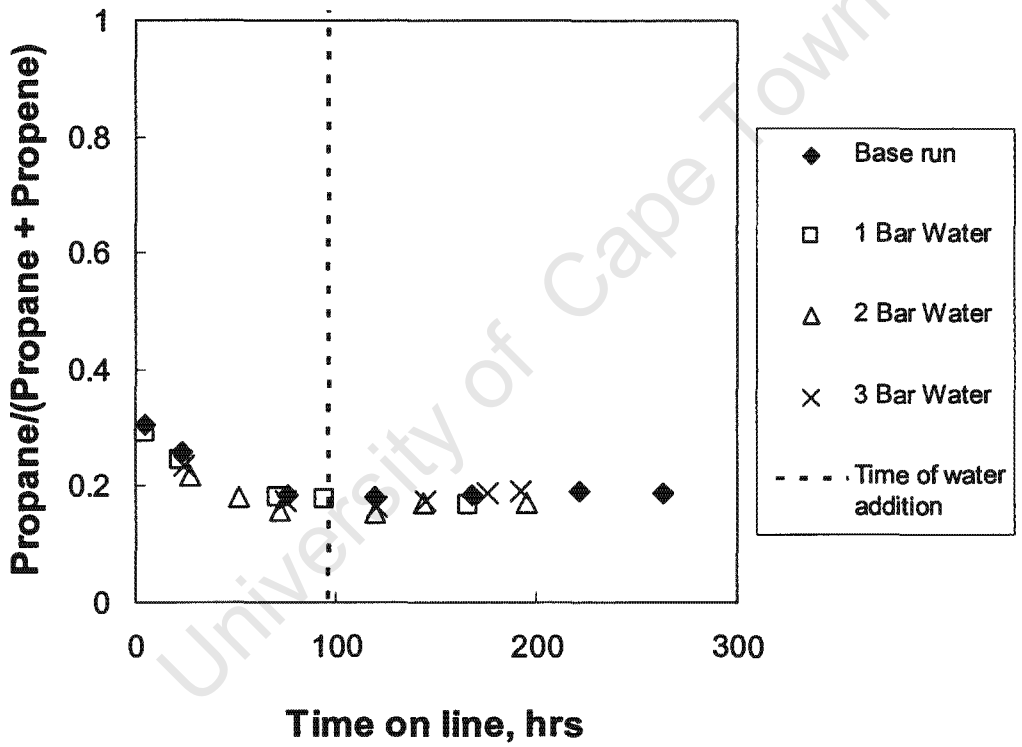

Figure 3.13: Paraffin content in the fraction of C_3-hydrocarbons in the hot tail gas as a function of time-on-line (dotted line: starting time of co-feeding water)

Figures 3.14 and 3.15 show the paraffin content in the fraction of linear C_{10}- and C_{14}-hydrocarbons, respectively. The paraffin content in the fraction of linear hydrocarbons increases with increasing carbon number. This can be ascribed to

the increase in the extent of secondary olefin reactions with increasing carbon number, which might be caused due to the increased solubility of the olefins with increasing carbon number (Schulz and Claeys, 1999a; 1999b). With increasing time-on-line the paraffin content in the fraction of the linear C_{10}- and C_{14}-hydrocarbons decreases indicating a decrease in the extent of secondary olefin hydrogenation. The paraffin content in the fraction of linear C_{14}-hydrocarbons decreases over a pro-longed time and a steady value was not obtained.

Upon the introduction of water in the feed, the paraffin content in the fraction of linear hydrocarbons decreases. This implies that water reduces the extent of

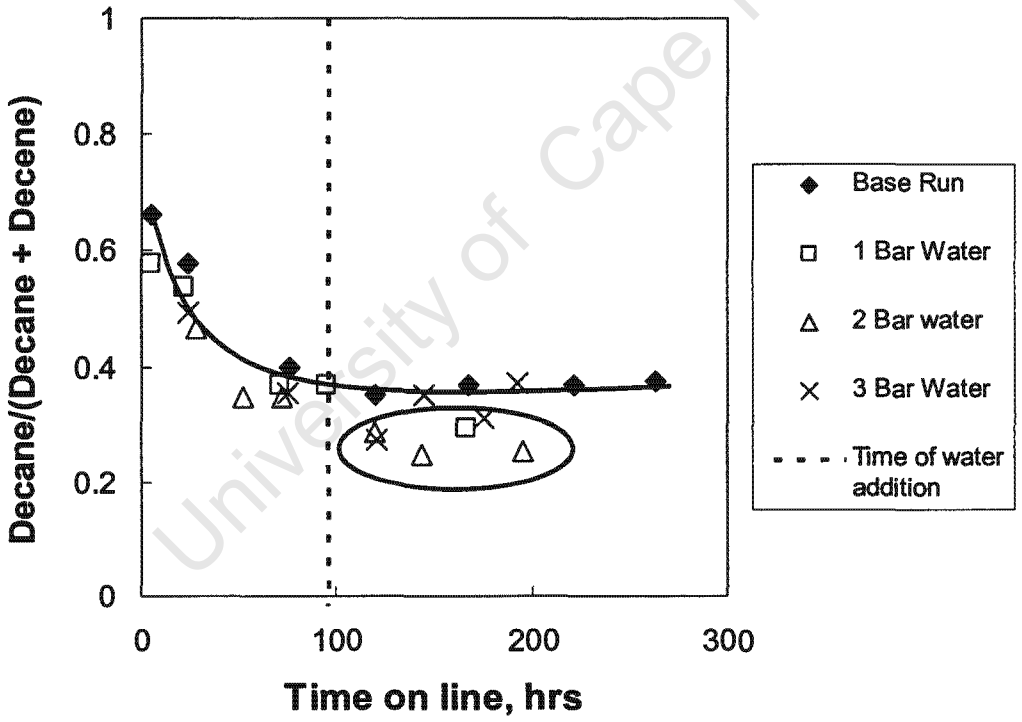

Figure 3.14: Paraffin content in the fraction of C_{10}-hydrocarbons in the hot tail gas as a function of time-on-line (dotted line: starting time of co-feeding water)

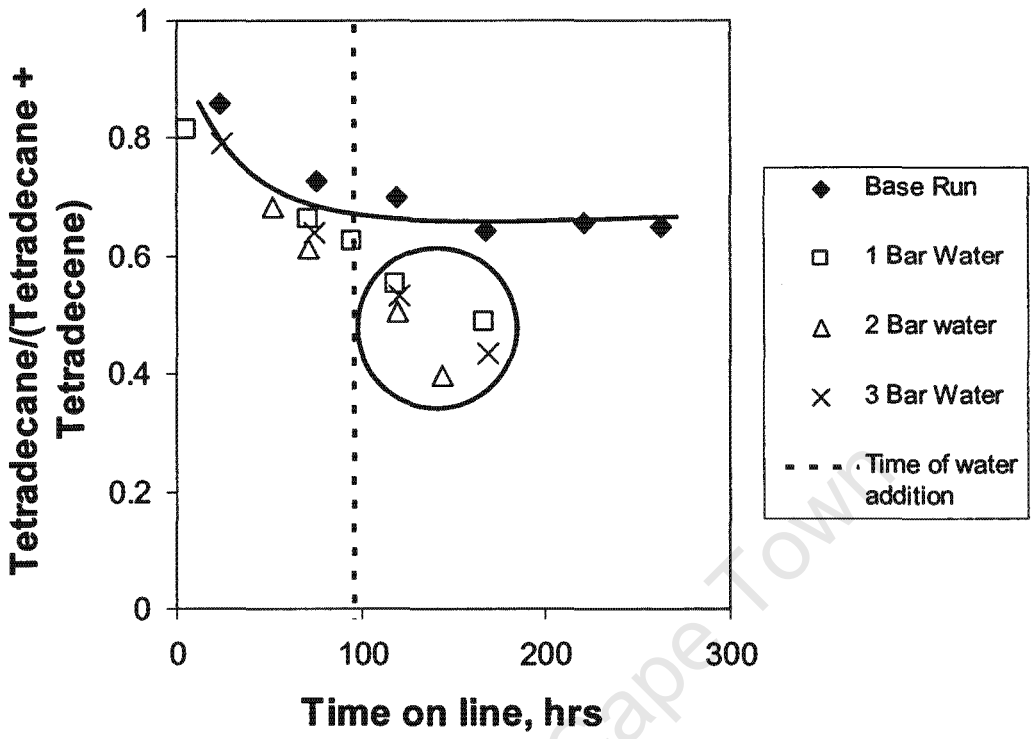

Figure 3.15: Paraffin content in the fraction of C_{14}-hydrocarbons in the oil fraction as a function of time-on-line (dotted line: starting time of co-feeding water)

secondary hydrogenation. A systematic decrease in the paraffin content can however not be detected. This might indicate that the observed effect is not a direct kinetic effect, but might be related to changes in the catalyst.

3.2.5.3 Double bond Isomerisation

Double bond isomers of α-olefins are generally considered to be secondary products in the Fischer-Tropsch synthesis (Schulz and Gökcebay, 1984b). However, data published by Bukur et al. (1990) imply that a small fraction of internal olefins might be formed primarily. The molar ratio of the amount of n-olefins with an internal double bond relative to the total amount of linear olefins within a carbon number fraction is a good indicator for the extent of the double

bond isomerisation (Schulz and Gökcebay, 1984b). The extent of the double bond isomerisation was investigated for C_5, C_{10} and C_{14}.

In all investigated carbon number fractions, the mol fraction of olefins with an internal double bond relative all linear olefins in a carbon number fraction passes a minimum with time-on-line (see Figures 3.16,3.17 and 3.18). Furthermore, it can be noted that the fraction of olefins with an internal double bond increases with increasing carbon number. This can be ascribed to the increase in the extent of secondary olefin reactions with increasing carbon number, which might be caused due to increased residence time of the olefins with increasing carbon number due to increased solubility (Schulz and Claeys, 1999a; 1999b).

The addition of water to the feed yields a strong decline in the content of olefins with an internal double bond in the fraction of linear hydrocarbons implying an inhibition of the secondary double bond isomerisation by water. With the addition of 2 and 3 bar of water to the feed the levels of internal olefins were mostly too low for the FID analysis of the hot tail gas to be able to detect. The GC analyses on the oil fraction show a clear decrease in internal olefins with water addition. The severity of decrease does however not seem to change with an increase in water co-feeding.

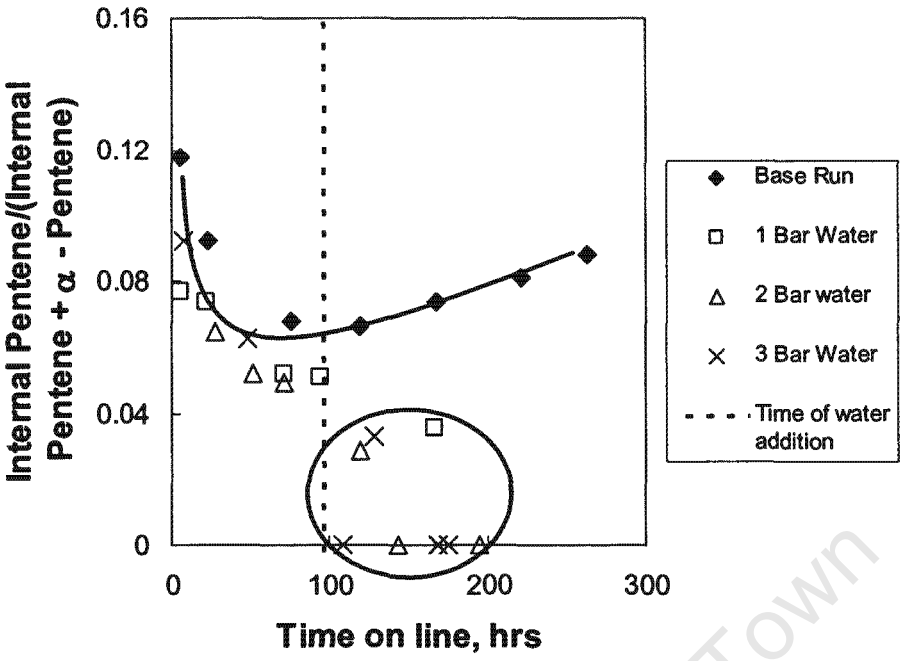

Figure 3.16: Molar ratio of the internal olefins relative to all linear olefins in C_5 in the hot tail gas as a function of time-on-line (dotted line: starting time of co-feeding water)

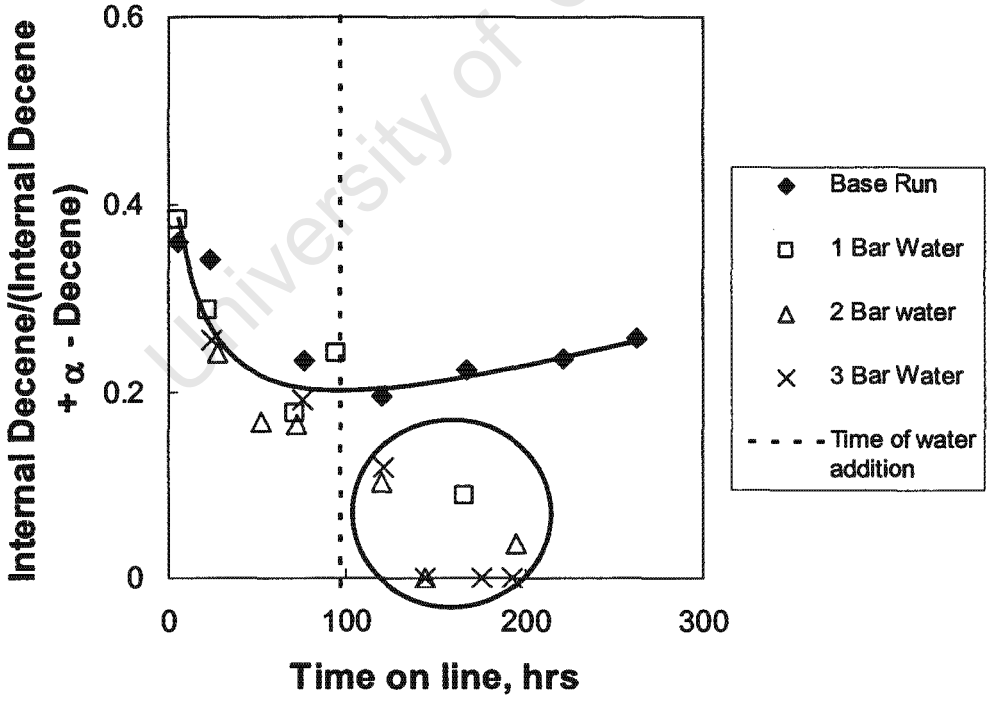

Figure 3.17: Molar ratio of the internal olefins relative to all linear olefins in C_{10} in the hot tail gas as a function of time-on-line (dotted line: starting time of co-feeding water)

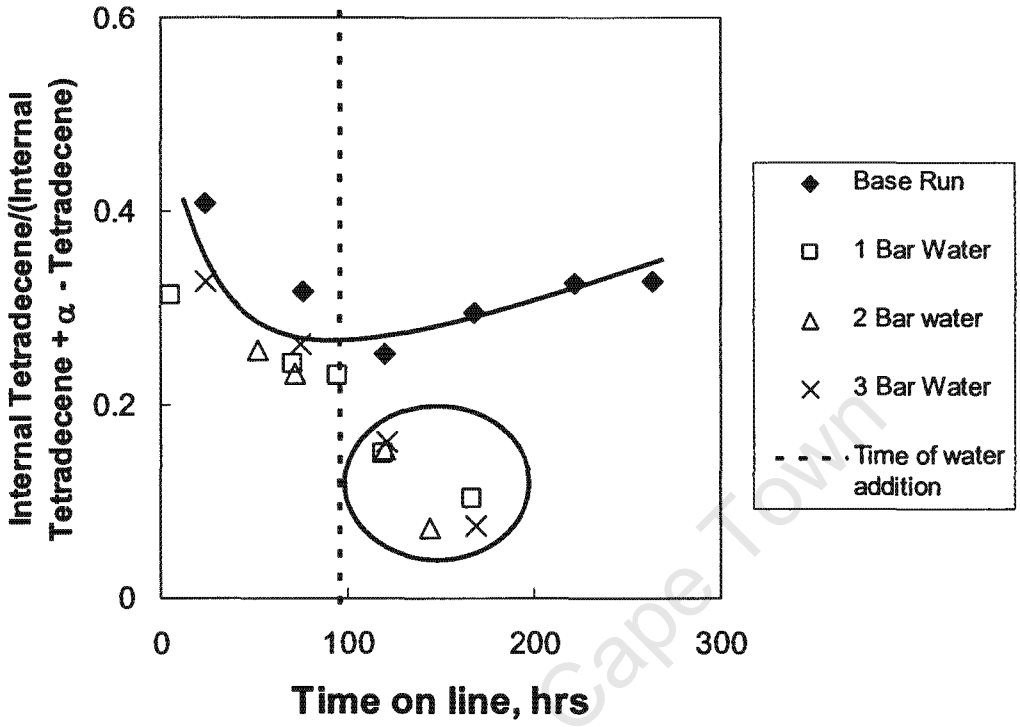

Figure 3.18: Molar ratio of the internal olefins relative to all linear olefins in C_{14} in the hot tail gas as a function of time-on-line (dotted line: starting time of co-feeding water)

3.2.5.4 Alcohol Selectivity

Alcohols form typically a minor part in the product of the Fischer-Tropsch synthesis. The methanol and ethanol peaks of the FID analyses on the hot tail were clearly distinguishable and were therefore used to evaluate alcohol selectivity. In addition tetradecanol selectivity was evaluated in the oil fraction. Figure 3.19 shows the methanol selectivity as a function of time-on-line. It is clear that water addition has a positive effect on methanol selectivity. This effect is also more predominant when the partial pressure of water in the feed (and thus in the reactor) is higher. Adding 3 bar of water to the feed yields the highest methanol selectivity. Again, the increase in methanol selectivity is not instantaneous, but shows rather a gradual increase over a prolonged period of ca. 100 hours.

The ethanol selectivity is within the error of measurement not affected by water co-feeding at all (see Figure 3.20).

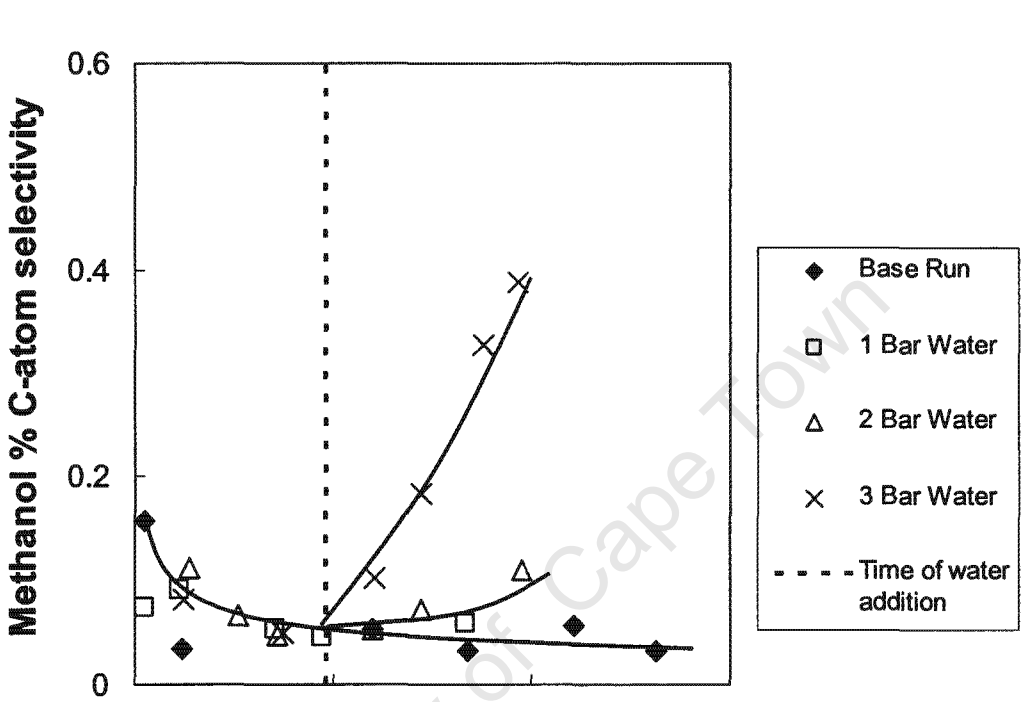

Figure 3.19: Methanol % C-atom selectivity (with regard to CO converted to all products excluding CO_2) as a function of time-on-line (dotted line: starting time of co-feeding water)

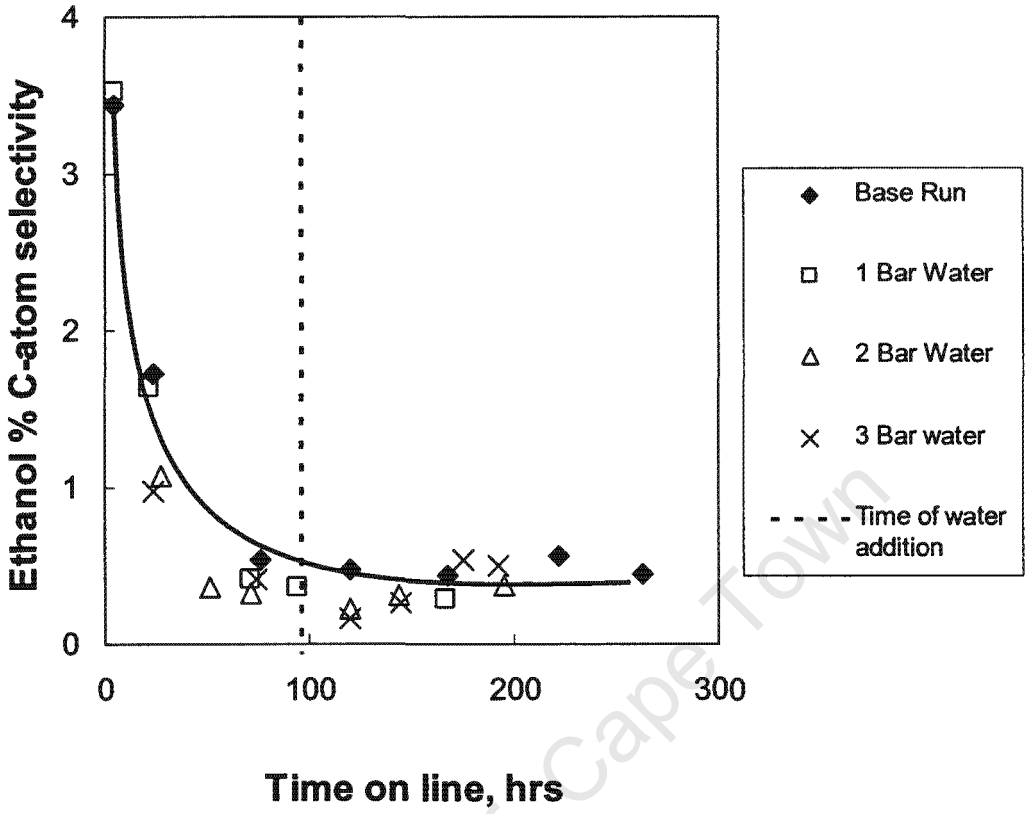

Figure 3.20: Ethanol % C-atom selectivity (with regard to CO converted to all products excluding CO_2) as a function of time-on-line (dotted line: starting time of co-feeding water)

For the oil fraction the content of tetradecanol in the fraction of the C_{14} organic product compounds hydrocarbon product is shown in Figure 3.21. As with methanol selectivity the tetradecanol content increases with an increase in water partial pressure.

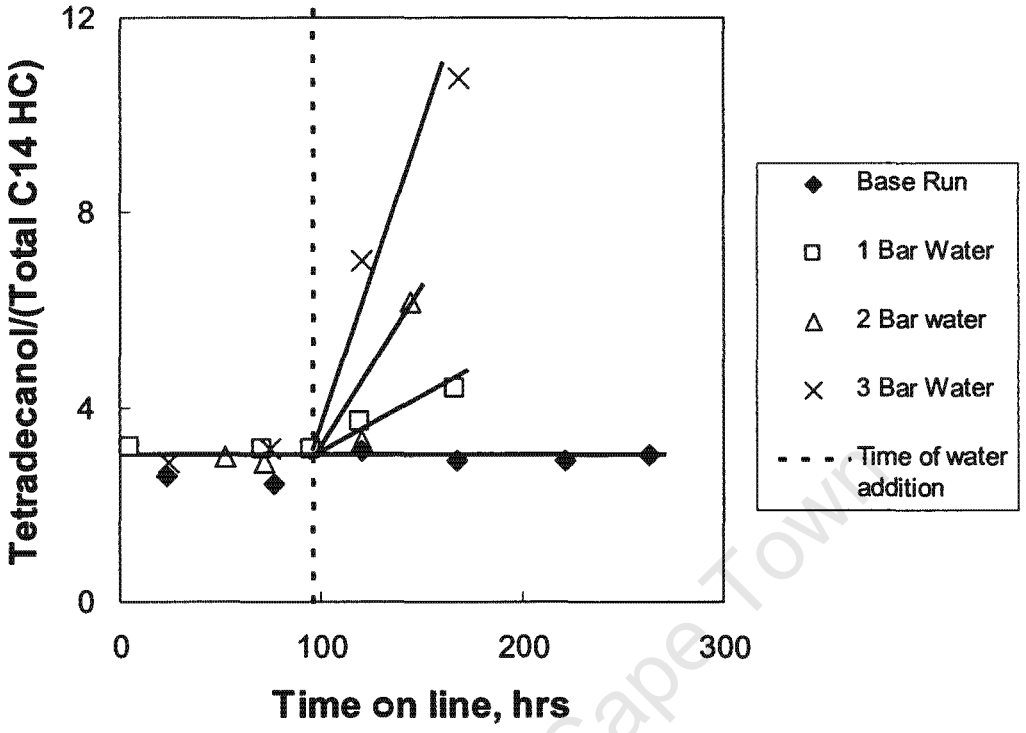

Figure 3.21: Mass ratio of tetradecanol relative to all hydrocarbons in C_{14} in the oil fraction as a function of time-on-line (dotted line: starting time of co-feeding water)

3.2.6 Reversibility of the Effects of Water Addition

It is of fundamental and economic importance whether removing the water from the feed can reverse the observed effects of the added water to the feed on the catalyst activity. In order to test whether the observed effects can be reversed, a run was performed, in which after 96 hrs on-line 2 bar of water was added to the feed. The co-feeding of water was stopped at 170 hours on-line.

The effect on co-feeding and stopping water on the water partial pressure in the reactor can be seen in Figure 3.22. Co-feeding water yields a strong increase in the partial pressure of water (this results reproduces the original experiment, in which 2 bar of water was added to the feed – see Chapter 3.2.2). Upon removal

of water from the feed the partial pressure of water drops to a value slightly lower than was obtained in the base case.

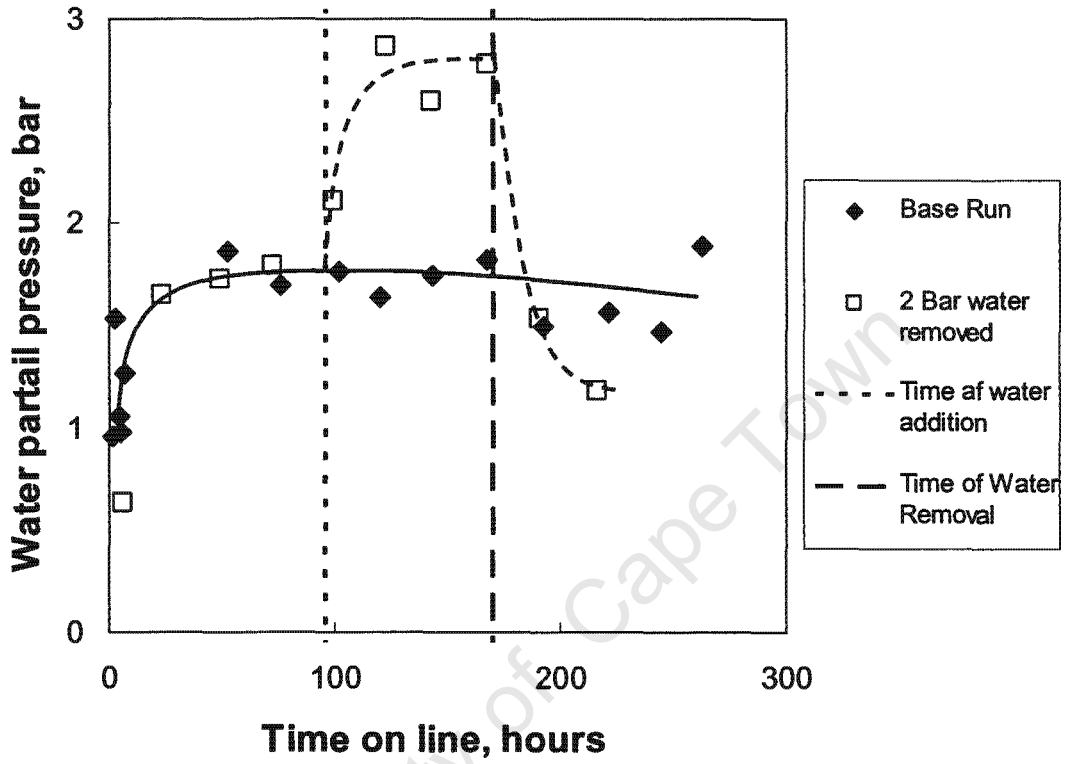

Figure 3.22: Water partial pressure in the reactor as a function of time on-line (dotted line: starting time and end-time of co-feeding water)

Figure 3.23 shows the effect of water addition to the feed and water removal from the feed on the synthesis gas (H_2+CO) conversion. Upon addition of 2 bar of water to the feed the synthesis gas conversion drops to ca. 20%. This was also observed in the previous experiment, in which 2 bar of water was added to the feed (see Figure 3.5). A recovery in the synthesis gas conversion is observed upon removal of water from the feed. The few data points collected in this study do not allow a firm conclusion on whether a full recovery is obtained or whether the conversion after the removal of water from the feed is slightly less. To observe this better the experiment should have been carried out for a longer time-on-line.

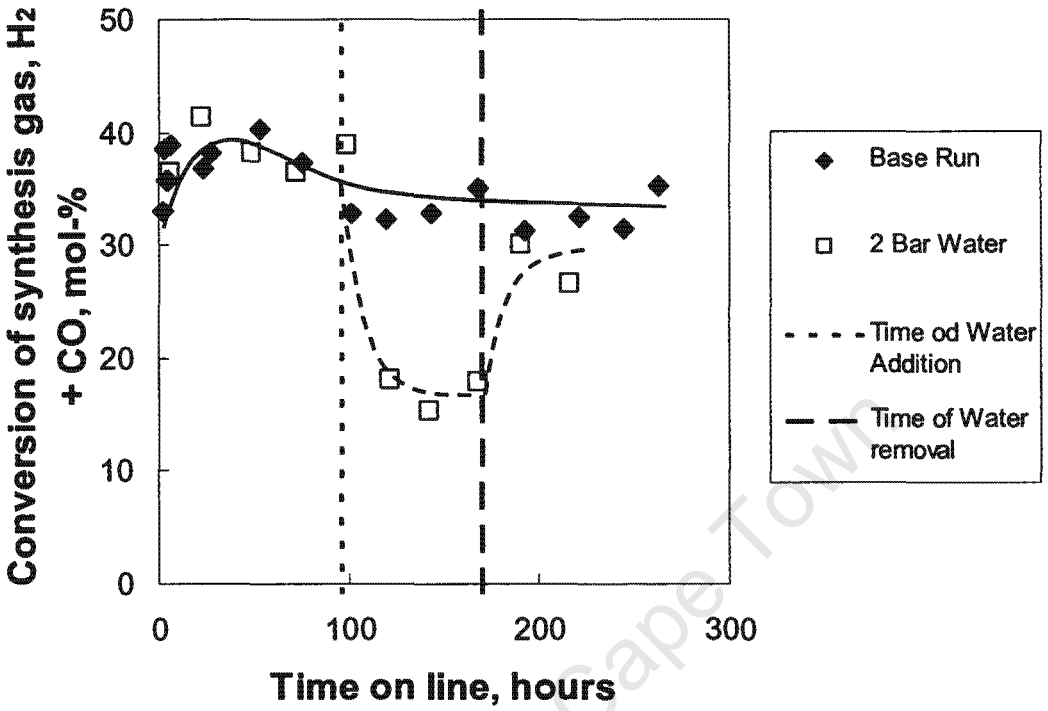

Figure 3.23: Conversion of synthesis gas as a function of time on-line (dotted line: starting time and end-time of co-feeding water)

Figure 3.24 shows the effect of water addition to the feed and water removal from the feed on the rate of formation of organic product compounds on carbon basis (rate of Fischer-Tropsch synthesis). Upon addition of 2 bar of water to the feed the rate of the Fischer-Tropsch synthesis and synthesis gas conversion drops by ca. 55%. This was also observed in the previous experiment, in which 2 bar of water was added to the feed (see Figure 3.8). A recovery in the rate of the Fischer-Tropsch synthesis is observed.

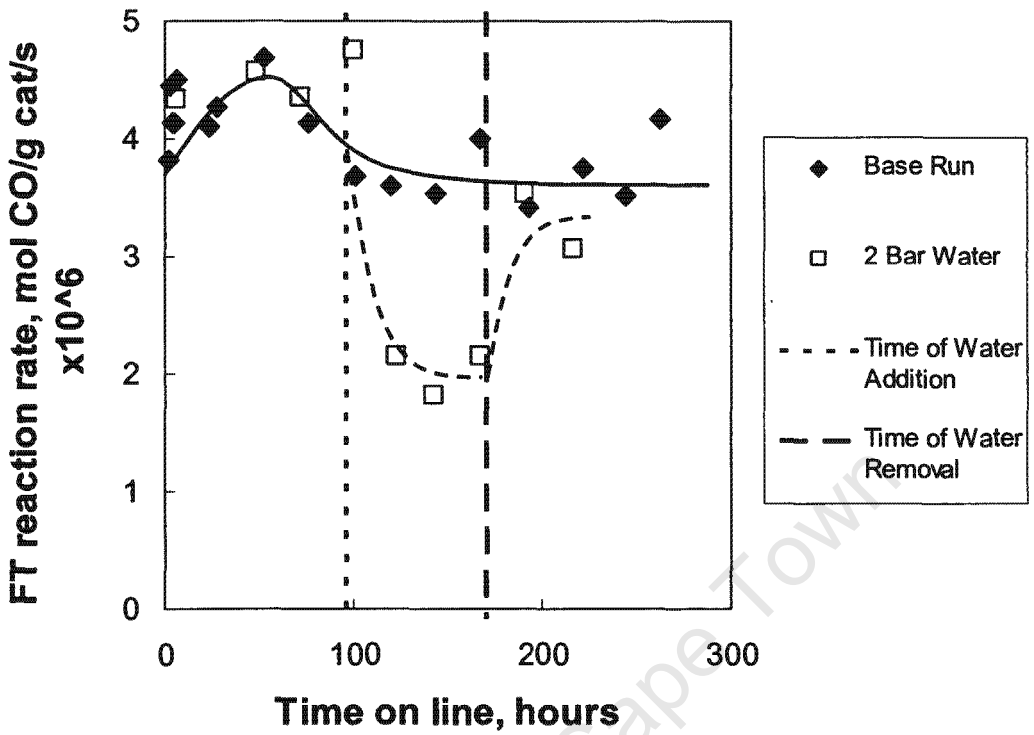

Figure 3.24: The rate of the Fischer-Tropsch synthesis (moles of CO converted for the formation of organic product compounds/gram of unreduced catalyst/second x 10^6) as a function of time on-line (dotted line: starting time and end-time of co-feeding water)

It is evident from Figures 3.23 and 3.24 that the effect of 2 bar water co-feeding on the FT reaction rate and synthesis gas conversion is reversible upon removal of water.

3.3 CHARACTERISATION OF SPENT CATALYST

3.3.1 Mössbauer Analyses

The Mössbauer spectra of the catalysts with various water co-feedings are presented in Figure 3.25. The hyperfine interaction parameters obtained from the deconvolution of the spectra are tabulated in Table 3.3.

The results obtained for all the catalysts indicate the presence of ε-Fe_2C and some unidentified Fe^{2+} and Fe^{3+} species. Fe_3O_4 was also identified for the catalysts exposed to a feed containing a water partial pressures exceeding 1 bar. The iron carbide identified for these catalysts is the transition phase between (hcp) ε'-$Fe_{2.2}C$ (hcp→ monoclinic) and (monoclinic) χ-$Fe_{2.5}C$. The Mössbauer adsorption spectra of both ε'-$Fe_{2.2}C$ and χ-$Fe_{2.5}C$ reveal the presence of three inequivalent magnetic Fe sites with almost similar hyperfine interaction parameters. Hence the type of iron carbide formed was confirmed by XRD technique (see chapter 3.3.2).

The Fe^{2+} and Fe^{3+} species observed in all the catalysts could be small crystallites of any of the iron phases present in these samples or Fe^{3+} inherent from the starting material. The total contribution of these small iron crystallites decreases with the increase in the water partial pressure.

In general all the catalysts show ε-Fe_2C as a major phase (>44%) for all catalysts exposed to a feed with a water partial pressures of up to 2 bar. The fact that the amount of this phase remained almost constant whilst that of Fe^{3+} decreased with the appearance of Fe_3O_4 at 2 bar, implies that there was no re-oxidation of bulk iron carbides using a feed containing 2 bar of water, instead the Fe^{3+} species were converted to magnetite. Removal of the water from the feed after three days of run had no effect on the extent of re-oxidation of this catalyst.

In the catalyst exposed to a feed with a water partial pressures of 3 bar, Fe^{3+} was further converted whilst about 50% of ε-Fe_2C was re-oxidized to Fe_3O_4 as evidenced by a decrease in both the amounts of Fe^{3+} and ε-Fe_2C with an increase in the amount of Fe_3O_4. The Fe^{2+} remained constant throughout the runs.

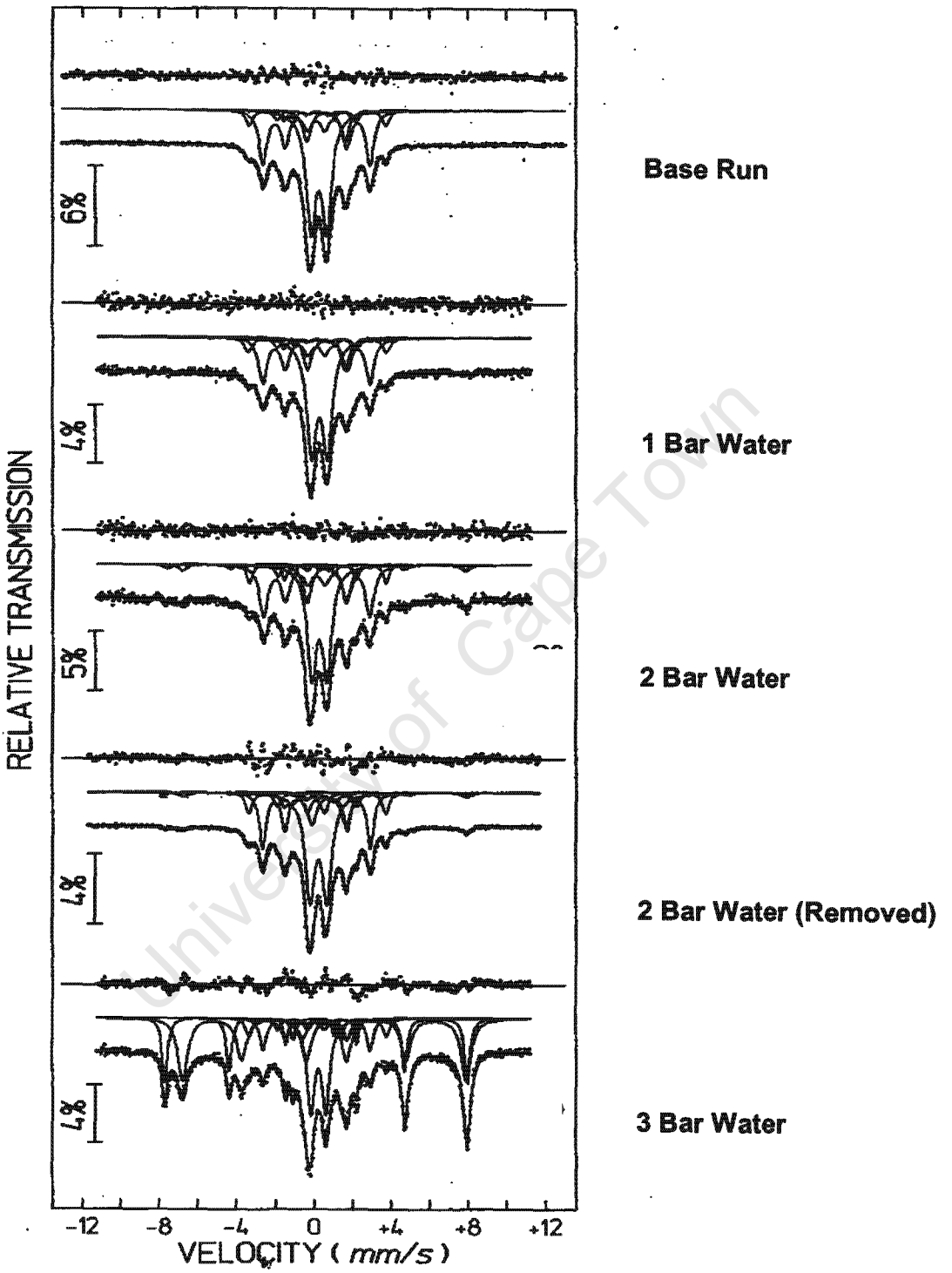

Figure 3.25: The Mössbauer spectra of all the catalysts with various amounts of water added to the feed

Table 3.3: Hyperfine interaction parameters obtained from the deconvolution of the Mössbauer spectra

Sample ID	Isomer Shift	Quadruple Splitting	Magnetic Field	Relative Absorption Area	Phase Composition
	(mm/s)Fe	(mm/s)		(Intensity)	
Base Run Catalyst	0.25	0.22	11.1		
	0.25	0.03	17.1	46.8	ε-Fe_2C
	0.29	0.04	22		
	0.74	1.98	-	9.8	Fe^{2+}
	0.38	0.81	-	43.4	Fe^{3+}
Catalyst after 1 bar water addition	0.25	0.2	11.1		
	0.24	0.01	17.2	44.6	ε-Fe_2C
	0.28	0.01	22.1		
	0.78	1.96	-	10.7	Fe^{2+}
	0.39	0.81	-	44.7	Fe^{3+}
Catalyst after 2 bar water addition	0.25	0.33	11.4		
	0.24	0.03	17	44.4	ε-Fe_2C
	0.3	0.01	22		
	0.64	0.05	45.5	7.1	Fe_3O_4
	0.27	-0.03	48.9		
	0.78	2.03	-	11.5	Fe^{2+}
	0.39	0.78	-	37	Fe^{3+}
Catalyst after 2 bar water addition and removal	0.27	0.3	11.4		
	0.24	0.03	17.3	45.3	ε-Fe_2C
	0.34	0.93	30		
	0.66	0.05	45.5	4.7	Fe_3O_4
	0.26	-0.02	48.3		
	0.88	1.77	-	11.5	Fe^{2+}
	0.35	0.87	-	38.5	Fe^{3+}
Catalyst after 3 bar water addition	0.41	0.28	11.4		
	0.24	0.03	17.1	21.7	ε-Fe_2C
	0.3	0.01	22		
	0.66	0.05	45.5		
	0.27	-0.03	48.6	50.1	Fe_3O_4
	0.78	2.08	-	10.2	Fe^{2+}
	0.35	0.77	-	18	Fe^{3+}

From these results, it can be concluded that the water in the feed (and thus the water partial pressure during Fischer-Tropsch synthesis) has a significant effect on the phase composition and the crystallite size of these catalysts. The iron species in these catalysts are initially present as small Fe^{2+}/Fe^{3+} and large ε-Fe_2C crystallites. Upon co-feeding of the feed with water at 2 bar the small Fe^{3+} crystallites are partially transformed to large crystallites of magnetite. Above 2 bar the iron carbide formed during FT gets re-oxidised back to magnetite.

The Fe^{2+} and Fe^{3+} species observed in all the catalysts could be small crystallites of any of the iron phases present in these samples or inherent of the starting material. Therefore unambiguous identification of the phases associated with these small crystallites is necessary for complete quantitative analyses, hence Mössbauer adsorption spectra of these samples should be recorded at cryogenic temperatures i.e. 80 or 4K.

3.3.2 XRD Analyses

The crystal phases present within the catalyst samples were analysed using X-ray diffraction (XRD). All the samples except one were analysed without extracting the catalyst from the wax. The catalyst sample from the 2 bar water addition run was extracted with xylene using Soxthlet extraction. The XRD-spectra are shown in Figure 3.26 and the detected crystal phases in the various catalysts and their crystallite sizes are listed in Table 3.4. The peaks of the Fe_2C and Fe_3O_4 phases were distinguished by doing Rietvelt refinement and subsequently the Debye-Scherrer equation was used to determine their crystallite sizes. The n-paraffin phases detected in the samples are not included in the table.

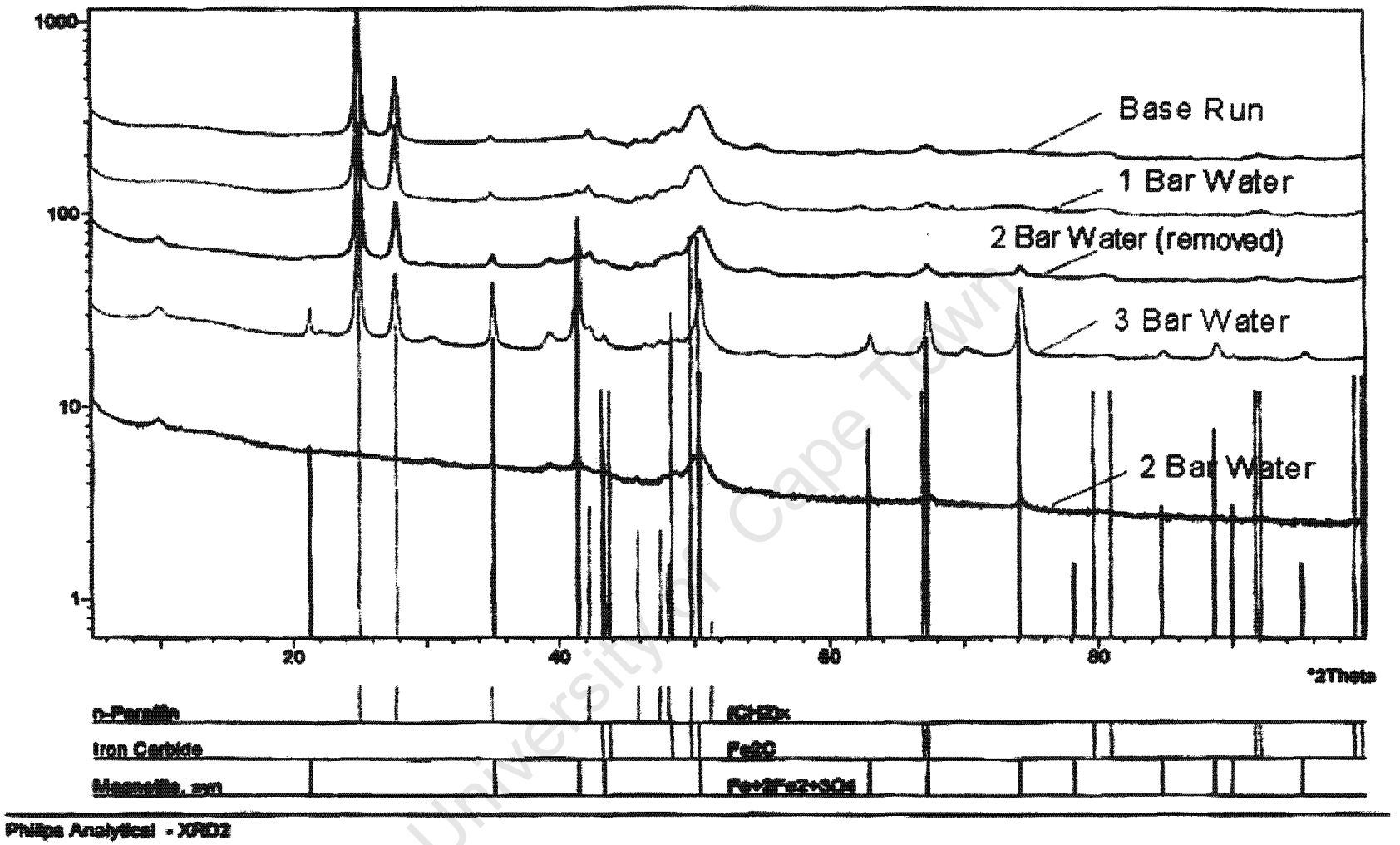

Figure 3.26: XRD spectra of the spent catalyst samples after being exposed to feeds containing various partial pressures of water

Table 3.4: Phases present in the spent catalyst samples and their crystallite sizes according to XRD

Catalyst Sample	Phase Detected			
	Fe_2C		Fe_3O_4	
	Mass %	Crystallite size (Å)	Mass %	Crystallite size (Å)
Base Run Catalyst	100	72	0	N/A
Catalyst after 1 bar water addition	100	75	0	N/A
Catalyst after 2 bar water addition	81	78	15	>1000
Catalyst after 2 bar water addition and removal	80	77	20	485
Catalyst after 3 bar water addition	22	171	78	818

The presence of magnetite was not detected in the base run and 1 bar water catalyst samples. It is however clear from the XRD-spectrum that iron carbide (ε-Fe_2C) is present as a major phase. The spectra of the catalysts that were exposed to a feed containing 2 bar water and 2 bar water (added/removed) are very similar to those of the base run and 1 bar water catalysts, except for the detection of magnetite as a minor phase. Magnetite was still detected in the sample, which had been exposed to a feed containing 2 bar of water, which was later removed. This indicates that a part of the re-oxidation during water addition was permanent or that the experiment was not carried out for long enough to reverse the effect of the added water to the feed. Except for the presence of the wax phase and the crystallite size, the XRD spectra of the two samples that underwent 2 bar water addition are almost identical.

The XRD spectrum of the catalyst sample that underwent 3 bar water addition differs from those of the other samples. Magnetite was detected in this sample as a major phase (78 wt%) and iron carbide only as a minor phase. This indicates that the addition of 3 bar water to the feed severely re-oxidises the catalyst to magnetite. The Fe_2C phases on the catalysts that underwent no water addition, 1 bar water addition, 2 bar water addition and 2 bar water addition and removal has within experimental error the same crystallite sizes. The Fe_2C phase of the

catalyst that underwent 3 bar water addition has a much larger crystallite size of 171Å. This indicates that the catalyst was severely sintered during the addition of 3 bar water to the feed.

The sizes of the magnetite crystallites are much larger than those of the Fe_2C phases. Both catalysts that underwent 2 bar water addition have magnetite present. The magnetite crystallite size of the catalyst that underwent 2 bar water addition and subsequent removal is too large to detect. This is most probably due to it being exposed after Soxthlet extraction. The magnetite crystallite size of the catalyst sample that underwent 3 bar water is almost double the size of the magnetite crystallite size of the catalyst sample that underwent 2 bar water addition. This is again evidence of catalyst sintering at high levels of water addition to the feed.

4

DISCUSSION

4.1 PHASES PRESENT IN THE IRON CATALYST

The catalyst used during the base run with no water co-feeding is reported to have Fe_2C as a major phase by both Mössbauer adsorption spectroscopy and XRD analyses. Furthermore, magnetite was not detected in the working active catalyst exposed to a feed without water. This phase did however start to appear at water co-feedings of 2 bar and higher.

After 1 bar water addition the Mössbauer adsorption spectroscopy analysis indicated a negligible decrease in Fe_2C phase and the XRD analysis indicated the presence of Fe_3O_4 as a minor phase. This indicates that even at very small amounts of water addition the catalyst structure does change slightly and is therefore rather sensitive for a change in water partial pressure.

With the addition of 2 bar of water to the feed the Mössbauer analyses detected a small amount of Fe_3O_4, but still no significant decrease in Fe_2C. The Mössbauer results of the catalyst that underwent 2 bar water addition, which was subsequently stopped shows a reduction in the magnetite content. The removal of 2 bar of water from the feed restored the catalytic activity.

The Mössbauer adsorption spectroscopy and XRD results of the catalyst that underwent 3 bar water addition differed greatly from the other catalysts. Both analyses indicated large decrease in the Fe_2C phase and at the same time a

large increase in the Fe_3O_4 phase. This coincides with a drastic decrease in Fischer-Tropsch reaction rate and conversion. It is clear from these results that the addition of 3 bar of water to the feed results in bulk re-oxidation of the carbide phases present, causing a decrease in reaction rate over and above that of kinetic inhibition.

The transition of Fe_2C into magnetite can be formally represented as:

$$3Fe_2C + 11H_2O \rightarrow 2Fe_3O_4 + 3CO + 11H_2 \qquad (4.1)$$

Thermodynamically, this reaction is for bulk Fe_2C at 240°C only feasible if

$$\left(\frac{p_{H_2O}}{p_{H_2}}\right)^{11} \cdot p_{CO}^{-3} > 1.09 \qquad (4.2)$$

(calculated using the data given by Kummer *et al.*(1948) and Browning *et al.* (1950))

These conditions were never obtained in these experiments (see Table 4.1). The catalyst, however, does not contain bulk iron carbide, but nano-sized iron carbide. Thermodynamically the oxidation of nano-sized iron carbide is more feasible than the oxidation of bulk iron carbide (van Steen, 2001).

Table 4.1: Ratio of the partial pressure of carbon dioxide relative to the partial pressure carbon monoxide at the end of the various runs and the amount of iron present as iron carbide and magnetite in the catalyst

	$\left(\frac{p_{H_2O}}{p_{H_2}}\right)^{11} \cdot p_{CO}^{-3}$	Fe in Fe_2C, %	Fe in Fe_3O_4
	bar^{-3}	%	%
No water added to feed	$1.7 \cdot 10^{-9}$	46.8	-
1 bar of water added to the feed	$1.7 \cdot 10^{-8}$	44.6	-
2 bar of water added to the feed	$3.4 \cdot 10^{-8}$	44.4	7.1
2 bar added to the feed and subsequent removal	$2.2 \cdot 10^{-12}$	45.3	4.7
3 bar added to the feed	$2.5 \cdot 10^{-7}$	21.7	50.1

4.2 EFFECT OF WATER ON FISCHER-TROPSCH ACTIVITY

During the experiments the reactor total pressure was not adjusted after the addition of water. The partial pressures of H_2 and CO in the feed to the reactor were thus diluted after water co-feeding started. However, in the reactor the partial pressure of hydrogen and carbon monoxide remained similar to that in the base run, whereas the water partial pressure in the reactor was increased upon increasing the water content in the reactor. In a CSTR, which is a good approximation for the type of reactor used in this study, the partial pressures in the reactor determine the rate of reaction and not the partial pressures in the feed.

It was observed that the rate of reaction decreased upon adding water to the feed. To evaluate the effect that water co-feeding had on the Fisher-Tropsch reaction rate, the average Fischer-Tropsch reaction rate was calculated for the period after water co-feeding started (96hours on line) until the end of each run. The decrease in rate of the Fischer-Tropsch synthesis relative to the rate of the Fischer-Tropsch synthesis, when no water was added to the feed, as a function of water partial pressure in the reactor is shown in Figure 4.1. The addition of water leads to a strong decrease in the rate of the Fischer-Tropsch synthesis.

Huff and Satterfield (1984) derived a rate expression for the rate of synthesis gas conversion based on a mechanistic model. The kinetic constants can be determined from a linearised form of the rate expression:

$$\frac{p_{CO} \cdot p_{H_2}^2}{-r_{H_2+CO} \cdot p_{H_2O}} = \frac{1}{a} + \frac{b}{a} \cdot \frac{p_{CO} \cdot p_{H_2}}{p_{H_2O}} \qquad (4.3)$$

Figure 4.2 shows the obtained data points in the linearised rate expression. As predicted by the rate expression a linear relationship is obtained for the data collected with a feed, to which no water was added, and with a feed, to which 1 bar of water was added. The data points collected with a feed containing 2 or more bar of water show a significant deviation from the expected correlation line.

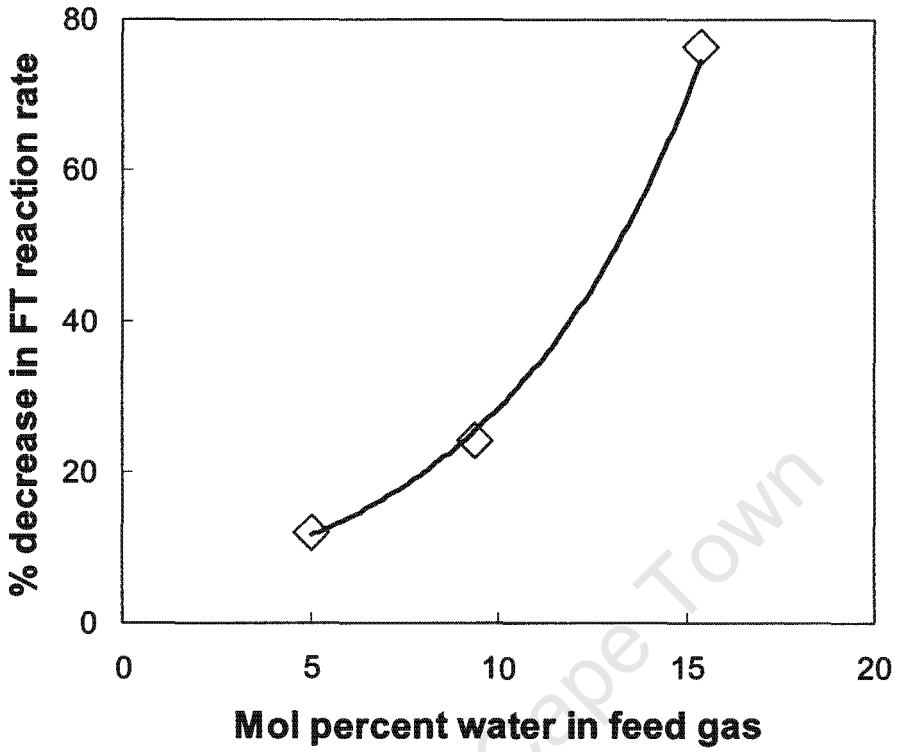

Figure 4.1: Effect of water addition to the feed on the decrease in Fischer-Tropsch reaction rate

The rate expression proposed by Satterfield and Huff (1984) cannot correspond to a physical realistic situation, despite the good correlation obtained for the linearised form with the data obtained when the catalyst was exposed to a feed containing less than 2 bar water, R^2 = 0.9611. The obtained intercept for the linear correlation, which should correspond to the reciprocal value of the activity factor a, is less than zero (similar unrealistic situations are obtained when using other linearised forms of the rate expression).

The observed rate of the Fischer-Tropsch synthesis was fitted to the rate expression proposed by van Steen and Schulz (1999). The proposed rate expression can be linearised as:

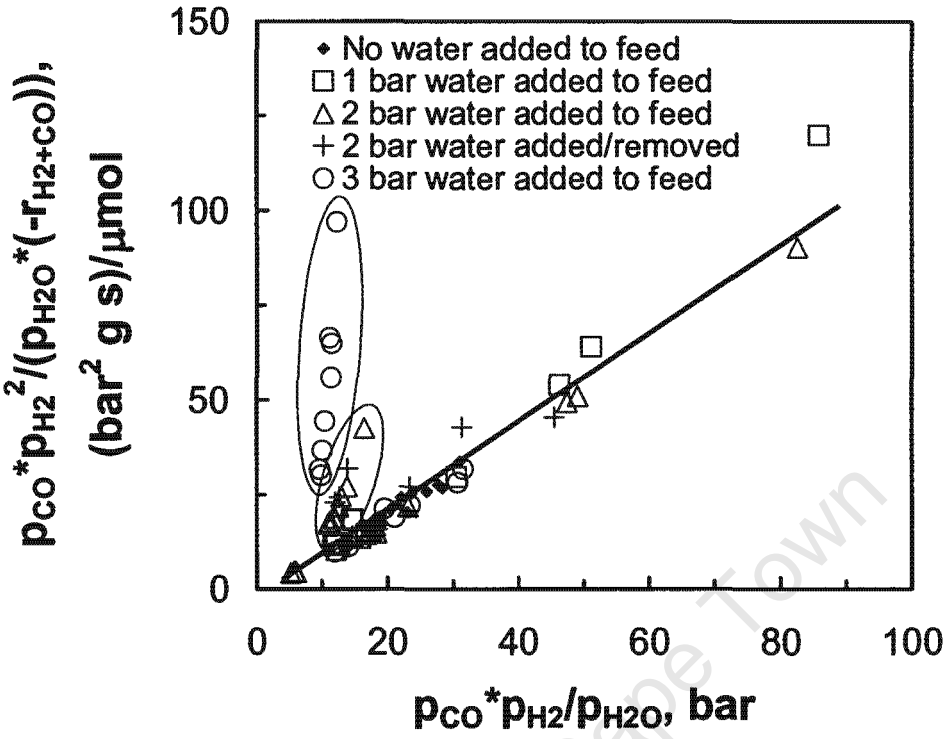

Figure 4.2: Graphical test of the linearised form of the rate expression describing the rate of hydrogen plus carbon monoxide consumption per gram of unreduced catalyst as proposed by Huff and Satterfield (1984) (encircled data points correspond to the data obtained, when the catalyst was exposed to a feed containing 2 bar of water or more)

$$\sqrt{\frac{p_{H_2}^{1.5} \cdot p_{CO}}{p_{H_2O} \cdot r_{FT}}} = \frac{1}{\sqrt{a}} + \frac{b}{\sqrt{a}} \cdot \frac{p_{H_2} \cdot p_{CO}}{p_{H_2O}} \qquad (4.4)$$

Figure 4.3 shows the fit of the measured data to the linearised form of the rate expression. The data obtained in the experiments without the addition of water to the feed and with the addition of 1 bar to the feed can be reasonably well described by the proposed rate expression. The obtained rate constant, a, and

the adsorption constant, b, using only the data, when the catalyst was exposed to a feed containing less than 2 bar of water, are given in Table 4.2. The value for the activity obtained in this study (a=2.2 10^{-4} μmol/(bar$^{1.5}$ g s)) is much higher then that reported by van Steen and Schulz (1999) for a precipitated iron catalyst (100 Fe/37 Al_2O_3/3 Cu/2 K_2O, which was tested at 250°C, but similar to the value reported by Claeys (1997) for a precipitated iron catalyst (100 Fe /13 Al_2O_3/10 Cu/ 5 K_2O), which was also tested at 250°C. The value obtained for the adsorption constant (b=0.04 bar^{-1}) is similar in all three studies.

Table 4.2: Kinetic parameters obtained from the linearised form of the rate expression describing the rate of the Fischer-Tropsch synthesis using the data obtained without water in the feed and with 1 bar of water in the feed (data given with 95% confidence interval)

a, μmol/(g s bar$^{1.5}$)	**b, bar^{-1}**	**R^2**
0.217 ± 0.037	$3.9 \cdot 10^{-2} \pm 0.038 \cdot 10^{-2}$	0.9467

The addition of 2 bar of water to the feed, and even more in the case of the addition of 3 bar of water to the feed leads to a deviation in the plot. The observed rate is much less than the expected rate of reaction based on the proposed rate expression. The Mössbauer analysis showed that the phase composition in the catalyst exposed to a feed containing 1 bar of water is similar to that of the catalyst exposed to a feed without water. The catalyst samples exposed to a feed with a larger amount of water had significant amounts of magnetite in it.

It is generally believed (Amelse *et al.*, 1978; Raupp and Delgass, 1979, Dictor and Bell, 1985; Datye *et al.*, 2000) that iron carbide is the catalytically active phase, whereas magnetite is relative inert.

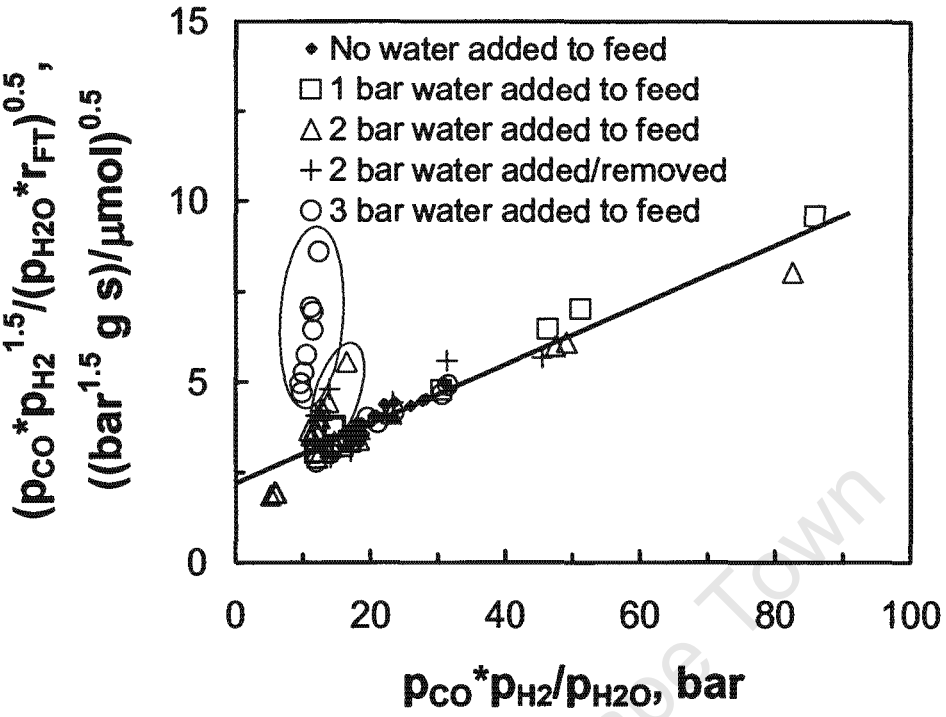

Figure 4.3: Graphical test of the linearised form of the rate expression describing the rate of the Fischer-Tropsch synthesis (equals the rate of formation of organic product compounds on carbon basis) per gram of unreduced catalyst as proposed by van Steen and Schulz (1999) (encircled data points correspond to the data obtained, when the catalyst was exposed to a feed containing 2 bar of water or more)

Figure 4.4 shows a graphical test for the rate of the Fischer-Tropsch synthesis per gram of Fe_2C as determined by Mössbauer adsorption spectroscopy. It is assumed here in the calculation of the rate of the Fischer-Tropsch synthesis, that Fe_2C content in the catalyst changes immediately, when the catalyst is exposed to a particular feed. A clear deviation can still be observed for the data points corresponding to the times that the catalyst was exposed to a feed containing 2 or more bar of water. The deviation from the correlation is however significantly reduced in comparison to the analysis, in which the rate of reaction per gram of unreduced catalyst was considered.

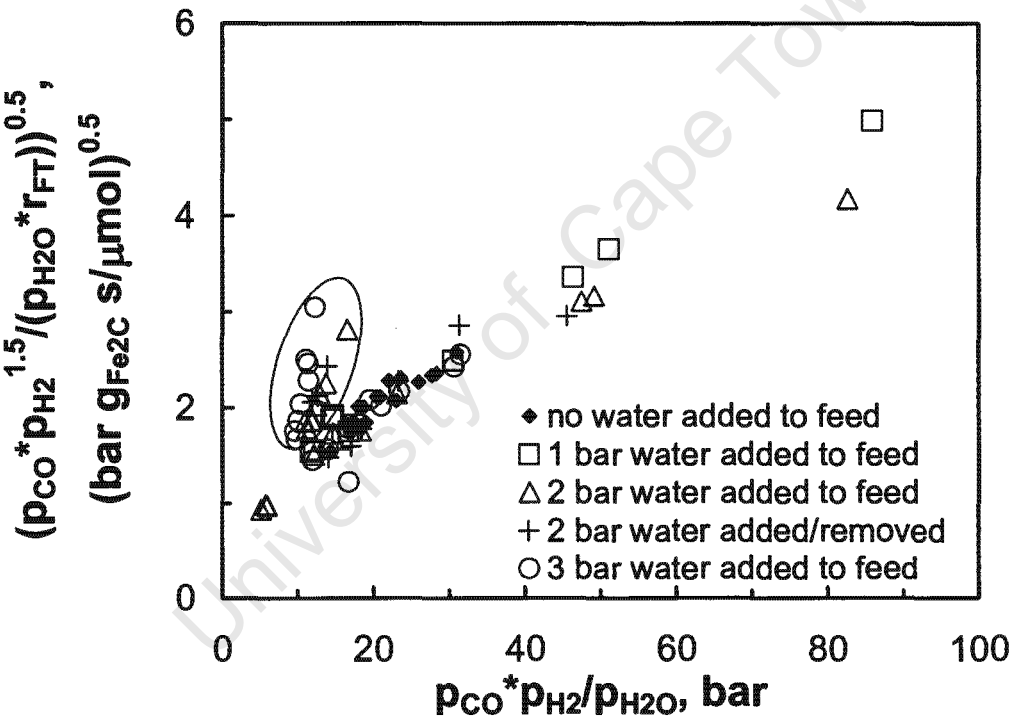

Figure 4.4: Graphical test of the linearised form of the rate expression describing the rate of the Fischer-Tropsch synthesis (equals the rate of formation of organic product compounds on carbon basis) per gram of Fe_2C as proposed by van Steen and Schulz (1999) (encircled data points correspond to the data obtained, when the catalyst was exposed to a feed containing 2 bar of water or more)

It must however be realised that the rate of reaction is proportional to the surface area of the active phase, which is not necessarily linearly related to its mass. Figure 4.5 shows a graphical test for the rate of the Fischer-Tropsch synthesis per gram of Fe_2C as determined by Mössbauer adsorption spectroscopy. A correction for a loss in surface area of the iron carbide has been made as determined from the average crystal size of Fe_2C using XRD. The crystallites are assumed to be spherical. It is also assumed in the calculation of the rate of the Fischer-Tropsch synthesis, that Fe_2C content in the catalyst and the crystallite size of the Fe_2C changes immediately, when the catalyst is exposed to a particular feed.

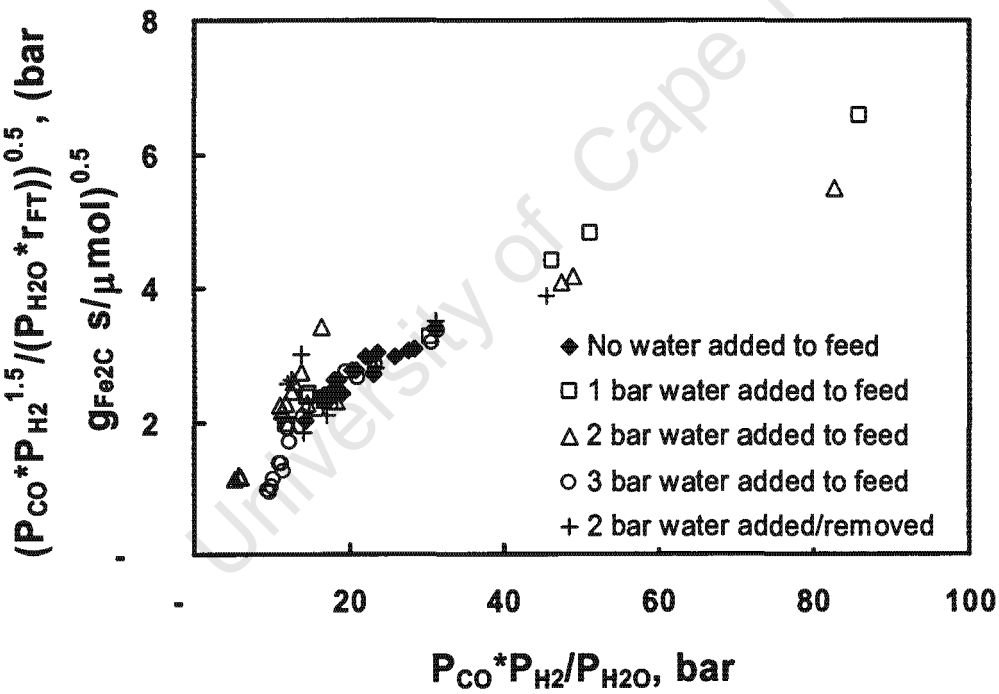

Figure 4.5: Graphical test of the linearised form of the rate expression describing the rate of the Fischer-Tropsch synthesis (equals the rate of formation of organic product compounds on carbon basis) per gram of Fe_2C corrected for a loss in surface area as proposed by van Steen and Schulz (1999)

The deviation from the model is for the data point corresponding to times when the catalyst was exposed to a feed containing 2 bar of water is greatly reduced by taking crystal growth into account. The deviation for the data points corresponding to the times that the catalyst was exposed to a feed containing 3 bar of water is also greatly reduced, but seems to be over-corrected. This is possibly due to the assumption that the Fe_2C content in the catalyst changes instantaneously when the catalyst is exposed to 3 bar water addition. The results here strongly support the hypothesis that iron carbide is the active phase.

4.3 EFFECT OF WATER ON WATER GAS SHIFT ACTIVITY

The water-gas-shift reaction rate did not seem to be affected by a change in the water partial pressure in the reactor. Only a few rate expressions have been proposed to describe the rate of CO_2-formation (rate of water-gas shift reaction) under Fischer-Tropsch conditions over a precipitated iron catalyst. Van der Laan and Beenackers (2000) proposed two rate expressions, which can be linearised to become:

$$\sqrt{\frac{\left(p_{CO} \cdot p_{H_2O} - \frac{p_{CO_2} \cdot p_{H_2}}{K_p}\right)}{r_{WGS}}} = \frac{1}{\sqrt{k_{WGS}}} + \frac{K_1}{\sqrt{k_{WGS}}} \cdot p_{CO} + \frac{K_2}{\sqrt{k_{WGS}}} \cdot p_{H_2O} \qquad (4.4)$$

$$\sqrt{\frac{\frac{P_{CO} \cdot P_{H_2O}}{\sqrt{P_{H_2}}} - \frac{P_{CO_2} \cdot \sqrt{P_{H_2}}}{K_P}}{r_{WGS}}} = \frac{1}{\sqrt{k_{WGS}}} + \frac{K_1}{\sqrt{k_{WGS}}} \cdot P_{CO} + \frac{K_3}{\sqrt{k_{WGS}}} \cdot P_{H_2O} \qquad (4.5)$$

The partial pressure of carbon monoxide changed relatively little. Hence a plot of the linearised form of equation 4.4, assuming a constant partial pressure of CO, should give a straight line (see Figure 4.6). A detailed multi-variable linear regression was performed as well. A reasonably good correlation was obtained (R^2 = 0.9659). However, the calculated intercept was within the 95% confidence interval less than zero. Hence, this rate expression must be rejected. A similar fit was obtained with equation 4.5.

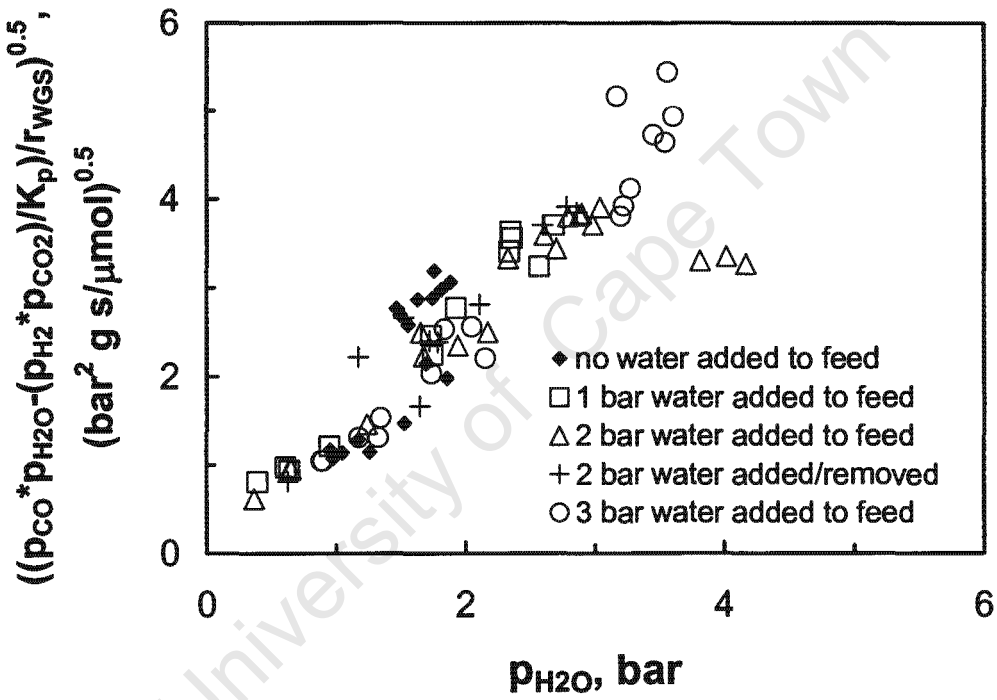

Figure 4.6: Graphical test of the linearised form of the rate expression describing the rate of the water gas shift reaction per gram of unreduced catalyst as proposed by van van der Laan and Beenackers (2000)

4.4 SELECTIVITY OF THE FISCHER-TROPSCH SYNTHESIS

The observed changes in the selectivity of the Fischer-Tropsch synthesis were mainly attributed to a reduction in the secondary reactions leading to a lower chain growth probability, decreased paraffin formation and decreased double bond isomerisation.

The chain growth probability decreases when the reactor water partial pressure increases. This was seen in both the light and heavy products. Again, the addition of 3 bar water in the feed to the reactor had a more drastic affect on the chain growth probability than 1 and 2 bar water addition. If water re-oxidises the active carbide phases on the catalyst to inactive oxide phases this result might have been expected. With less active phases present there will be a lower probability for readsorption of olefins and therefore the chain growth probability will decrease.

Figure 4.7 shows the behaviour of chain growth probability (α) as determined from the ASF plot for the products between C_4 and C_{10} as a function of synthesis gas conversion. The encircled data points indicate the first 100 hours on line when the catalyst phases were still stabilising. At a conversion below 10% (3 bar water addition) the chain growth probability experiences a drastic decrease compared to that of 20% and above. This indicates that, in addition to the conversion effect, the chain growth probability is decreased as a result of a decrease in active sites on the catalyst surface. This supports the theory of olefin readsorption as there would be less probability of readsorption as the number of active sites decreases with catalyst deactivation (through re-oxidation).

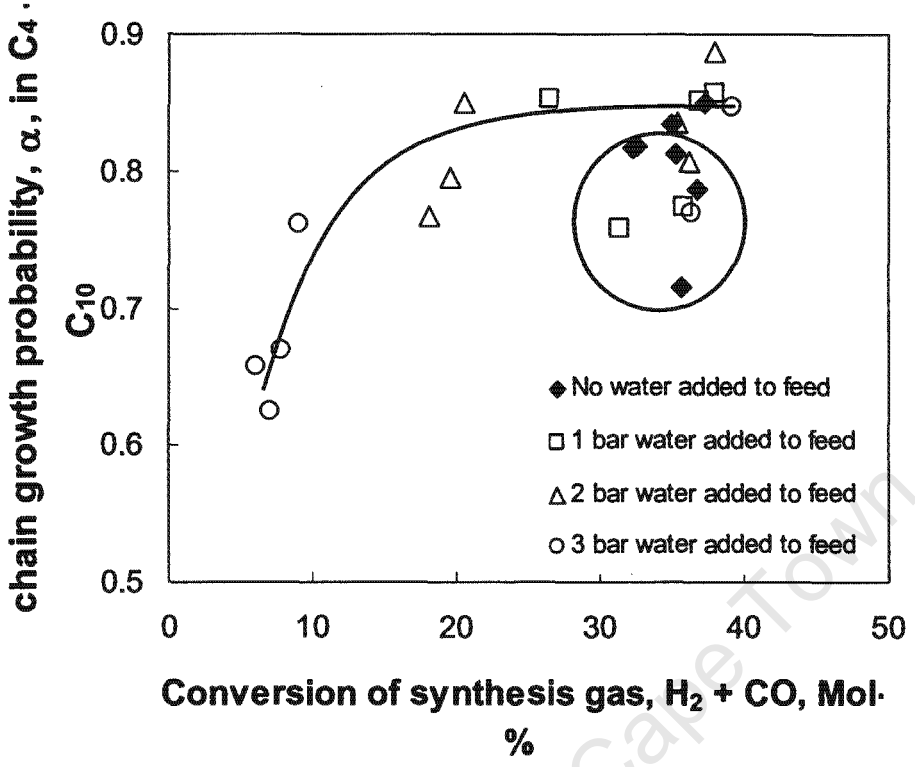

Figure 4.7: Chain growth probability in the range C4 – C10 from the product analysis of the hot tail gas as a function of synthesis gas conversion (encircled data points are from before 100 hours on line)

Water co-feeding had a negligible effect on the paraffin content in the fraction of C_3-hydrocarbons. A plausible reason for this is that negligible readsorption occurs in the case of short chain hydrocarbons and the paraffins that were formed are therefore mainly primary products. Water co-feeding significantly decreases the amount of paraffins in the fraction of linear hydrocarbons at high carbon numbers. A systematic decrease in the paraffin content could however not be detected and a plot of paraffin content as a function of conversion did not reveal a trend. The inhibition of the formation of paraffins by secondary reactions at higher water partial pressures may indicate a deactivation of the catalyst.

Also the double bond isomerisation is inhibited by water as evidenced by the strong decrease of the content of internal olefins in the fraction of linear olefins with the introduction of water in the feed. As with the paraffin content, a systematic decrease in the molar ratio of the internal olefins relative to all linear olefins could not be detected and a plot of the internal olefin content as a function of conversion did not reveal a trend.

Oxygenates formed in Fischer-Tropsch are mainly n-aldehydes and n-alcohols-(1) and to a lesser extent methyl ketones, secondary alcohols, carboxylic acids and esters. On the FID analyses of the tail gas only alcohols up to carbon number 5 were detected. The FID peaks of the alcohols in the tail gas also became more inaccurate with increasing carbon number. Alcohols were however detected easily in the oil fraction.

In analogy to olefins oxygenates can readsorb on a catalyst surface and undergo secondary reactions, namely dehydration yielding olefins, hydrogenation to form a paraffin and incorporation into growing chains as shown in co-feeding experiments (Kummer *et al.*, 1951; Kummer, 1953). The selectivity for methanol and tetradecanol increased with increasing water content in the feed. This increase was gradual over a period of 100 hours and most prominent at 3 bar water addition.

Figure 4.8 shows the behaviour of methanol selectivity as a function of synthesis gas conversion. The encircled data points indicate the first 100 hours on line when the catalyst phases were still stabilising. At conversions below 10% (3 bar water addition) the methanol selectivity experiences a drastic increase compared to that of 20% and above. An identical trend is obtained when the mass ratio of tetradecanol to all hydrocarbons in C_{14} in the oil fraction was plotted as a function of conversion. This indicates that, in addition to the conversion effect, the alcohol selectivity is increased as a result of a decrease in active sites on the catalyst surface.

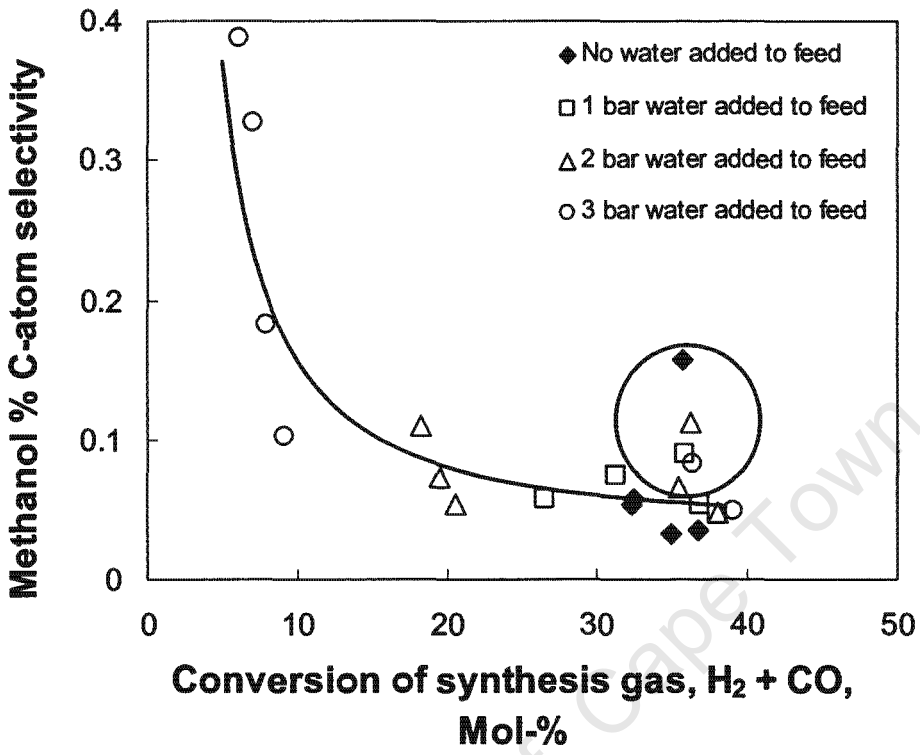

Figure 4.8: Methanol % C-atom selectivity (with regard to CO converted to all products excluding CO_2) as a function of synthesis gas conversion (encircled data points are from before 100 hours on line)

These results may support the theory of oxygenate readsorption as there would be less probability of readsorption as the number of active sites decreases with catalyst deactivation (through re-oxidation). This may well be evidence that alcohol readsorption leads mainly to chain growth and paraffin formation.

5

CONCLUSIONS

The effect of the addition of water to the feed of the Fischer-Tropsch reactor was investigated. The addition of water to the feed resulted in a change in the water partial pressure, but the partial pressure of the reactants CO and H_2 and the partial pressure of the product CO_2 remained almost constant. The addition of water to the feed resulted in a decrease in the partial pressure of the co-fed inert compounds and the organic product compounds.

The increase in the water partial pressure resulted in a change in the phases present in the catalyst. It was shown by both Mössbauer and XRD analyses that the spent base case catalyst (no water co-feeding) had Fe_2C present as the major phase. In addition, these analyses indicated that the spent catalyst that underwent 3 bar water addition contains magnetite as a major phase, which coincided with a drastic decrease in Fischer-Tropsch reaction rate and conversion. This strongly supports the argument which states that iron carbides are active for the Fischer-Tropsch synthesis and magnetite is inactive. The addition of 1 and 2 bar water to the feed did not lead to a drastic change in the catalyst structure, but did however show that it is very sensitive for small changes in water partial pressure. Hence, the addition of two bar water to the feed did cause a decrease in Fischer-Tropsch conversion and reaction rate, but upon removal of water the catalytic activity was almost fully restored. Evidence of catalyst sintering at 3 bar water addition was obtained from XRD analyses.

The reaction rate data generated during this study fitted the rate expressions proposed by both Satterfield and Huff (1984) and van Steen and Schulz (1999) well when the catalyst was exposed to a feed containing less than 2 bar water. The addition of 2 bar water to the feed and even more so, the addition of 3 bar water did however lead to a deviation in the plot. Calculating the reaction rate of Fischer-Tropsch synthesis per gram of Fe_2C significantly reduced this deviation, which again suggests that the Fe_2C crystallites are the active sites for Fischer-Tropsch synthesis. Furthermore, when catalyst surface area loss is taken into account due to crystal growth the deviation even at 3 bar water addition is very little again showing evidence of catalyst sintering at high water partial pressures. The water-gas-shift reaction rate was not affected by any amount of water co-feeding. This is however not surprising as the WGS reaction is far from equilibrium at the conditions at which the experiments were done.

The changes in the selectivity of the Fischer-Tropsch synthesis were mainly attributed to a reduction in the secondary reactions leading to a lower chain growth probability, decreased paraffin formation and decreased double bond isomerisation. Alcohol selectivity was however enhanced by the addition of water. The selectivity results obtained during this study support the following theories:

- Negligible olefin readsorption occurs at low carbon numbers
- Paraffins form both as primary and secondary products
- Internal olefins form mostly as secondary products
- Alcohol readsorption leads mainly to chain growth and paraffin formation

Evaluation of the chain growth probability and alcohol selectivity as a function of synthesis gas conversion revealed that the decrease in product readsorption is not only caused by a decrease in conversion after water addition, but also by a decrease in active iron carbide sites which are reoxidised to inactive magnetite.

REFERENCES

AKARI, H. AND PONEC, V.
Methanation of carbon monoxide on nickel and nickel copper alloys
Journal of Catalysis **44** (1976), 340

AMELSE, J.A., BUTT, J.B., SCHWARTZ, L.H.
Carburization of supported iron synthesis catalysts
Journal of Physical Chemistry **82** (1978), 558

ANDERSON R. B., FRIEDEL, K., STORCH, H.
Journal of Physical Chemistry **19** (1951), 313

ANDERSON R. B.
In "Catalysis" (P.H. Emmet, Ed.), *Vol. IV*, Reinhold, New York (1956), Chapters 1-3.

ANDERSON, K. G., EKERDT, J.G.
Study of Fisher-Tropsch synthesis over Fe/SiO_2: Effect of diethylamine on hydrocarbon and alcohol production
Journal of Catalysis **95** (1985), 602

BLYHOLDER, G.
Molecular orbital view of chemisorbed carbon monoxide
Journal of Physical Chemistry **68** (1964), 2772

BONZEL, H.P., KREBS, H.J.
On the chemical nature of the carbonaceous deposits on iron after CO hydrogenation
Surface Science **91** (1980), 499

BONZEL, H.P., KREBS, H.J.
Surface science approach to heterogeneous catalysis: CO hydrogenation on transition metals
Surface Science **117** (1982), 639

BRADY, R., PETTIT, R.
Reactions of diazomethane on transition-metal surfaces and their relationship to the mechanism of the Fischer-Tropsch reaction
Journal of the American Chemical Society **102** (1980), 6181

BRADY, R., PETTIT, R.
Mechanism of the Fischer-Tropsch reaction. The chain propagation step
Journal of the American Chemical Society **103** (1981), 1287

BROWN, J., FESHARAKI, S.
GTL: Future prospects and passible impacts on the Asia Pacific region
An East West Centre Report, Honolulu, Hawaii (2002)

BROWNING, L.C., DEWITT, T.W., EMMETT, P.H.
J. Am. Chem. Soc. **72** (1950), 4211

BUKUR, D., MUKESH, D., PATEL, S.
Promoter effects on precipitated iron catalysts for the Fischer-Tropsch synthesis
Industrial Engineering Chemistry Research **29** (1990)

CLAEYS, M.
Selektivität, Elementarschritte und kinetische Modellierung bei der Fischer-Tropsch Synthese
PhD Thesis, University of Karlsruhe (1997)

CLAEYS, M., VAN STEEN, E.
On the effect of water during Fischer-Tropsch synthesis with a ruthenium catalyst
Catalysis Today **71** (2002), 419

CRAXFORD, S.R.
Reactions of the Fischer-Tropsch process. Fischer-Tropsch synthesis and some related reactions
Transactions of the Faraday Society **35** (1939), 946-958/966-967

DATYE, A.K., JIN, Y., MANSKER, L., MOTJOPE, R.T., DLAMINI, T.H., COVILLE, N.
The nature of the active phase in iron Fischer-Tropsch catalysts
Studies in Surface Science and Catalysis **130** (2000), 1139

DAUBERT, T.E., DANNER, R.P., SIBUL, H.M., STEBBINS, C.C.
DIPPR Data Compilation of Pure Compound Properties
AIChE, New York (1993)

DICTOR, R.A., BELL, A.T.
Fischer-Tropsch Synthesis over reduced and unreduced iron oxide catalysts.
Journal of Catalysis **97** (1985), 121

DRY, M.E.
The Fischer-Tropsch Synthesis
In "Catalysis, Science and Technology" (J. Anderson, M. Boudard, Eds.), Volume 1, p. 319, Springer Verlag, Berlin (1981)

Dry, M. E.
Catalytic aspects of industrial Fischer-Tropsch synthesis
Journal of Molecular Catalysis **17** (1982a), 133

DRY, M.E.
Sasol's Fischer-Tropsch Experience
Hydrocarbon Processing. **61(8)** (1982b), 121

DRY, M.E.
The Sasol Route to Chemicals and Fuels
Proc. Methane Conversion (D.M. Bibby, C.D. Chang, R.F. Howe, S. Yurchuk, Eds.), p. 447, Elsevier Science Publishers, Amsterdam (1988)

DRY, M.E.
The Fischer-Tropsch process – commercial aspects
Catalysis Today **6** (1990), 183

DRY, M. E.
Practical and theoretical aspects of the catalytic Fischer-Tropsch Process
Applied Catalysis A: General **138** (1996), 319

DWYER, D.J., SOMORJAI, G.A.
Hydrogenation of CO and CO_2 over iron foils
Journal of Catalysis, **52** (1978), 291

DWYER, D.J., HARDENBERGH, J.H.
The catalytic reduction of carbon monoxide over iron surfaces: a surface science investigation
Journal of Catalysis **87** (1984), 66

EILERS, J., POSTHUMA, S.A., SIE, S.T.
The Shell Middle Distillate Synthesis Process (SMDS).
Catalysis Letters **7**((1990), 253

ESPINOZA, R. L., STEYNBERG, A. P., JAGER, B., VOSLOO, A. C.
Low Temperature Fischer Tropsch synthesis from a Sasol perspective
Applied Catalysis A: General **186** (1999), 13

FISCHER, F. AND TROPSCH, H.
Die Erdölsynthese bei gewöhnlichem Druck aus den Vergassungsprodukten der Kohlen
Brennstoff-Chemie **7** (1926), 97

FLORY, P.
Journal of the American Chemical Society **58** (1936), 1877

FROHNING, C., KÖLBEL, H., RALEK, M., ROTTIG, W., SCHNURR, F., SCHULZ, H.,
Fischer-Tropsch Synthese
In "Chemierohstoffe aus Kohle" (J. Falbe, Ed.), Georg Thieme Verlag, Stuttgart (1977)

GRADASSI, M.J.
Economics of gas to liquids manufacture
Studies in Surface Science and Catalysis **119** (1998), 35

HERRINGTON, E.
Chemical Industry **65** (1946), 346

HILMEN, A.M., SCHANKE, D., HANSSEN, K.F., HOLMEN, A.
Study of the effect of water on alumina supported cobalt Fischer-Tropsch catalysts
Applied Catalysis A: General **186** (1999), 169

HUANG, C.S., XU, B.H., DAVIS, B.H.
Fuel Science and Technology International **11** (1993), 639

HUFF jr., G., SATTERFIELD, C.N.
Intrinsic kinetics of the Fischer-Tropsch synthesis on a reduced fused magnetite catalyst
Industrial Engineering Chemistry Process Design Development **23** (1984), 696

IGLESIA, E., REYES, S. C., MADON, R. J.
Transport enhanced alpha olefin readsorption pathways in Ru-catalysed hydrocarbon synthesis
Journal of Catalysis **129** (1991), 238

JAGER, B., DRY, M.E., SHINGLES, T., STEYNBERG, A.P.
Experience with a new type of reactor for Fischer-Tropsch synthesis
Catalysis Letters **7** (1990), 293

JAGER, B., DRY, M.E., SHINGLES, T., STEYNBERG, A.P., YUKAWA, Y.
A new and more efficient Synthol reactor for Fischer-Tropsch synthesis
Proc. 6th National Meeting of the South African Institution of Chemical Engineers, Durban (1991)

JAGER, B., ESPINOZA, R.
Advances in low temperature Fischer-Tropsch synthesis
Catalysis Today **23** (1995a), 17

JAGER, B.
Improved Sasol Fischer-Tropsch processes
Proc. 12th International Pittsburgh Coal Conference (1995b), 1171

KAMINSKY, M., WINOGRAD, N., GEOFFRY, G., VANNICE, M.

Direct SIMS observation of methylidyne, mehylene and methyl intermediates on Ni(III) methanation catalyst
Journal of American Chemical Society **108** (1986), 1315

KARN, F.S., SHULTZ, J.F., ANDERSON, R.B.
Kinetics of the Fischer-Tropsch synthesis on iron catalysts – III. Influence of water vapor
Actes Congr. Int. Catal. 2nd, **2** (1960), 2439

KNOTTENBELT, C.
Mossgas "gas-to-liquid" diesel fuels – an environmentally friendly option
Catalysis Today **71** (2002), 437

KÖLBEL, H., RALEK, M.
Catalysis Review – Science and Engineering **21** (1980), 225

KREBS, H.J., BONZEL, H.P.
A model study of the hydrogenation of CO over polycrystalline iron
Surface Science **88** (1979), 269

KUMMER, J.T., BROWNING, L.C., EMMETT, P.H.
J. Chem. Phys. **16** (1948), 740

MANSKER, L.D., JIN, Y., BUKUR, D.B., DATYE, A.K.
Characterisation of slurry phase iron catalysts for Fischer-Tropsch synthesis.
Applied Catalysis A: General, **186** (1999), 277

PICHLER, H. SCHULZ, H.
Neuere Erkenntnisse auf dem Gebiet der Synthese von Kohlenwasserstoffen aus CO und H_2

Chemie Ingenieur Technik **42** (1970), 1162

RAUPP, G.B., DELGASS, W.N.
Mössbauer investigation of supported Fe catalysts III. In-situ kinetics and spectroscopy during FT synthesis
Journal of Catalysis **58** (1979), 361

REYMOND, J.P., MERIAUDEAU, P., POMMIER, B., BENETT, C.O.
Further results on the reaction of H_2/CO on fused iron by the transient method.
Journal of Catalysis **64** (1980), 163

ROGINSKI, S.
Proc. 3rd Congr. on Catalysis, Amsterdam (1965), 939

SACHTLER, J.W.A., KOOL, J.M., PONEC, V.
The role of carbon in methanation by cobalt and ruthenium
Journal of Catalysis **56** (1979), 284

SATTERFIELD, C.N., HANLON, R.T., TUNG, S.E., ZOU, Z.M., PAPAEFTHYMIOU, G.C.
Effect of water on the iron-catalysed Fischer-Tropsch synthesis
DOE Report DOE/PC/80015-T1 (1986a)

SATTERFIELD, C.N., HANLON, R.T., TUNG, S.E., ZOU, Z.M., PAPAEFTHYMIOU, G.C.
Effect of water on the iron-catalysed Fischer-Tropsch synthesis
Industrial Engineering Chemistry Product Research Development **25** (1986b), 407

SCHULZ, G.V.
Zeitschrift fur physikalische Chemie **B30** (1935), 379

SCHULZ, H., BÖHRINGER, W., KOHL, C., RAHMAN, N., WILL, A.
Entwicklung und Anwendung der Kapillar-GC-Gesamtprobentechnik für Gas/Dampf-Vielstoffgemische
DGMK-Forschungsbericht 320, DGMK, Hamburg (1984a)

SCHULZ, H. GÖKCEBAY, H.
Fischer-Tropsch CO hydrogenation as a means for linear olefin production
In "Catalysis of Organic Reactions" (J. Kosak, Ed.), p. 153, M. Dekker, New York (1984b)

SCHULZ, H., BECK, K., ERICH, E.
Mechanism of the Fischer-Tropsch process
Studies in Surface Science and Catalysis **36** (1988), 457

SCHULZ, H., GORRE, H., ERICH, E., VAN STEEN, E.
Regularities of selectivity as a key for discrimination FT-surface reactions and formation of the dynamic system
Catalysis Letters **7** (1990), 157

SCHULZ, H., CLAEYS, M., HARMS, S.
Effect of water partial pressure on steady state Fischet-Tropsch activity and selectivity of a promoted cobalt catalyst
Studies in Surface Science and Catalysis **107** (1997), 193

SCHULZ. H., CLAEYS, M.
Kinetic modelling of Fischer-Tropsch product distributions

Applied Catalysis A: General **186** (1999a), 91-107

SCHULZ., H., CLAEYS, M.
Reactions of α-olefins of different chain length added during the Fischer-Tropsch synthesis on a cobalt catalyst in a slurry reactor
Applied Catalysis A: General **186** (1999b), 71-90

SCHULZ., H., NIE, Z., OUSMANOV, F.
Construction of the Fischer-Tropsch regime with cobalt catalysts
Catalysis Today **71** (2002), 351-360

SENDEN, M.M.G.
The Shell Middle Distillate Synthesis Process commercial plant experience and outlook into the future
Petroleum Technology **415** (1995), 94

SENZI, L., MEITZNER, G.D., IGLESIA, E.
Structure and site evaluation of iron oxide catalyst precursors during the Fischer-Tropsch synthesis
Journal of Physical Chemistry B **105** (2001), 5743

SIE, S.T., SENDEN, M.M.G., VAN WECHEM, H.M.H.
Conversion of natural gas to transportation fuels via the Shell Middle Distillate Synthesis Process (SMDS)
Catalysis Today **8** (1991), 371

STERNBERG, A., WENDER, J.

Proc. Intern. Conf. Coordination Chem., The Chemical Society, London (1959), 53

STERNBERG, A., WENDER, J.
Distributed chain growth probabilities for the Fischer-Tropsch synthesis
Journal of Catalysis **92** (1985), 426

STEYNBERG, A.P., ESPINOZA, R.L., JAGER, B., VOSLOO, A.C.
High temperature Fischer-Tropsch synthesis in commercial practice
Applied Catalysis A: General **186** (1999), 41

STORCH, H.H., GOLUMBIC, N., ANDERSON, R.B.
The Fischer-Tropsch and Related Synthesis
John Wiley & Sons, New York, 1951

VAN BERGE, P.J., EVERSON, R.C.
Cobalt as an alternative Fischer-Tropsch catalyst to iron for the production of middle distillates
Studies in Surface Science and Catalysis **107** (1997), 207

VAN DER LAAN, G.P., BEENACKERS, A.A.C.M.
Intrinsic kinetics of the gas–solid Fischer–Tropsch and water gas shift reactions over a precipitated iron catalyst
Applied Catalysis A: General **193** (2000), 39

VANNICE, M.A.
Catalytic synthesis of hydrocarbons from hydrogen-carbon monoxide mixtures over the Group VIII metals. I. Specific activities and product distributions of supported metals
Journal of Catalysis **37** (1975), 449

VAN STEEN, E., SCHULZ, H.
Polymerisation Kinetics of the Fischer Tropsch CO Hydrogenation using Iron Based and Cobalt Based Catalysts
Applied Catalysis A: General **186** (1999), 309-320

VAN STEEN, E
Personal Communications
(2001)

XU, L., BAO, S., O'BRIEN R.J., RAJE, A., DAVIS, B.H.
Don't rule out iron catalysts for Fischer-Tropsch synthesis
CHEMTECH **28(1)** (1998), 47

APPENDIX A

A1. Calculation of feed gas water partial pressure

The molar flow rate of a component in the feed is calculated from the TCD peak areas and composition of the calibration gas and the TCD peak areas of the feed gas ampoule by the following equation:

$$MolarFlow = \frac{CG\%_x \times CGA_{Ar}}{CGA_x \times CG\%_{Ar}} \times \frac{Flow_{Ar} \times FGA_x}{FGA_{Ar}}$$

Where:

Molar flow:	The molar flow rate of a component x in moles/s
CG%:	Mole percent of component in calibration gas
CGA:	TCD peak area of component in calibration gas
Flow:	Molar flow of component in moles/s
FGA:	TCD peak area of component in feed gas

Typical molar flow rates of the components in the feed during this study were calculated in Table A1 using a representative ampoule TCD analysis.

Table A1.

Component	Calibration Gas Composition	Calibration Gas TCD Peak Areas	Feedgas TCD Peak Areas	Feed Gas Molar Flow Rate
	Mole %			mole/s
H_2	39.99	148.3	100.6	4.52E-04
Ar	10.02	237.0	99.0	6.97E-05
N_2	5	111.0	6.6	4.98E-06
CO	19.97	427.5	319.3	2.48E-04
CH_4	15.01	282.2	114.9	1.02E-04
CO_2	10.01	274.0	11.7	7.13E-06

Water is a sub-cooled liquid at 20 bar and 25°C with a density of 994,9kg/m^3. If water is added at a flow rate of x µl/min at these conditions the mass flow rate can be calculated as follows:

$$\dot{m}_{water} = \frac{x}{\rho}$$

and the molar flow rate as follows:

$$\dot{M}_{water} = \frac{\dot{m}_{water}}{Mr_{water}}$$

The molar flow rate for 50µl/min of water was calculated in table A2.

Table A2.

Water Flow rate		Density	Water Flow rate	Mr	Water Flow rate
µl/min	m3/s	kg/m3	kg/s	kg/mol	mol/s
50	8.33E-10	994.9	8.29E-07	0.018	4.61E-05

After heating the feed stream to 240°C the water is a superheated vapour at 20 bar. The molar flow rate of all the components stay constant and the partial pressures of the components are calculated as follows:

Table A3.

Component	Feed Gas Molar Flow Rate	Mole Fraction	Partial Pressure
	mole/s		Bar
H^2	4.52E-04	0.49	9.7
Ar	6.97E-05	0.07	1.5
N_2	4.98E-06	0.01	0.1
CO	2.48E-04	0.27	5.3
CH_4	1.02E-04	0.11	2.2
CO_2	7.13E-06	0.01	0.2
H_2O	4.61E-05	0.05	
Total	9.30E-04	1	20

Therefore, the water partial pressure in the feed is increased to 1 bar if 50ml/min of water is co-fed to the reactor. Table A4 and A5 show the different flow rates of water used during the runs and the effect they had on the feed partial pressures and molar flow rates of the other component.

Table A4.

Component	Partial pressure of component in the feed, bar			
	Base run	50µl co-fed	100µl co-fed	175µl co-fed
H_2	10.22	9.72	9.26	8.65
Ar	1.58	1.50	1.43	1.33
N_2	0.11	0.11	0.10	0.10
CO	5.62	5.34	5.09	4.75
CH_4	2.30	2.19	2.09	1.95
CO_2	0.16	0.15	0.15	0.14
H_2O	**0**	**1.0**	**1.9**	**3.1**
H_2/CO Ratio	1.82	1.82	1.82	1.82
% Decrease in CO and H_2 Partial Pressure	0	5.0	9.4	15.4

Table A5.

Component	Molar percentage of component in the feed			
	Base run	50μl co-fed	100μl co-fed	175μl co-fed
H_2	51.12	48.59	46.30	43.24
Ar	7.89	7.50	7.15	6.67
N_2	0.56	0.53	0.51	0.48
CO	28.11	26.71	25.45	23.77
CH_4	11.51	10.94	10.43	9.74
CO_2	0.81	0.77	0.73	0.68
H_2O	**0**	**5.0**	**9.4**	**15.4**
H_2/CO Ratio	1.82	1.82	1.82	1.82

A2. Calculation of reactor water partial pressure

The flow rates of CO and CO_2 in the feed and tail gas are calculated from the TCD peak areas as in section A1. For every mole of hydrocarbon formed in the FT synthesis one mole of water is formed. The molar flow rate of water formed by the FT reaction can therefore be calculated as follows if the WGS reaction is taken into account:

$$\dot{V}_{H_2O}^{FT} = \left(\dot{V}_{CO}^{F} - \dot{V}_{CO}^{T} \right) - 2\left(\dot{V}_{CO_2}^{T} - \dot{V}_{CO_2}^{F} \right)$$

where:

$\dot{V}_{H_2O}^{FT}$ = normalised volumetric flow rate of the water produced by the FT reaction

$\dot{V}_{CO}^{F}$ = normalised volumetric flow of CO in the feed gas

$\dot{V}^{T}_{CO}$ = normalised volumetric flow rate of CO in the tail gas

$\dot{V}^{F}_{CO_2}$ = normalised volumetric flow rate of CO_2 in the feed gas

$\dot{V}^{T}_{CO_2}$ = normalised volumetric flow rate of CO_2 in the tail gas

The flow rate of the water that is co-fed to the reactor is measured. Therefore, the total water flow rate in the tail gas is calculated as follows:

$$\dot{V}^{Total}_{H_2O} = \dot{V}^{FT}_{H_2O} + \dot{V}^{co-fed}_{H_2O}$$

If the reactor is assumed to be well mixed the water partial pressure in the tail gas will be equal to the water partial pressure in the reactor. The reactor water partial pressure can therefore be calculated as follows:

$$P_{H_2O} = \frac{\dot{V}^{Total}_{H_2O}}{\dot{V}_{Total}} P_T$$

where:

P_{H_2O} = water partial pressure in the reactor

$\dot{V}^{Total}_{H_2O}$ = normalised total volumetric flow rate of water on the tail gas

$\dot{V}_{Total}$ = normalised total tail gas flow rate

P_T = total reactor pressure

APPENDIX B

The data gathered during the 5 experimental micro reactor runs are presented in this section.

Table B1. Experimental data for Run 1 (Base run)

Period :		1	2	3	4	5	6	7	8	9	10	11	12	13
Time :		14:00	08:30	14:00	13:00	08:45	14:30	08:50	08:20	08:30	09:30	14:30	13:30	08:10
Stirring speed	rpm	450	450	450	450	450	450	450	450	450	450	450	450	450
Reactor Pressure Inlet	bar	20.1	20.1	20.1	20.1	20	20.1	20.1	20.1	20.1	20.1	20.1	20	20.1
Reactor Temperature	°C	240.1	240	240	240	239.8	240	240	240	240	240	240	240	240
Measured indicator temp.	°C	240	239.43	239.44	239.43	239.4	239.4	239.44	239.4	239.4	239.44	239.4	239.4	239.4
Hot condensate pot temp	°C	190	190	190	190	190	190	190	190	190	190	190	190	190
Hot condensate line temp	°C	200	200	200	200	200	200	200	200	200	200	200	200	200
Sample point temp	°C	220	220	220	220	220	220	220	220	220	220	220	220	220
APG flow	Brooks %	26.19	26.18	26.18	26.18	26.18	26.11	26.18	26.2	26.18	26.2	26.2	26.18	26.19
Ar flow	Brooks %	18.15	18.01	18.07	18.07	18.07	18.07	18.05	18.05	18.08	18.09	18.01	18.08	18.06
Hot trap drainings	[g]	12.04	11.57	59.38	52.43	2.03	8.99	35.66	50.08	52.65	52.93	58.97	46.47	37.92
Cold trap drainings	[g]	10.86	57.19	144.30	104.43	2.45	20.73	81.78	102.64	106.77	111.55	128.33	100.18	81.31
Water drained	[g]		40.08	88.87	83.61			67.76	86.13	88.62	92.37	105.85	82.44	66.48
Oil drained	[g]		15.98	24.10	19.64			12.74	16.13	17.26	18.15	22.14	16.62	13.66
Drain time		14:30	09:10	14:25	13:40	09:00	14:30	09:40	08:50	09:00	10:10	14:50	13:50	08:50

Table B2. Experimental data for Run 2 (1 bar water added)

Period :		1	2	3	4	5	6	7	8	9
Time :		15:00	08:10	10:30	09:00	08:30	16:30	08:40	08:50	08:30
Stirring speed	rpm	450	450	450	450	450	450	450	450	450
Reactor Pressure Inlet	bar	20	20.2	20.2	20	20	20.1	20.1	20.1	20
Reactor Temperature	°C	240	240	240	240	240	240	240	240	240
Measured indicator temp.	°C	239.5	239.5	239.4	239.4	239.4	239.4	239.4	239.4	
Hot condensate pot temp	°C	190	190	190	190	190	190	190	190	190
Hot condensate line temp	°C	200	200	200	200	200	200	200	200	200
Sample point temp	°C	220	220	220	220	220	220	220	220	220
APG flow	Brooks %	26.20	26.20	26.20	26.20	26.20	26.18	26.21	26.19	26.19
Ar flow	Brooks %	18.10	18.10	18.10	18.10	18.10	18.05	18.10	18.08	18.1
Hot trap drainings	[g]	8.30	2.18	49.40	55.45	58.75	17.90	32.31	40.26	
Cold trap drainings	[g]	10.36	54.00	107.84	107.13	114.08	43.22	112.37	160.55	
Water drained	[g]		38.37	74.22	87.19	93.40	36.42	98.03	141.81	124.54
Oil drained	[g]		14.85	20.86	18.95	19.70	6.14	13.60	18.02	17.18
Drain time		15:15	08:30	11:00	09:30	09:30	16:50	09:20	09:20	09:00
Water Addition	ml/min	0	0	0	0	0	0.05	0.05	0.05	0.05

Note: Water co-feeding started at 96 hours on line.

Table B3. Experimental data for Run 4 (2 bar water added)

Period :		1	2	3	4	5	6	7	8	9	10	11	12	13
Time :		14:00	12:30	12:50	08:40	08:30	15:10	08:40	16:00	08:50	16:05	08:35	15:35	12:00
Stirring speed	rpm	450	450	450	450	450	450	450	450	450	450	450	450	450
Reactor Pressure Inlet	bar	20	20	20	20	20	20.1	20.1	20	20	20	19.9	19.9	20.1
Reactor Temperature	°C	240	240	240	240	240	240	240	240	240	240	240	240	240
Measured indicator temp.	°C	239.5	239.6	239.6	239.6	239.6	239.6	239.6	239.6	239.6	239.6	239.6	239.6	239.6
Hot condensate pot temp	°C	190	190	190	190	190	190	190	190	190	190	190	190	190
Hot condensate line temp	°C	200	200	200	200	200	200	200	200	200	200	200	200	200
Sample point temp	°C	220	220	220	220	220	220	220	220	220	220	220	220	220
APG flow	Brooks %	26.18	26.18	26.18	26.24	26.17	26.18	26.17	26.18	26.18	26.18	26.18	26.17	26.17
Ar flow	Brooks %	18.01	18.08	18.08	18.07	18.00	18.08	18.07	18.08	18.08	18.08	18.08	18.08	18.07
Hot trap drainings	[g]		8.47	49.13	50.66	62.31	17.52	41.65	11.28	19.05	7.37	15.25	5.43	15.82
Cold trap drainings	[g]	9.91	76.89	104.95	94.94	117.04	30.85	146.46	59.61	134.00	56.63	126.53	53.65	157.96
Water drained	[g]		55.69	85.15	78.14	96.09	25.25	131.81	54.27	123.72	52.40	118.01	49.26	147.72
Oil drained	[g]		20.73	18.77	16.20	19.92	5.08	13.66	4.63	9.46	3.48	7.68	2.96	9.43
Drain time		14:00	12:50	13:00	08:55	08:50	15:00	08:50	16:10	08:50	16:00	08:40	15:40	12:15
Water Addition	ml/min	0	0	0	0	0	0.10	0.10	0.10	0.10	0.10	0.10	0.10	0.10

Note: Water co-feeding started: 96 hours on line

Table B4. Experimental data for Run 3 (3 bar water added)

Period :		1	2	3	4	5	6	7	8	9	10	11	12	13
Time :		15:15	08:10	08:40	10:45	11:30	20:30	08:20	16:00	08:30	15:25	08:30	15:40	08:40
Stirring speed	rpm	450	450	450	450	450	450	450	450	450	450	450	450	450
Reactor Pressure Inlet	bar	20.1	20.1	20.1	20.1	20.1	19.9	20	20	20	20	20	20	20
Reactor Temperature	°C	240	240	240	240	240	240	240	240	240	240	240	240	240
Measured indicator temp.	°C	239.5	239.5	239.6	239.6	239.6	239.6	239.5	239.5	239.5	239.5	239.5	239.5	239.5
Hot condensate pot temp	°C	190	190	190	190	190	190	190	190	190	190	190	190	190
Hot condensate line temp	°C	200	200	200	200	200	200	200	200	200	200	200	200	200
Sample point temp	°C	220	220	220	220	220	220	220	220	220	220	220	220	220
APG flow	Brooks %	26.20	26.20	26.20	26.17	26.17	26.15	26.18	26.16	26.18	26.1	26.18	26.16	26.15
Ar flow	Brooks %	18.08	18.09	18.08	18.04	18.05	18.00	18.05	18	18.05	18.03	18.06	18.05	18.06
Hot trap drainings	[g]	0.95	34.91	49.05	54.20	62.64	16.57	10.62	2.30	3.22	0.88	2.14	0.00	2.16
Cold trap drainings	[g]	17.97	56.31	96.52	114.62	111.12	83.18	137.32	80.76	175.37	76.20	181.80	74.14	176.95
Water drained	[g]		41.43	76.37	93.15	91.33	76.26	131.19	77.52	170.74	73.79	177.51	72.19	173.66
Oil drained	[g]		15.05	19.37	20.33	18.85	6.04	5.03	2.13	3.48	1.24	3.30	1.18	2.43
Drain time		15:30	08:45	09:30	11:20	12:10	20:30	09:00	16:20	08:30	15:40	09:00	15:45	09:00
Water Addition	ml/min	0	0	0	0	0	0.175	0.175	0.175	0.175	0.175	0.175	0.175	0.175

Note: Water co-feeding started: 96 hours on line

Table B5. Experimental data for Run 5 (2 bar water added and removed)

Period :		1	2	3	4	5	6	7	8	9	10
Time :		15:15	08:00	09:45	09:25	12:30	11:20	07:30	08:25	07:50	09:00
Stirring speed	rpm	450	450	450	450	450	450	450	450	450	450
Reactor Pressure Inlet	bar	19.8	20.1	20	20	20	20.1	20.1	20	20	20
Reactor Temperature	°C	239.9	240	239.9	240	240	240	240	240	240	240
Measured indicator temp.	°C										
Hot condensate pot temp	°C	190	190	190	190	190	190	190	190	190	190
Hot condensate line temp	°C	200	200	200	200	200	200	200	200	200	200
Sample point temp	°C	220	220	220	220	220	220	220	220	220	220
APG flow	Brooks %	26.24	26.24	26.24	26.23	26.24	26.24	26.23	26.25	26.25	26.25
Ar flow	Brooks %	18.05	18.08	18.09	18.09	18.10	18.10	18.10	18.1	18.1	18.1
Hot trap drainings	[g]		1.31	47.92	64.73	72.73	49.07	20.56	34.55	51.45	20.63
Cold trap drainings	[g]	13.96	50.37	110.75	117.04	138.91	187.99	160.31	181.96	86.37	98.11
Water drained	[g]		35.81	91.77	97.42	114.56	169.82	148.32	170.05	74.43	82.14
Oil drained	[g]		11.45	18.25	18.74	23.33	17.25	10.76	11.09	11.12	15.07
Drain time		15:15	08:20	10:00	09:40	12:50	11:50	08:20	09:00	08:15	09:15
Water Addition	ml/min	0	0	0	0	0	0.1	0.1	0.1	0	0

Note: Water co-feeding started: 96 hours on line

Water co-feeding stopped: 170 hours on line

APPENDIX C

The results for calculations done from the TCD analyses are given in this section.

Table C1. Results obtained from TCD analyses for Run 1 (Base Run).

Time on Line, hrs	2	3	4	5	7	24	28	53	76	102	120	143	168	193	222	245	263
Calculated Syngas GHSV (ml(n) / g-cat / hr)	2800	2800	2800	2800	2800	2696	2696	2823	2677	2722	2702	2607	2763	2652	2790	2700	2862
Calculated APG GHSV (ml(n) / g-cat / hr)	3238	3238	3238	3238	3238	3112	3112	3269	3102	3148	3126	3017	3198	3066	3226	3126	3312
Reactor Feedgas Flow Rates (ml(n) / s)																	
H2	10.00	10.00	10.00	10.00	10.00	9.61	9.61	10.20	9.65	9.90	9.74	9.45	10.10	9.79	10.24	9.82	10.45
CO	5.55	5.55	5.55	5.55	5.55	5.37	5.37	5.48	5.23	5.22	5.27	5.03	5.25	4.94	5.26	5.18	5.45
SYNGAS	15.56	15.56	15.56	15.56	15.56	14.98	14.98	15.68	14.87	15.12	15.01	14.49	15.35	14.73	15.50	15.00	15.90
CH4	2.27	2.27	2.27	2.27	2.27	2.16	2.16	2.30	2.19	2.21	2.20	2.14	2.27	2.16	2.27	2.21	2.33
CO2	0.16	0.16	0.16	0.16	0.16	0.16	0.16	0.18	0.16	0.16	0.15	0.14	0.15	0.14	0.16	0.16	0.16
Reactor Tail Gas Flow Rates (ml(n) / s)																	
H2	7.67	7.12	7.47	7.49	7.26	6.98	6.76	6.76	6.57	6.99	6.93	6.79	6.90	7.10	7.30	6.99	7.12
CO	2.76	2.45	2.53	2.51	2.24	2.49	2.48	2.62	2.74	3.18	3.23	2.95	3.07	3.03	3.16	3.29	3.18
SYNGAS	10.44	9.57	10.00	10.00	9.50	9.47	9.25	9.38	9.32	10.17	10.16	9.74	9.98	10.14	10.46	10.27	10.30
CH4	2.36	2.18	2.36	2.39	2.36	2.32	2.28	2.29	2.27	2.21	2.28	2.23	2.26	2.28	2.43	2.25	2.27
CO2	1.15	1.08	1.23	1.27	1.30	1.21	1.14	0.85	0.73	0.46	0.50	0.49	0.49	0.49	0.56	0.50	0.50
H2O	0.81	1.25	0.87	0.82	1.04	0.77	0.93	1.52	1.34	1.45	1.34	1.39	1.49	1.21	1.31	1.20	1.59
HC's	0.56	0.76	0.61	0.60	0.69	0.56	0.60	0.73	0.61	0.56	0.54	0.55	0.61	0.48	0.51	0.50	0.67
Ar	1.55	1.55	1.55	1.55	1.55	1.55	1.55	1.55	1.55	1.55	1.55	1.55	1.55	1.55	1.55	1.55	1.55
Reactor Partial Pressures [bar] - H2	9.08	8.68	8.97	9.00	8.82	8.79	8.60	8.28	8.30	8.51	8.46	8.51	8.43	8.80	8.68	8.56	8.43
Reactor Partial Pressures [bar] - CO	3.27	2.99	3.04	3.02	2.72	3.14	3.15	3.21	3.47	3.87	3.95	3.70	3.75	3.75	3.75	4.04	3.77
Reactor Partial Pressures [bar] - H2O	0.96	1.53	1.05	0.98	1.26	0.97	1.18	1.86	1.70	1.76	1.63	1.75	1.82	1.50	1.58	1.47	1.89
Reactor Partial Pressures [bar] - CO2	1.36	1.32	1.48	1.53	1.58	1.52	1.44	1.05	0.92	0.55	0.61	0.61	0.60	0.61	0.66	0.62	0.59
% Conversion - H2	23.28	28.85	25.31	25.17	27.46	27.40	29.60	33.72	31.87	29.36	28.87	28.19	31.65	27.46	28.69	28.88	31.90
% Conversion - CO	50.28	55.85	54.44	54.76	59.67	53.54	53.78	52.25	47.49	39.19	36.68	41.45	41.43	36.59	39.97	36.51	41.63
% Conversion - SYNGAS	32.92	38.49	35.71	35.73	38.96	36.77	36.27	40.20	37.36	32.76	32.32	32.79	34.99	31.19	32.51	31.51	35.23
% Conversion - CO+CO2	32.43	39.21	35.09	34.73	39.18	33.98	35.53	39.95	36.61	33.45	32.04	34.55	34.90	31.56	32.47	29.81	35.43
FT Reaction Rate (mole CO / g-cat / s)	3.81E-06	4.45E-06	4.13E-06	4.13E-06	4.51E-06	4.09E-06	4.26E-06	4.69E-06	4.13E-06	3.68E-06	3.61E-06	3.53E-06	3.99E-06	3.42E-06	3.75E-06	3.52E-06	4.17E-06
WGS-Reaction Rate (mole CO2 formed / g-cat / s)	2.21E-06	2.06E-06	2.40E-06	2.48E-06	2.54E-06	2.34E-06	2.19E-06	1.51E-06	1.27E-06	6.69E-07	7.81E-07	7.74E-07	7.65E-07	7.75E-07	8.80E-07	7.74E-07	7.54E-07
WGS Rate/FT Rate	0.56	0.46	0.58	0.60	0.56	0.57	0.51	0.32	0.31	0.18	0.22	0.22	0.19	0.23	0.23	0.22	0.18
H2/CO-Feed Ratio	1.80	1.80	1.80	1.80	1.80	1.79	1.79	1.86	1.85	1.89	1.85	1.88	1.92	1.98	1.95	1.90	1.92
H2/CO-Reactor Ratio	2.78	2.90	2.95	2.98	3.24	2.80	2.73	2.58	2.40	2.20	2.14	2.30	2.25	2.34	2.31	2.13	2.24
% CO (Of total Reacted) Converted to CO2	35.51	29.79	35.54	36.59	34.34	36.54	33.94	23.55	22.92	14.65	17.18	16.64	15.77	18.23	18.76	18.35	14.90
Usage Ratio (Delta H2 / Delta CO)	0.83	0.93	0.84	0.83	0.83	0.92	0.99	1.20	1.24	1.42	1.36	1.28	1.47	1.41	1.40	1.50	1.47

Table C2. Results obtained from TCD analyses for Run 2 (1 bar water added).

Time on Line (h)	2	3	5	22	49	71	95	103	119	143	149	167
Calculated Syngas GHSV (ml(n) / g-cat / hr)	2624	2624	2624	2689	2719	2695	2797	2794	2737	2734	2734	2822
Calculated APG GHSV (ml(n) / g-cat / hr)	3039	3039	3039	3111	3141	3115	3222	3216	3147	3136	3136	3238
Reactor Feedgas Flow Rates (ml(n) / s)												
H2	9.53	9.53	9.53	9.75	9.79	9.73	10.08	10.00	9.76	9.69	9.69	10.18
CO	5.05	5.05	5.05	5.19	5.31	5.25	5.46	5.52	5.44	5.50	5.50	5.50
SYNGAS	14.58	14.58	14.58	14.94	15.11	14.97	15.54	15.52	15.21	15.19	15.19	15.68
CH4	2.15	2.15	2.15	2.18	2.18	2.17	2.20	2.18	2.13	2.10	2.10	2.17
CO2	0.16	0.16	0.16	0.16	0.16	0.16	0.16	0.16	0.14	0.13	0.13	0.14
Reactor Tail Gas Flow Rates (ml(n) / s)												
H2	7.78	7.61	7.47	7.01	6.57	6.54	6.58	7.15	6.93	7.50	7.42	7.83
CO	2.92	2.70	2.55	2.59	2.82	2.92	3.05	3.43	3.44	3.69	3.76	3.69
SYNGAS	10.70	10.31	10.02	9.59	9.39	9.46	9.63	10.58	10.38	11.19	11.17	11.53
CH4	2.37	2.32	2.33	2.29	2.23	2.24	2.20	2.19	2.12	2.13	2.20	2.20
CO2	1.06	1.08	1.15	1.09	0.71	0.63	0.58	0.58	0.49	0.50	0.47	0.47
H2O [produced]	0.32	0.50	0.51	0.75	1.39	1.38	1.56	1.25	1.31	1.07	1.08	1.14
H2O [co-fed]	0.00	0.00	0.00	0.00	0.00	0.00	0.00	1.03	1.03	1.03	1.03	1.03
H2O [total]	0.32	0.50	0.51	0.75	1.39	1.38	1.56	2.28	2.34	2.10	2.11	2.17
HC's	0.33	0.42	0.44	0.52	0.63	0.59	0.66	0.55	0.55	0.47	0.44	0.48
Ar	1.55	1.55	1.55	1.55	1.55	1.55	1.55	1.55	1.55	1.55	1.55	1.55
Reactor Partial Pressures [bar] - H2	9.52	9.40	9.33	8.87	8.26	8.24	8.12	8.06	7.95	8.35	8.27	8.51
Reactor Partial Pressures [bar] - CO	3.57	3.34	3.19	3.28	3.55	3.69	3.77	3.87	3.95	4.12	4.19	4.01
Reactor Partial Pressures [bar] - H2O	0.40	0.61	0.64	0.95	1.75	1.74	1.93	2.57	2.68	2.34	2.35	2.36
Reactor Partial Pressures [bar] - CO2	1.29	1.34	1.44	1.38	0.89	0.80	0.72	0.65	0.56	0.56	0.52	0.51
% Conversion - H2	18.39	20.21	21.69	28.12	32.95	32.82	34.76	28.53	29.01	22.66	23.46	23.02
% Conversion - CO	42.09	46.49	49.43	50.19	46.85	44.28	44.09	37.86	36.71	32.86	31.70	32.87
% Conversion - SYNGAS	26.59	29.30	31.29	35.79	37.84	36.83	38.04	31.84	31.77	26.35	26.44	26.48
% Conversion - CO+CO2	24.26	28.16	29.81	32.33	36.54	35.27	36.35	30.21	30.37	26.12	25.64	26.79
FT Reaction Rate (mole CO / g-cat / s)	2.88E-06	3.18E-06	3.39E-06	3.98E-06	4.25E-06	4.10E-06	4.40E-06	3.68E-06	3.59E-06	2.98E-06	2.99E-06	3.09E-06
WGS-Reaction Rate (mole CO2 formed / g-cat / s)	2.01E-06	2.06E-06	2.21E-06	2.07E-06	1.22E-06	1.05E-06	9.43E-07	9.42E-07	7.69E-07	8.26E-07	7.44E-07	7.46E-07
WGS Rate/FT Rate	0.70	0.65	0.65	0.52	0.29	0.26	0.21	0.26	0.21	0.28	0.25	0.24
H2/CO-Feed Ratio	1.89	1.89	1.89	1.88	1.84	1.85	1.85	1.81	1.79	1.76	1.76	1.85
H2/CO-Reactor Ratio	2.66	2.82	2.93	2.71	2.33	2.24	2.15	2.08	2.01	2.03	1.98	2.12
% CO (Of total Reacted) Converted to CO2	42.38	39.42	39.70	35.57	22.02	20.33	17.55	20.20	17.26	20.50	19.13	18.50
Usage Ratio (Delta H2 / Delta CO)	0.83	0.82	0.83	1.05	1.30	1.37	1.45	1.36	1.42	1.22	1.30	1.30

Table C3. Results obtained from TCD analyses for Run 4 (2 bar water added).

Time on Line (h)	1	2	5	27	52	72	79	95	99	101	102	120	123	127	144	151	168	175	195
Calculated Syngas GHSV (ml(n) / g-cat / hr)	2823	2823	2823	2681	2630	2630	2630	2800	2751	2800	2751	2747	2691	2891	2871	2851	2842	2997	2856
Calculated APG GHSV (ml(n) / g-cat / hr)	3222	3222	3222	3083	3020	3020	3020	3343	3170	3343	3170	3160	3314	3314	3290	3268	3246	3412	3268
Reactor Feedgas Flow Rates (ml(n) / s)																			
H2	10.29	10.29	10.29	9.60	9.31	9.31	9.31	10.34	9.85	10.34	9.85	9.54	10.46	10.46	10.46	10.46	10.40	10.90	10.42
CO	5.39	5.39	5.39	5.29	5.31	5.31	5.31	5.21	5.63	5.21	5.63	5.72	5.60	5.60	5.47	5.36	5.39	5.75	5.44
SYNGAS	15.68	15.68	15.68	14.90	14.61	14.61	14.61	15.55	15.26	15.55	15.28	15.26	16.06	16.06	15.95	15.84	15.79	16.85	15.87
CH4	2.06	2.06	2.06	2.11	2.05	2.05	2.05	2.87	2.19	2.87	2.19	2.16	2.18	2.18	2.15	2.13	2.07	2.12	2.09
CO2	0.15	0.15	0.15	0.12	0.12	0.12	0.12	0.15	0.13	0.15	0.13	0.13	0.18	0.18	0.18	0.18	0.18	0.18	0.20
Reactor Tail Gas Flow Rates (ml(n) / s)																			
H2	7.45	7.51	7.75	6.89	6.56	6.46	6.76	6.43	6.79	6.77	6.96	8.07	8.58	8.61	8.80	8.97	9.34	9.09	9.02
CO	2.63	2.77	2.61	2.61	2.88	2.57	2.69	3.00	2.95	2.63	2.75	4.05	4.05	4.03	4.03	4.07	4.28	3.97	3.97
SYNGAS	10.29	10.28	10.36	9.50	9.44	9.05	9.45	9.43	9.73	9.59	9.73	12.12	12.63	12.64	12.63	13.04	13.62	13.06	12.99
CH4	2.33	2.36	2.23	2.23	2.17	2.26	2.13	2.25	2.17	2.13	2.16	2.21	2.05	2.07	2.06	2.06	2.11	2.02	2.08
CO2	1.17	1.20	1.40	0.97	0.87	0.62	0.85	0.59	0.64	0.63	0.64	0.50	0.54	0.53	0.52	0.54	0.57	0.55	0.59
H2O [produced]	0.53	0.54	0.30	0.98	1.32	1.73	1.55	1.32	1.66	1.42	1.85	0.95	0.63	0.85	0.75	0.57	0.32	1.04	0.68
H2O [co-fed]	0.00	0.00	0.00	0.00	0.00	0.00	0.00	0.00	2.06	2.06	2.06	2.06	2.06	2.06	2.06	2.06	2.06	2.06	2.06
H2O [total]	0.53	0.54	0.30	0.98	1.32	1.73	1.55	1.32	3.73	3.48	3.92	3.01	2.90	2.92	2.82	2.63	2.38	3.10	2.74
HC's	0.43	0.43	0.46	0.57	0.56	0.87	0.87	0.80	0.73	0.88	0.80	0.42	0.44	0.44	0.40	0.33	0.22	0.51	0.36
Ar	1.55	1.55	1.55	1.55	1.55	1.55	1.55	1.55	1.55	1.55	1.55	1.55	1.55	1.55	1.55	1.55	1.55	1.55	1.55
Reactor Partial Pressures [bar] - H2	9.15	9.18	9.51	8.72	8.33	8.16	8.44	8.07	7.31	7.41	7.42	8.15	8.53	8.54	8.72	8.90	9.13	8.74	8.87
Reactor Partial Pressures [bar] - CO	3.47	3.39	3.21	3.30	3.66	3.24	3.37	3.77	3.18	3.09	2.93	4.08	4.03	4.00	3.99	4.03	4.19	3.82	3.91
Reactor Partial Pressures [bar] - H2O	0.85	0.68	0.37	1.24	1.68	2.17	1.94	1.66	4.02	3.81	4.17	3.04	2.88	2.90	2.79	2.61	2.33	2.98	2.70
Reactor Partial Pressures [bar] - CO2	1.44	1.46	1.71	1.23	0.85	0.78	0.81	0.74	0.69	0.69	0.68	0.50	0.53	0.53	0.52	0.54	0.56	0.53	0.59
% Conversion - H2	27.54	27.03	24.70	28.26	29.51	30.34	27.40	37.82	29.70	34.56	27.73	15.34	18.01	17.75	15.99	14.37	10.22	16.57	13.51
% Conversion - CO	47.53	46.63	51.59	50.72	45.73	51.52	49.23	42.43	47.64	45.77	51.10	29.32	27.66	27.89	26.34	24.10	20.46	30.98	27.04
% Conversion - SYNGAS	34.42	34.46	33.95	36.24	35.40	38.03	35.33	39.36	38.31	38.32	36.34	20.58	21.37	21.29	19.54	17.68	13.72	21.54	18.15
% Conversion - CO+CO2	28.65	29.29	28.58	34.66	35.34	42.04	39.27	33.87	38.61	36.46	42.02	22.95	21.28	21.56	20.05	17.33	13.18	24.51	19.75
FT Reaction Rate (mole CO / g-cat / s)	4.01E-06	4.02E-06	3.96E-06	4.01E-06	3.85E-06	4.13E-06	3.84E-06	4.55E-06	4.13E-06	4.43E-06	4.13E-06	2.34E-06	2.55E-06	2.54E-06	2.32E-06	2.08E-06	1.61E-06	2.67E-06	2.14E-06
WGS-Reaction Rate (mole CO2 formed / g-cat / s	2.27E-06	2.33E-06	2.77E-06	1.90E-06	1.23E-06	1.12E-06	1.16E-06	9.95E-07	1.13E-06	1.08E-06	1.14E-06	8.13E-07	7.95E-07	7.68E-07	7.69E-07	8.10E-07	8.76E-07	8.27E-07	8.68E-07
WGS Rate/FT Rate	0.57	0.58	0.70	0.47	0.32	0.27	0.31	0.22	0.27	0.24	0.28	0.35	0.31	0.31	0.33	0.39	0.54	0.31	0.41
H2/CO-Feed Ratio	1.91	1.91	1.91	1.81	1.75	1.75	1.75	1.98	1.72	1.98	1.72	1.87	1.87	1.87	1.91	1.98	1.93	1.89	1.92
H2/CO-Reactor Ratio	2.63	2.71	2.97	2.64	2.28	2.52	2.51	2.14	2.30	2.39	2.53	2.00	2.12	2.13	2.18	2.21	2.18	2.29	2.27
% CO (Of total Reacted) Converted to CO2	39.72	39.78	44.60	31.68	22.72	16.40	20.24	20.16	18.98	20.29	17.77	21.71	23.04	22.82	23.90	28.11	35.62	20.63	26.99
Usage Ratio (Delta H2 / Delta CO)	1.11	1.06	0.91	1.01	1.13	1.03	0.98	1.77	1.07	1.50	0.93	0.87	1.22	1.19	1.16	1.17	0.98	1.01	0.98

Table C4. Results obtained from TCD analyses for Run 3 (3 bar water added).

Time on Line (h)	1	5	7	24	31	49	55	75	99	108	120	128	144	151	168	176	193
Calculated Syngas GHSV (ml(n) / g-cat / hr)	2688	2688	2688	2655	2655	2709	2709	2694	2700	2735	2803	2744	2791	2867	2714	2782	2765
Calculated APG GHSV (ml(n) / g-cat / hr)	3101	3101	3101	3054	3054	3118	3118	3101	3107	3143	3224	3171	3211	3302	3131	3206	3187
Reactor Feedgas Flow Rates (ml(n) / s)																	
H2	9.49	9.49	9.49	9.38	9.38	9.50	9.50	9.46	9.53	9.66	9.90	9.69	9.75	10.14	9.47	9.74	9.74
CO	5.45	5.45	5.45	5.39	5.39	5.55	5.55	5.51	5.47	5.54	5.68	5.55	5.76	5.79	5.61	5.72	5.62
SYNGAS	14.93	14.93	14.93	14.75	14.75	15.05	15.05	14.97	15.00	15.19	15.57	15.24	15.51	15.93	15.08	15.46	15.38
CH4	2.15	2.15	2.15	2.07	2.07	2.13	2.13	2.11	2.14	2.16	2.23	2.27	2.22	2.28	2.17	2.20	2.19
CO2	0.15	0.15	0.15	0.15	0.15	0.14	0.14	0.15	0.12	0.11	0.10	0.11	0.11	0.13	0.14	0.15	0.15
Reactor Tail Gas Flow Rates (ml(n) / s)																	
H2	7.59	7.15	6.84	6.86	6.63	6.71	6.56	6.23	6.57	9.06	9.34	9.46	9.41	9.45	9.38	9.48	9.64
CO	2.39	2.52	2.49	2.53	2.63	2.83	2.56	2.87	3.03	4.62	4.83	5.14	4.87	4.76	4.83	4.90	4.79
SYNGAS	9.98	9.68	9.33	9.38	9.26	9.55	9.13	9.11	9.59	13.68	14.16	14.59	14.28	14.21	14.20	14.38	14.43
CH4	2.31	2.30	2.26	2.24	2.21	2.22	2.22	2.11	2.21	2.17	2.19	2.25	2.22	2.20	2.23	2.20	2.20
CO2	1.12	1.26	1.28	1.11	1.00	0.80	0.77	0.66	0.61	0.39	0.34	0.38	0.41	0.44	0.52	0.56	0.57
H2O [produced]	1.11	0.71	0.71	0.93	1.06	1.41	1.74	1.62	1.48	0.35	0.39	-0.07	0.29	0.41	0.03	0.00	-0.01
H2O [co-fed]	0.00	0.00	0.00	0.00	0.00	0.00	0.00	0.00	0.00	3.61	3.61	3.61	3.61	3.61	3.61	3.61	3.61
H2O [total]	1.11	0.71	0.71	0.93	1.06	1.41	1.74	1.62	1.48	3.97	4.00	3.54	3.90	4.03	3.65	3.62	3.60
HC's	0.64	0.55	0.57	0.56	0.59	0.66	0.76	0.71	0.63	0.21	0.22	0.06	0.20	0.27	0.12	0.14	0.13
Ar	1.55	1.55	1.55	1.55	1.55	1.55	1.55	1.55	1.55	1.55	1.55	1.55	1.55	1.55	1.55	1.55	1.55
Reactor Partial Pressures [bar] - H2	9.08	8.91	8.71	8.68	8.46	8.30	8.12	7.91	8.17	8.25	8.31	8.46	8.34	8.32	8.42	8.44	8.57
Reactor Partial Pressures [bar] - CO	2.86	3.14	3.17	3.20	3.38	3.50	3.17	3.65	3.76	4.21	4.30	4.60	4.32	4.19	4.34	4.37	4.26
Reactor Partial Pressures [bar] - H2O	1.33	0.89	0.90	1.18	1.35	1.74	2.15	2.05	1.84	3.61	3.56	3.17	3.46	3.55	3.27	3.22	3.20
Reactor Partial Pressures [bar] - CO2	1.34	1.56	1.63	1.41	1.27	0.99	0.95	0.84	0.75	0.35	0.30	0.32	0.38	0.39	0.47	0.50	0.51
% Conversion - H2	20.01	24.56	27.91	26.71	29.14	29.38	30.93	34.06	31.07	6.21	5.66	2.41	3.46	6.83	0.97	2.66	1.09
% Conversion - CO	56.11	53.65	54.30	53.16	51.16	48.95	53.80	47.88	44.69	16.49	14.96	7.49	15.38	17.81	13.94	14.36	14.73
% Conversion - SYNGAS	33.17	35.18	37.54	38.38	37.19	38.56	39.38	39.15	38.04	9.96	9.05	4.26	7.89	10.82	5.79	6.99	6.08
% Conversion - CO+CO2	38.26	33.38	33.65	35.24	35.40	37.15	42.57	38.61	35.87	11.43	10.88	3.09	10.18	12.46	7.27	7.21	7.23
FT Reaction Rate (mole CO / g-cat / s)	3.68E-06	3.91E-06	4.17E-06	3.99E-06	4.08E-06	4.09E-06	4.41E-06	4.36E-06	4.02E-06	1.12E-06	1.05E-06	4.83E-07	9.10E-07	1.28E-06	6.50E-07	8.04E-07	6.94E-07
WGS-Reaction Rate (mole CO2 formed / g-cat / s)	2.17E-06	2.46E-06	2.51E-06	2.15E-06	1.90E-06	1.46E-06	1.39E-06	1.14E-06	1.08E-06	6.25E-07	5.17E-07	5.45E-07	6.68E-07	6.90E-07	8.35E-07	9.13E-07	9.40E-07
WGS Rate/FT Rate	0.59	0.63	0.60	0.54	0.46	0.36	0.32	0.26	0.27	0.56	0.49	1.13	0.73	0.54	1.29	1.14	1.35
H2/CO-Feed Ratio	1.74	1.74	1.74	1.74	1.74	1.71	1.71	1.72	1.74	1.74	1.74	1.74	1.69	1.75	1.69	1.70	1.73
H2/CO-Reactor Ratio	3.18	2.84	2.75	2.72	2.52	2.37	2.56	2.17	2.17	1.96	1.93	1.84	1.93	1.98	1.94	1.93	2.01
% CO (Of total Reacted) Converted to CO2	31.81	37.79	38.04	33.70	30.80	24.11	20.87	19.35	19.74	30.68	27.26	56.73	33.81	30.00	47.86	49.80	50.90
Usage Ratio (Delta H2 / Delta CO)	0.62	0.80	0.90	0.87	0.99	1.03	0.98	1.22	1.21	0.66	0.66	0.56	0.38	0.67	0.12	0.32	0.13

Table C5. Results obtained from TCD analyses for Run 5 (2 bar water added and removed).

Time on Line (h)	6	23	49	72	100	122	142	167	190	216
Calculated Syngas GHSV (ml(n) / g-cat / hr)	2870	3086	3471	3472	2959	2889	2868	2896	2843	2793
Calculated APG GHSV (ml(n) / g-cat / hr)	3275	3532	3968	3960	3388	3300	3286	3315	3239	3193
Reactor Feedgas Flow Rates (ml(n) / s)										
H2	10.48	11.17	10.52	10.52	10.74	10.42	10.46	10.49	10.29	10.26
CO	5.46	5.97	5.56	5.56	5.70	5.63	5.47	5.60	5.51	5.26
SYNGAS	15.94	17.15	16.09	16.09	16.44	16.05	15.93	16.09	15.79	15.52
CH4	2.10	2.31	2.15	2.15	2.21	2.13	2.17	2.17	2.05	2.07
CO2	0.15	0.17	0.16	0.16	0.17	0.15	0.15	0.16	0.15	0.15
Reactor Tail Gas Flow Rates (ml(n) / s)										
H2	7.62	7.24	6.82	7.19	7.01	9.12	9.32	9.07	7.62	7.99
CO	2.51	2.82	3.13	3.05	3.05	4.04	4.17	4.14	3.43	3.40
SYNGAS	10.12	10.06	9.95	10.23	10.06	13.16	13.49	13.21	11.04	11.40
CH4	2.23	2.18	2.15	2.21	2.22	2.18	2.19	2.15	2.11	2.25
CO2	1.37	1.04	0.67	0.66	0.60	0.49	0.49	0.48	0.54	0.57
H2O [produced]	0.51	1.41	1.41	1.50	1.79	0.91	0.63	0.81	1.31	1.01
H2O [co-fed]	0.00	0.00	0.00	0.00	0.00	2.06	2.06	2.06	0.00	0.00
H2O [total]	0.51	1.41	1.41	1.50	1.79	2.97	2.69	2.87	1.31	1.01
HC's	0.54	0.80	0.64	0.65	0.74	0.40	0.31	0.38	0.54	0.42
Ar	1.56	1.56	1.56	1.56	1.56	1.56	1.56	1.56	1.56	1.56
Reactor Partial Pressures [bar] - H2	9.33	8.50	8.33	8.55	8.26	8.78	8.99	8.78	8.91	9.29
Reactor Partial Pressures [bar] - CO	3.07	3.31	3.82	3.62	3.59	3.90	4.02	4.01	4.01	3.96
Reactor Partial Pressures [bar] - H2O	0.63	1.65	1.73	1.79	2.11	2.86	2.60	2.78	1.53	1.18
Reactor Partial Pressures [bar] - CO2	1.68	1.22	0.81	0.79	0.71	0.47	0.47	0.47	0.63	0.66
% Conversion - H2	27.30	35.18	35.19	31.69	34.74	12.55	10.86	13.56	25.94	22.09
% Conversion - CO	54.14	52.80	43.80	45.28	46.53	28.10	23.85	26.05	37.78	35.26
% Conversion - SYNGAS	36.50	41.32	38.17	36.39	38.83	18.00	15.32	17.91	30.07	26.55
% Conversion - CO+CO2	31.77	38.18	34.61	36.16	38.99	22.11	17.65	20.25	30.76	27.24
FT Reaction Rate (mole CO / g-cat / s)	4.33E-06	5.27E-06	4.57E-06	4.35E-06	4.75E-06	2.15E-06	1.82E-06	2.14E-06	3.53E-06	3.06E-06
WGS-Reaction Rate (mole CO2 formed / g-cat / s)	2.73E-06	1.95E-06	1.14E-06	1.13E-06	9.59E-07	7.52E-07	7.57E-07	7.25E-07	8.63E-07	9.41E-07
WGS Rate/FT Rate	0.63	0.37	0.25	0.26	0.20	0.35	0.42	0.34	0.24	0.31
H2/CO-Feed Ratio	1.92	1.87	1.86	1.88	1.88	1.85	1.91	1.87	1.87	1.95
H2/CO-Reactor Ratio	3.04	2.57	2.18	2.36	2.30	2.25	2.24	2.19	2.22	2.35
% CO (Of total Reacted) Converted to CO2	41.32	27.68	13.22	12.66	16.21	21.34	25.99	22.29	18.58	22.74
Usage Ratio (Delta H2 / Delta CO)	0.97	1.25	1.58	1.48	1.41	0.83	0.87	0.98	1.28	1.22

APPENDIX D

The results for calculations done from the FID analyses are given in this section.

Figure D1. Selectivity results for Run 1 (base run)

Time on Line, hrs	5	24	76	120	168	222	263
% C-atom Selectivities (Calculated w.r.t. CO converted to all products excluding CO2)							
METHANE	6.15	8.62	4.01	4.64	-0.24	9.60	-3.41
METHANOL	0.16	0.03	0.00	0.05	0.03	0.06	0.03
ETHYLENE	1.27	0.84	0.52	1.09		0.37	0.47
ETHANE	4.72	3.71	2.44	2.61	2.35	3.07	2.64
ETHANOL	3.44	1.73	0.54	0.47	0.43	0.56	0.45
PROPENE	4.09	3.39	2.24	2.30	2.25	2.88	2.46
PROPANE	1.79	1.18	0.51	0.51	0.51	0.68	0.57
n-PROPANOL	1.16	0.53	0.13	0.16	0.12	0.23	0.12
α - BUTENE	3.96	2.44	1.79	1.80	1.73	2.24	1.76
n-BUTANE	1.73	1.20	0.55	0.49	0.52	0.64	0.55
trans-2-BUTENE	0.12	0.09	0.04	0.04	0.04	0.06	0.05
cis-2-BUTENE	0.19	0.16	0.09	0.00	0.10	0.13	0.12
n-BUTANOL	0.93	0.20	0.14	0.11	0.10	0.14	0.10
α - PENTENE	2.17	2.08	1.70	1.55	1.56	1.89	1.52
n-PENTANE	1.65	1.11	0.53	0.47	0.48	0.60	0.49
trans-2-PENTENE	0.16	0.09	0.05	0.04	0.05	0.06	0.06
cis-2-PENTENE	0.13	0.12	0.07	0.07	0.08	0.11	0.09
n-PENTANOL	0.81	0.06	0.08	0.08	0.00	0.05	0.02
α - HEXENE	1.64	1.74	1.62	1.43	1.46	1.77	1.36
n-HEXANE	1.65	1.14	0.57	0.49	0.50	0.61	0.49
trans-2-HEXENE	0.13	0.11	0.05	0.11	0.05	0.07	0.05
cis-2-HEXENE	0.12	0.12	0.08	0.10	0.08	0.11	0.09
n-HEXANOL	0.53	0.02	0.06	0.10	0.00	0.09	0.00
C7 (total)	3.53	3.06	2.44	2.20	2.13	2.58	2.06
C8 (total)	3.29	2.82	2.50	2.20	2.18	3.13	1.98
C9 (total)	2.77	2.68	2.54	2.08	2.16	2.58	2.01
C10 (total)	2.19	2.60	2.60	2.23	2.16	2.36	2.00
C11 (total)	1.92	2.69	2.89	2.27	2.37	2.34	2.04
C12 (total)	1.66	2.42	2.90	2.11	2.36	2.15	1.70
C13 (total)	1.25	2.25	3.31	1.89	2.29	2.27	1.58
C14 (total)	0.75	0.00	2.99	1.52	1.74	1.75	1.44
C15+	43.94	50.77	60.03	64.80	70.40	54.83	75.11

Figure D2. Selectivity results for Run 2 (1 bar water added)

Time on Line, hrs	5	22	71	95	166
% C-atom Selectivities (Calculated w.r.t. CO converted to all products excluding CO2)					
METHANE	11.99	6.35	3.56	0.07	1.57
METHANOL	0.07	0.09	0.05	0.05	0.06
ETHYLENE	2.43	2.18	1.48	1.58	0.27
ETHANE	3.25	1.95	0.89	0.81	2.54
ETHANOL	3.53	1.64	0.41	0.37	0.29
PROPENE	4.76	3.45	2.12	1.97	2.26
PROPANE	1.96	1.12	0.47	0.42	0.45
n-PROPANOL	1.28	0.40	0.14	0.10	0.07
α - BUTENE	3.42	2.56	1.77	1.62	1.91
n-BUTANE	2.00	1.09	0.47	0.42	0.45
trans-2-BUTENE	0.12	0.08	0.03	0.03	0.02
cis-2-BUTENE	0.18	0.14	0.07	0.07	0.05
n-BUTANOL	1.19	0.34	0.10	0.07	0.09
α - PENTENE	2.86	2.22	1.70	1.56	1.83
n-PENTANE	1.89	1.07	0.50	0.44	0.46
trans-2-PENTENE	0.12	0.08	0.04	0.03	0.03
cis-2-PENTENE	0.12	0.10	0.06	0.05	0.04
n-PENTANOL	0.90	0.26	0.09	0.00	0.09
α - HEXENE	2.27	1.90	1.66	1.52	1.80
n-HEXANE	1.84	1.07	0.54	0.48	0.49
trans-2-HEXENE	0.14	0.09	0.04	0.04	0.03
cis-2-HEXENE	0.12	0.10	0.06	0.06	0.03
n-HEXANOL	0.50	0.09	0.05	0.00	0.05
C7 (total)	5.06	3.13	2.45	2.16	2.48
C8 (total)	4.19	2.88	2.39	2.16	2.58
C9 (total)	4.65	2.67	2.45	2.28	2.57
C10 (total)	3.65	2.48	2.54	2.35	2.60
C11 (total)	3.86	2.41	2.81	2.64	2.80
C12 (total)	2.89	2.54	3.24	2.81	3.03
C13 (total)	2.09	2.52	0.00	2.56	2.80
C14 (total)	1.48	2.11	3.00	2.18	2.37
C15+	24.58	49.29	62.47	67.40	61.94

Figure D3. Selectivity results for Run 4 (2 bar water added)

Time on Line, hrs	28	52	72	120	144	195
Calculated %C-atom Selectivities (Calculated w.r.t. CO converted to all products excluding CO2)						
METHANE	6.88	6.82	9.59	3.49	-8.53	-1.47
METHANOL	0.11	0.07	0.05	0.05	0.07	0.11
ETHYLENE	1.72	1.28	2.24	2.02	1.81	2.91
ETHANE	1.28	0.76	0.68	0.69	0.89	1.09
ETHANOL	1.07	0.37	0.33	0.22	0.32	0.37
PROPENE	2.70	2.05	1.88	1.99	2.35	3.19
PROPANE	0.75	0.45	0.35	0.37	0.49	0.66
n-PROPANOL	0.12	0.06	0.09	0.00	0.06	0.11
α - BUTENE	2.10	1.83	1.50	1.70	1.90	2.37
n-BUTANE	0.73	0.46	0.36	0.36	0.41	0.52
trans-2-BUTENE	0.05	0.15	0.03	0.02	0.08	0.11
cis-2-BUTENE	0.10	0.07	0.06	0.04	0.05	0.05
n-BUTANOL	0.06	0.00	0.05	0.04	0.00	0.09
α - PENTENE	1.89	1.71	1.46	1.65	1.59	1.82
n-PENTANE	0.71	0.48	0.39	0.37	0.37	0.46
trans-2-PENTENE	0.05	0.04	0.03	0.02	0.00	0.00
cis-2-PENTENE	0.08	0.06	0.04	0.03	0.00	0.00
n-PENTANOL	0.01	0.00	0.00	0.00	0.00	0.11
α - HEXENE	1.70	1.68	1.45	1.64	1.48	1.65
n-HEXANE	0.74	0.52	0.43	0.38	0.36	0.42
trans-2-HEXENE	0.07	0.04	0.03	0.02	0.00	0.00
cis-2-HEXENE	0.09	0.06	0.05	0.02	0.00	0.00
n-HEXANOL	0.09	0.00	0.00	0.04	0.04	0.00
C7 (total)	2.91	2.36	2.35	2.06	1.75	1.90
C8 (total)	2.63	2.32	2.35	2.13	1.94	1.79
C9 (total)	2.54	2.32	2.51	2.21	1.60	1.85
C10 (total)	2.33	2.19	2.80	2.16	1.53	1.77
C11 (total)	2.27	2.14	3.44	2.22	1.53	1.69
C12 (total)	2.16	1.94	3.87	2.33	1.41	1.58
C13 (total)	1.96	1.59	3.58	2.29	1.31	1.52
C14 (total)	1.63	1.26	2.78	2.22	1.18	1.43
C15+	58.46	64.94	55.21	67.23	84.02	71.89

Figure D4. Selectivity results for Run 3 (3 bar water added)

Time on Line, hrs	24	75	120	144	176	193
Calculated %C-atom Selectivities (Calculated w.r.t. CO converted to all products excluding CO2)						
METHANE	8.61	-0.22	-7.32	-0.17	-1.39	2.54
METHANOL	0.08	0.05	0.10	0.18	0.33	0.39
ETHYLENE	0.63	0.94	-0.05	0.38	-0.57	0.22
ETHANE	3.42	2.24	5.84	6.49	10.34	10.95
ETHANOL	0.97	0.41	0.16	0.26	0.54	0.51
PROPENE	3.27	1.87	3.02	4.28	7.24	7.88
PROPANE	1.00	0.40	0.60	0.90	1.68	1.86
n-PROPANOL	0.27	0.11	0.00	0.11	0.31	0.35
α - BUTENE	2.52	1.41	1.99	2.82	5.20	4.99
n-BUTANE	0.96	0.37	0.44	0.65	1.19	1.32
trans-2-BUTENE	0.14	0.03	0.00	0.06	0.27	0.20
cis-2-BUTENE	0.13	0.13	0.07	0.11	0.16	0.00
n-BUTANOL	0.11	0.12	0.21	0.18	0.41	0.38
α - PENTENE	2.11	1.33	1.55	1.98	3.33	3.42
n-PENTANE	0.93	0.38	0.37	0.52	0.92	1.01
trans-2-PENTENE	0.09	0.03	0.00	0.07	0.00	0.00
cis-2-PENTENE	0.12	0.05	0.00	0.00	0.00	0.00
n-PENTANOL	0.00	0.06	0.13	0.09	0.38	0.00
α - HEXENE	1.90	1.28	1.30	1.50	2.59	2.44
n-HEXANE	0.93	0.41	0.33	0.44	0.73	0.81
trans-2-HEXENE	0.09	0.04	0.00	0.00	0.00	0.00
cis-2-HEXENE	0.12	0.06	0.00	0.00	0.00	0.00
n-HEXANOL	0.00	0.04	0.13	0.07	0.00	0.18
C7 (total)	3.17	1.82	1.39	1.49	2.78	3.15
C8 (total)	2.98	1.98	1.42	1.27	1.84	3.26
C9 (total)	2.53	1.99	1.50	1.12	1.51	2.04
C10 (total)	2.27	2.10	1.45	0.94	1.24	1.42
C11 (total)	2.23	2.42	1.52	1.10	1.11	1.30
C12 (total)	1.97	2.78	1.71	1.07	0.94	1.27
C13 (total)	1.57	2.68	1.93	0.99	0.87	1.14
C14 (total)	0.95	2.37	2.30	0.98	0.59	1.04
C15+	53.24	68.37	74.55	69.05	54.84	45.01

Figure D5. Selectivity results for Run 5 (2 bar water added and removed)

Time on Line, hrs	23	49	100	122	167	216
Calculated %C-atom Selectivities (Calculated w.r.t. CO converted to all products excluding CO2)						
METHANE			0.38	3.99		12.53
METHANOL	0.07	0.00	0.00	0.00	0.15	0.28
ETHYLENE	1.90	1.57	1.41	2.06	2.40	2.90
ETHANE	0.76	0.42	0.34	0.35	0.43	0.00
ETHANOL	0.83	0.40	0.21	0.06	0.29	0.53
PROPENE	2.05	1.79	1.67	2.03	2.65	3.35
PROPANE	0.53	0.36	0.32	0.38	0.53	0.76
n-PROPANOL	0.23	0.03	0.06	0.00	0.12	0.00
α - BUTENE	1.54	1.58	1.54	1.71	1.99	2.48
n-BUTANE	0.52	0.38	0.33	0.36	0.44	0.67
trans-2-BUTENE	0.03	0.02	0.02	0.04	0.02	0.06
cis-2-BUTENE	0.06	0.05	0.04	0.07	0.06	0.13
n-BUTANOL	0.10	0.12	0.07	0.11	0.12	0.46
α - PENTENE	1.31	1.49	1.50	1.55	1.63	2.00
n-PENTANE	0.49	0.38	0.35	0.34	0.39	0.60
trans-2-PENTENE	0.04	0.02	0.02	0.04	0.02	0.06
cis-2-PENTENE	0.05	0.04	0.03	0.00	0.04	0.09
n-PENTANOL	0.07	0.05	0.00	0.00	0.00	0.41
α - HEXENE	1.21	1.51	1.51	1.53	1.45	1.75
n-HEXANE	0.49	0.41	0.38	0.34	0.37	0.58
trans-2-HEXENE	0.04	0.03	0.02	0.07	0.02	0.07
cis-2-HEXENE	0.05	0.04	0.04	0.04	0.01	0.08
n-HEXANOL	0.00	0.00	0.00	0.00	0.00	0.00
C7 (total)	1.73	2.00	1.97	1.91	1.67	2.24
C8 (total)	1.72	2.06	2.00	1.93	1.63	2.30
C9 (total)	1.58	2.04	2.13	1.83	1.56	2.38
C10 (total)	1.50	2.03	2.18	1.80	1.35	2.36
C11 (total)	1.51	2.09	2.14	1.94	1.28	2.24
C12 (total)	1.51	2.15	2.08	2.06	1.14	1.90
C13 (total)	1.45	2.10	1.73	2.14	0.74	1.73
C14 (total)	1.16	1.64	0.22	1.16	0.00	1.58
C15+	80.97	73.31	75.29	70.15	79.09	53.48